AD-A249 982

REPORT DOCUMENTATION PAGE

Form Approved
OMB No. 0704-0188

Estimated to average 1 hour per response, including the time for reviewing instructions, searching existing data sources, gathering and maintaining the data needed, and completing and reviewing the collection of information. Send comments regarding this burden estimate or any other aspect of this collection of information, including suggestions for reducing this burden, to Washington Headquarters Services, Directorate for Information Operations and Reports, 1215 Jefferson Davis Highway, Suite 1204, Arlington, VA 22202-4302, and to the Office of Management and Budget, Paperwork Reduction Project (0704-0188), Washington, DC 20503.

REPORT DATE	3. REPORT TYPE AND DATES COVERED
1991	THESIS/~~DISSERTATION~~

4. TITLE AND SUBTITLE
Development of Instrumentation for Boundary Layer Transition Detection

5. FUNDING NUMBERS

6. AUTHOR(S)
Steven B. Harrison, 1st Lt

7. PERFORMING ORGANIZATION NAME(S) AND ADDRESS(ES)
AFIT Student Attending: University of Oxford

8. PERFORMING ORGANIZATION REPORT NUMBER
AFIT/CI/CIA- 91-100

9. SPONSORING/MONITORING AGENCY NAME(S) AND ADDRESS(ES)
AFIT/CI
Wright-Patterson AFB OH 45433-6583

10. SPONSORING/MONITORING AGENCY REPORT NUMBER

11. SUPPLEMENTARY NOTES

12a. DISTRIBUTION/AVAILABILITY STATEMENT
Approved for Public Release IAW 190-1
Distributed Unlimited
ERNEST A. HAYGOOD, Captain, USAF
Executive Officer

12b. DISTRIBUTION CODE

13. ABSTRACT *(Maximum 200 words)*

DISTRIBUTION STATEMENT A
Approved for public release;
Distribution Unlimited

DTIC
ELECTE
MAY 11 1992
S B D

14. SUBJECT TERMS

15. NUMBER OF PAGES
128

16. PRICE CODE

17. SECURITY CLASSIFICATION OF REPORT	18. SECURITY CLASSIFICATION OF THIS PAGE	19. SECURITY CLASSIFICATION OF ABSTRACT	20. LIMITATION OF ABSTRACT

NSN 7540-01-280-5500

Standard Form 298 (Rev. 2-89)
Prescribed by ANSI Std. Z39-18
298-102

AD-A-249782

92-11946

92 5 01 030

DISCLAIMER NOTICE

THIS DOCUMENT IS BEST QUALITY AVAILABLE. THE COPY FURNISHED TO DTIC CONTAINED A SIGNIFICANT NUMBER OF COLOR PAGES WHICH DO NOT REPRODUCE LEGIBLY ON BLACK AND WHITE MICROFICHE.

Development of Instrumentation for Boundary Layer Transition Detection

Steven B. Harrison

The Queen's College

Oxford

A thesis submitted in partial fulfilment of the requirements for the degree of

Master of Science at the University of Oxford.

Trinity Term, 1991.

Department of Engineering Science

Parks Road, Oxford

To Jill

Development of Instrumentation for Boundary Layer Transition Detection

Steven B. Harrison
The Queen's College
Submitted in partial fulfilment of the requirements of the degree of Master of Science at the University of Oxford, Trinity Term 1991.

Abstract

A steady state heat transfer technique is developed and evaluated for detecting boundary layer transition on a flat plate in incompressible flow. The method involves adhering encapsulated temperature sensitive liquid crystals to a constant heat flux surface. A heater composed of unidirectional carbon fibres is developed and tested with the aim of in-flight boundary layer transition detection on a natural laminar flow nacelle. The individual and combined influences of surface heating and favourable pressure gradient on boundary layer transition are considered. Heating is found to be a destabilising influence on the boundary layer while a favourable pressure gradient is a stabilising influence. A Stanton number correlates the movement of transition with heating for zero pressure gradient flat plate boundary layers. No similar correlation is found when a favourable pressure gradient accompanies the heating. Heating is more destabilising in a favourable pressure gradient than in zero pressure gradient. Shear sensitive liquid crystal is used to detect transition and to obtain, for the first time, quantitative measurements of surface shear stress in a transitional boundary layer. This involves calibrating the time required for the liquid crystal film to experience a texture change when subjected to a shearing force. Using this technique, shear sensitive liquid crystal shows promise for full coverage measurement of surface shear stress in low speed flows.

Accession For
NTIS GRA&I ☑
DTIC TAB ☐
Unannounced ☐
Justification
By
Distribution/
Availability Codes
Dist | Avail and/or Special
A-1

Acknowledgements

I wish to express by gratitude to the entire crew at the Osney Laboratory for their support and assistance in completing this project. Their humour and expertise in areas as diverse as fluid mechanics and shove-ha'penny have made my work easier and more enjoyable. Although each member of the Osney Laboratory deserves a personal acknowledgement, space permits the mention of only a few individuals. First and foremost, I am deeply indebted to 'The Master', Dr. David Mee, for his guidance and assistance throughout the project. The pleasure that Dr. Mee draws from performing his job well is apparent and contagious--and it has certainly made my work more enjoyable throughout. I am also grateful to Prof. Terry Jones for giving me the opportunity to study at Osney, and for his remarkable enthusiasm and ingenuity. My warm appreciation goes out to Dr. Peter Ireland, Dr. Simon Hogg, Terry Cain and John Clark for their assistance and ready commentary (both political and not). Sarah-Jane Harrison's assistance in all things administrative was invaluable. I am also grateful to Andy Fowler for graciously granting me the use of his equipment, and to Dr. Trevor Walton for sharing his expertise concerning the physics of liquid crystals.

I am tremendously thankful to my wife, Jill, and daughters Hilary and Mollie for their unconditional love, support and encouragement. Their presence keeps my work in perspective. Finally, I am indebted to my parents and sisters who are always confident of my success, even when I am not.

The Rhodes Trust has provided the opportunity and financial support for my studies at Oxford. *Rolls-Royce plc.* funded this research. I was also supported by the Air Force Institute of Technology (AFIT). I am particularly grateful to AFIT and the Board of Trustees of the Rhodes Trust for generously allowing me a third year at Oxford in order to study in the Dept. of Engineering Science. The encouragement and assistance of Maj. Aaron Byerley were largely responsible for my decision to stay on.

Contents

Abstract

Acknowledgements

Nomenclature

Chapter 1: ***Introduction and Literature Survey*** 1.1
1.1 *Natural Laminar Flow* 1.1
1.2 *Transition* 1.5
1.2.1 *A Model of Transition* 1.6
1.2.2 *Factors Affecting Transition* 1.12
1.2.2.1 *Curvature* 1.13
1.2.2.2 *Free-stream Turbulence* 1.13
1.2.2.3 *Surface Roughness* 1.15
1.2.2.4 *Heating and Pressure Gradient* 1.16
1.2.3 *Techniques for Transition Detection* 1.19
1.3 *Liquid Crystals* 1.22

Chapter 2: ***Experimental Techniques*** 2.1
2.1 *Test Facilities* 2.1
2.1.1 *Tunnel* 2.1
2.1.2 *Flat Plate* 2.2
2.1.3 *Pressure Fairing* 2.2
2.2 *Temperature Sensitive Liquid Crystal Experiments* 2.3
2.2.1 *Aluminium Heater* 2.4
2.2.1.1 *Experimental Apparatus* 2.4
2.2.1.2 *Experimental Program* 2.9
2.2.1.2.1 *Flat Plate, Zero Pressure Gradient* 2.9
2.2.1.2.2 *Flat Plate, Constant Pressure Gradient* 2.12
2.2.2 *Carbon Heater* 2.15
2.2.2.1 *Experimental Apparatus* 2.15
2.2.2.2 *Experimental Program* 2.20
2.3 *Shear Sensitive Liquid Crystal Experiments* 2.23
2.3.1 *Experimental Apparatus* 2.23
2.3.2 *Experimental Program* 2.25

Chapter 3: ***Results and Discussion*** 3.1
3.1 *Temperature Sensitive Liquid Crystals* 3.1
3.1.1 *Aluminium Heater* 3.1
3.1.1.1 *Flat Plate, Zero Pressure Gradient* 3.1
3.1.1.2 *Flat Plate, Constant Pressure Gradient* 3.5
3.1.2 *Carbon-Fibre Heater* 3.11
3.1.3 *Preliminary Results from a Curved Carbon-Fibre Heater* 3.15

3.2 *Shear Sensitive Liquid Crystal* 3.17
3.2.1 *Natural Transition* 3.17
3.2.2 *Induced Transition* 3.20

Chapter 4: *Conclusions and Recommendations* 4.1
4.1 *Heat Transfer Measurements* 4.1
4.1.1 *Future Work* 4.3
4.2 *Unidirectional Carbon-Fibre Heater* 4.4
4.3 *Surface Shear Stress Measurements* 4.5

Appendix A: *Dimensional Analysis* A.1

Appendix B: *Uncertainty Analysis* B.1
B.1. *Uncertainty in Reynolds and Stanton Numbers at Transition End* B.4
B.2. *Uncertainty in Transition Length* B.5

Appendix C: *Estimates of Longitudinal Conduction* C.1

References

Figures

Nomenclature

C_p	specific heat at constant pressure, J/kg·K
h	coefficient of heat transfer, W/m^2·K
i	electric current, Amps
k	thermal conductivity, W/m·K
K	acceleration parameter
p	pressure, N/m^2
Pr	Prandtl number
q	heat flux, W/m^2
R	electrical resistance, Ω
Re	Reynolds number
St	Stanton number
t	thickness, m
t	time, sec
T	temperature, K
T_c	liquid crystal colour play temperature, K
T_g	gas temperature, K
T_s	surface temperatue, K
Tu	turbulence intensity
U	fluid velocity, m/sec
u	fluid velocity component, m/sec
u_l	local fluid velocity component, m/sec
x	distance parallel to surface, m
y	distance normal to surface, m

Greek

α	temperature coefficient of resistance, Ω/K
γ	intermittency
δ	boundary layer thickness, m
δ	uncertainty
ε	emissivity
η	transition length, m
μ	viscosity, kg/sec·m
ν	kinematic viscosity, m^2/sec
ξ	unheated starting length, m
ρ	mass density, kg/m^3
σ	Stefan-Boltzman constant
τ	shear stress, N/m^2

Subscripts

ad	adiabatic
cond	conduction
conv	convection
crit	critical
ref	reference conditions
t	transition start
T	transition end
w	conditions at the wall

Chapter 1: *Introduction and Literature Survey*

1.1 *Natural Laminar Flow*

The Oxford University Engineering Laboratory is to be involved in experiments to detect boundary layer transition in flight tests on a natural laminar flow (NLF) engine nacelle. The skin friction drag associated with a laminar boundary layer is substantially smaller than that of an equivalent length of turbulent boundary layer. Laminar flow technology is, therefore, directed at reducing viscous drag on aircraft by delaying the point of boundary layer transition from laminar to turbulent flow. Transition may be delayed by using either active or passive means. The latter is advantageous in that the power requirements of active systems, such as suction, diminish the benefits of delayed transition. One such passive measure is *natural* laminar flow technology, in which the geometry of an aerodynamic body is designed so as to delay transition.

It has been established that the point of transition in the boundary layer is strongly influenced by the pressure gradient in the external stream. A negative (or favourable) pressure gradient in the stream-wise direction leads to delayed transition and an adverse pressure gradient advances transition location. NLF technology seeks to extend the length of laminar flow by developing a body geometry which has a favourable pressure gradient over as much of its length as possible (Fig 1.1). There

is, however, a trade-off to be considered when attempting to reduce drag by this means. A favourable pressure gradient is formed at the expense of an increase in wing thickness (or nacelle diameter) which leads to increased form drag.

HASTINGS et al. (1987) have noted that the external nacelle on large turbofan-powered aircraft are particularly attractive candidates for the application of natural laminar flow technology. These nacelles have lower characteristic Reynolds numbers than other possible candidates, such as fuselages and wings. Furthermore, nacelles are not required to provide lift and can, therefore, be shaped to have pressure gradients favourable to laminar boundary layers without the concern for lift and moment characteristics which influences the design of NLF wings.

The practical importance of NLF work is considerable. By contouring the NLF nacelle so as to have accelerating flow over as much as 70% of its length, HASTINGS et al. suggest that nacelle friction drag may be reduced by as much as 40-50%. This equates to a reduction in total aircraft drag and cruise fuel burn of 1-2% for a large commercial transport. The potential savings in fuel costs (see Fig. 1.2) as well as benefits in terms of increased flight range and payload and reduced environmental pollution are substantial. These benefits may be increased considerably by NLF applications to other aircraft structures (Fig. 1.3). GODARD (1989) has noted that viscous drag accounts for ~ 50% of total aircraft drag. SZODRUCH (1991) estimates that NLF technology offers a potential reduction of this drag by 13.5%.

Although there is presently no commercial aircraft designed for laminar

boundary layers, there have been a number of laminar flow projects over the last decade. Since the early 1980's, General Electric and NASA's Langley Research Center have combined to perform NLF wind tunnel and flight tests. Tests were performed at unit Reynolds numbers of ~ 3.5-6.0 x 10^6 m^{-1} on Citation and OV-1B aircraft. Phase I of these experiments suggests that NLF could be maintained as far aft as 50% of nacelle length.

COUSTEIX et al. (1991) have reported that ONERA/CERT have performed laminar flow flight experiments on the vertical tail of a Falcon 50 aircraft. Flight conditions included the transonic range with unit Reynolds numbers of 4-7 x 10^6 m^{-1}.

In 1985 Germany also initiated a national research program intended to develop transonic laminar flow technology. REDEKER et al. (1990), HORSTMANN et al. (1990 and 1990a) and HENKE et al. (1990) describe flight tests employing a wing glove on a light aircraft and the corresponding wind tunnel tests using a 1/2 scale model of the wing. The program has thus far been focused on performing flight and wind tunnel transition investigations on wings. The goal is to use the results to develop a reliable transition prediction procedure and a reasonable correlation between flight and wind tunnel data. Tests were conducted at altitudes of 4000-10000 ft, and at Reynolds numbers based on mean aerodynamic chord length of 3-10 x 10^6. This program has demonstrated the NLF concept with laminar flow in flight of up to 50% of the chord.

The experiments presented herein are related to tests which are to be performed on an NLF nacelle as part of a joint venture involving Rolls-Royce plc., DLR, Hurel-Dubois (UK) ltd., Oxford University, and MTU. Two series of flight tests are to be performed as a means of demonstrating NLF technology. In the first tests, measurements will be made of drag and transition location on the nacelle of a Rolls-Royce M45 turbofan engine over a range of flight conditions. This nacelle is constructed to the original coordinates for the machine and to typical standards for a modern production engine. It is referred to as the datum nacelle. This nacelle will then be replaced with a second nacelle whose geometry has been designed by Rolls-Royce and DLR to extend laminar flow. Transition location and drag will be measured on this NLF nacelle over a range of flight conditions and engine settings similar to those for which the datum nacelle was tested. This program will enable direct comparisons to be made between the datum and NLF nacelles under similar free-stream conditions and power settings and with identical engines. DLR's VFW614 (Fig. 1.4) will serve as the test vehicle and the port-side M45 engine will be instrumented.

DLR and Oxford University are charged with transition detection. DLR will utilise infrared imaging while Oxford will measure transition using temperature sensitive liquid crystals applied to a carbon-fibre heater which is integrated into the structure of the nacelle. Resistance temperature detectors beneath the carbon-fibre heater will provide an alternative means of measuring surface temperature and serve as feedback units to the heater's temperature control system. A series of hot film gauges developed and manufactured by Oxford University will provide a third means

of detecting transition location. Cameras mounted in a wing pod, as well as in the cabin, will enable DLR and Oxford each to accomplish transition measurements on both sides of the nacelle. Drag on the external nacelle will be assessed by DLR using pressure rakes mounted downstream of the nacelle.

The instrumented nacelles are to be manufactured to the specifications of Rolls-Royce, Oxford University, and DLR by Hurel-Dubois (UK) ltd., of Burnley, England. The design condition for the nacelle is M = 0.6 at 30,000 ft., although drag and transition location will be measured throughout a prescribed flight envelope.

1.2 *Transition*

The transition from laminar to turbulent flow represents one of the most important and perplexing problems in fluid mechanics. REYNOLDS (1883) initiated the study of transition more than a century ago with his classic series of dye filament experiments. REYNOLDS observed that a thread of dye flowing down a pipe, while initially sharply defined, suddenly diffused into the stream at what came to be known as the location of 'transition' from laminar to turbulent flow. Furthermore, he established that this phenomenon occurred at a unique numerical value of the dimensionless parameter, $U\,d/\nu$ -- the transition Reynolds number.

Since that time, a vast amount of research has been directed at better understanding, predicting and controlling the phenomenon of transition from laminar to turbulent flow, particularly within boundary layers. Nevertheless, a complete understanding of boundary layer transition remains elusive.

1.2.1 *A Model of Transition*

There currently exists no generalised theory which would find its foundation in a comprehensive appreciation of the physical mechanisms responsible for transition and extend to a prediction of transition onset and length. Nevertheless, many links in the chain of events involved with transition have been exposed. In particular, the initial stage leading to transition, the 'linear' portion of transition, is now fairly well understood. REYNOLDS (1895) postulated that transition is a consequence of the instability of the laminar flow. However, it was the theoretical studies of PRANDTL (1922) which eventually led to a 'linear stability theory' capable of predicting a 'critical' Reynolds number at which small disturbances in the flow (Tollmien-Schlichting waves) become unstable. The results of linear stability theory were later confirmed experimentally by SCHUBAUER and SKRAMSTAD (1948). SCHLICHTING (1979) provides a detailed account of the history and development of linear stability theory. Here linear stability theory (or 'classical small perturbation analysis') will only be mentioned briefly as a convenient means of approaching the processes of transition and the effects of the disturbance environment on transition.

Stability analysis is based on the assumption that laminar flows are affected by certain small disturbances which may originate from surface imperfections or irregularities in the external flow. The theory investigates the behaviour of these disturbances as they are superimposed on the Navier-Stokes equations of motion. If the disturbances decay with time, the flow is considered stable. Disturbances which amplify with time are unstable and may cause transition. The object is to predict the value of the critical Reynolds number for a prescribed flow.

The fundamental differential equation for a disturbance is the well known Orr-Summerfeld (O-S) equation (the derivation of which may be found in texts such as SCHLICHTING (1979)):

$$(U - c)(\phi'' - \alpha^2 \phi) - U''\phi = \frac{i}{\alpha R_\delta}(\phi'''' - 2\alpha^2 \phi'' + \alpha^4 \phi) \quad . \quad (1.1)$$

Here, R_δ represents the Reynolds number based on boundary layer thickness, δ, α is the wave number, ϕ is the amplitude function of the fluctuation, and c is a complex function of which the real portion denotes the velocity of propagation of the wave while the imaginary portion determines the degree of damping (or amplification) of the disturbance. Equation 1.1 is obtained by writing each dependent variable in the Navier-Stokes equations as a dependent variable plus a time dependent term. The resulting equations are linearised and the mean flow equation is subtracted out. Parallel flow is assumed and the equations are nondimensionalised with free-stream quantities. Suitable boundary conditions can then be imposed.

By omitting the viscous terms (RHS) of the O-S equation, RAYLEIGH (1913) was able to derive the important 'point of inflection criterion' which states that the existence of a point of inflection in the velocity profile, $U(y)$ constitutes a *necessary* condition for the occurrence of instability. TOLLMIEN (1936) later showed that such an inflection also constitutes a *sufficient* condition for the amplification of disturbances.

The solution to the O-S equation for a prescribed laminar flow is a curve of neutral stability as shown in Fig. 1.5. The point on the curve at which the Reynolds

number has its smallest value (tangent parallel to the vertical axis) is of particular interest since it indicates the limit of stability. Below that critical Reynolds number, Re_{crit}, all individual oscillations decay; for Reynolds numbers > Re_{crit}, disturbances at at least some frequencies are amplified. It is worth noting, however, that Re_{crit} is not the same as the Reynolds number at transition start, Re_t (the *experimental* critical Reynolds number). Re_{crit} represents the Reynolds number at which some individual disturbances will *begin* to amplify. As will be discussed below, the culmination of the amplification process is turbulence. The point at which isolated patches of turbulence first begin to appear is designated Re_t. The amplification process, however, takes some time. Therefore, Re_t must be downstream of Re_{crit}.

The relationship between Re_{crit} and Re_t is not yet well understood. More specifically, no theoretical model exists which is capable of explaining the means by which two-dimensional Tollmien-Schlichting (T-S) waves experience non-linear amplification, eventually leading to turbulence. The temporal and spatial scales required for this amplification may be influenced by a number of environmental factors (discussed in Section 1.2.2.). The means by which the boundary layer responds to these factors is little understood. Consequently, a reliable method for prediction of transition location is still a utopia.

Studies involving this 'non-linear' region of instability began soon after the aforementioned work of SCHUBAUER and SKRAMSTAD (1948). From observations of the flow on a water table, EMMONS (1951) postulated that transition is not initiated along a continuous front but, rather, involves a transition *region* in which

'spots' of turbulence form and expand as they move downstream. Fully turbulent flow occurs where these turbulent spots merged to cover the entire span of the surface. Passage of the spots over points on the surface results in alternations of laminar and turbulent flow. The alternations may be quantitatively described by an *intermittency factor*, γ, which represents the fraction of time any point spends in turbulent flow. Hence, $\gamma = 0$ at the onset of transition and $\gamma = 1$ when the transition to turbulent flow is complete. SCHUBAUER and KLEBANOFF (1955) provided details of the geometry of turbulent spots and their growth as they move downstream by using an electrical spark to introduce turbulent spots into a laminar boundary layer (Fig. 1.6). NARASIMHA (1957) postulated that the spots formed at a preferred stream-wise position but randomly in time and span-wise location. The resulting intermittency distribution through the transition region,

$$\gamma = 1 - e^{-.412\,\xi^2} \quad , \tag{1.2}$$

where

$$\xi = \frac{x - x_t}{\lambda} \quad , \tag{1.3}$$

fits the experimental data well. Here, λ represents the distance between the location at which $\gamma = 0.25$ and the location at which $\gamma = 0.75$, and x_t marks the beginning of transition. DHAWAN and NARASIMHA (1958) showed that the velocity profile and skin friction variations within the transition region at subsonic speeds could be predicted by weighting the average of the laminar and turbulent values by the intermittency factor. The validity of this proposition has recently been supported by the results of DEY and NARASIMHA (1990).

SCHUBAUER (1957) and KLEBANOFF and TIDSTROM (1959) began studies into the manner in which these turbulent spots arise from the two-dimensional disturbances in the boundary layer. These studies indicated that there is a definite and reproducible progression of events by which T-S waves evolve into turbulence. Using a vibrating ribbon technique for the introduction of forced oscillations in the boundary layer, KLEBANOFF et al. (1962) were able to show that even in nominally two-dimensional flow, the T-S waves that develop in regions of instability increasingly warp or bend in the span-wise direction as they move downstream. This warping is responsible for secondary flows to and from the surface which eventually evolve into turbulent spots.

Many features of this evolution from T-S waves to turbulent spots have become widely accepted (see Fig. 1.7). STUART (1965) and TANI (1969) provide general reviews of the transition process. It may be summarised as follows:

(1) *Stable laminar flow develops a region of instability to small wavy disturbances.* Provided the Reynolds number is above a critical level (as predicted by linear stability theory), T-S waves begin to amplify.

(2) *Three dimensional waves and vortices form.* Minor irregularities in the free stream, test surface, etc. give rise to a rate of wave growth which varies with span-wise position. Thus, as shown in Fig. 1.8, an initially two-dimensional wave takes on three-dimensional form. Vortex filaments within the boundary layer distort with the wave front. The vortex filaments, in turn, induce secondary flows to and

from the surface which help to intensify the warping. As the generated three-dimensional waves with vorticity progress downstream, the wave front distortion increases. The disturbance lines thus form 'Λ' or 'hairpin' vortices (Fig. 1.9). As these grow, the vorticity lines stretch and strengthen. 'Peaks' and 'hollows' of high and low disturbance intensity form (see Fig. 1.10).

(3) *Bursts of turbulence appear in regions of very high vorticity.* The instantaneous velocity profile develops a region of high shear (with an associated inflection) at span-wise stations corresponding to a peak (Fig. 1.11). As the point of inflection criterion suggests, these inflectional velocity profiles are associated with higher amplification rates. The vortices act as a mixing mechanism, introducing low speed flow from the lower layers of the boundary layer to the upper layers and vice versa. Thus, additional regions of inflectional velocity profiles are created, thereby adding additional sources of instability and disturbance growth. At some stage high frequency bursts of turbulence (embryonic 'turbulent spots') form in the regions of high vorticity.

(4) *Turbulent spot growth.* The embryonic turbulent spots travel downstream and spread span-wise at rates as observed by SCHUBAUER and KLEBANOFF (1955) (refer to Fig. 1.6). The initiation of turbulent spots is generally considered to be the 'start' of transition. At some distance downstream, these spots coalesce to form a fully turbulent boundary layer.

The details of transition presented above are primarily derived from

'controlled' experiments (e.g. those in which the boundary layer is disturbed in a controlled manner) such as those performed by KLEBANOFF et al. (1962) employing a vibrating ribbon. Nevertheless, the features discussed are thought to be common to most forms of 'natural' transition as well, although the events perhaps occur in a less regular manner. In some cases, however, it seems that the disturbance environment may be so intrusive upon the boundary layer as to 'bypass' the initial T-S wave stage of the transition process and introduce directly disturbances of large enough amplitude to readily generate turbulent spots. For example, SUDER and O'BRIEN (1988) and SOHN et al. (1989) have reported bypass transition due to high levels of free stream turbulence. MORKOVIN (1984) has also addressed the issue in depth.

1.2.2 *Factors Affecting Transition*

Most of the difficulty in understanding and predicting transition is due to the large number of independent factors which affect transition. It is known, for example, that transition may be influenced by free stream turbulence, pressure gradient, heat transfer between the surface and the fluid, surface roughness, surface curvature, Mach number, Reynolds number, angle of attack, sweep angle, acoustic radiation, surface vibration and injection or suction of fluid at the wall. STUART (1965) and TANI (1969) and, more recently, RESHOTKO (1976) and HERBERT (1988) have produced excellent general reviews of transition and the various factors affecting it*. The more

*STUART and TANI focus on low speed flows. RESHOTKO is primarily concerned with heating and the *receptivity* of the boundary layer, i.e. the means by which a particular forced disturbance enters the boundary layer and the nature of its signature in the disturbance flow. HERBERT is interested in the means by which small two-dimensional disturbances in flat plate boundary layers grow into the violent three-dimensional disturbances and high-frequency motions that characterise turbulence.

general works of SCHLICHTING (1979), YOUNG (1989) and WHITE (1991) also discuss the various factors affecting transition.

The effects of heating and pressure gradient on transition are of primary interest in the present study. Curvature, surface roughness and turbulence are of subsidiary interest and will, consequently, be discussed briefly. The remaining factors will not be discussed further.

1.2.2.1 *Curvature*

While of little bearing for the flat plate experiments presented in this study, curvature may be of interest for experiments performed on the NLF nacelle. LIEPMAN (1943) has shown that Re_t is virtually unaffected by convex curvature when the radius of curvature is large in relation to the boundary layer thickness, δ (Fig. 1.12).

1.2.2.2 *Free-stream Turbulence*

Qualitatively, transition is hastened by an increase in free-stream turbulence. Most studies involved with turbulence to date have only measured free-stream turbulence intensity,

$$Tu = \frac{\left(\frac{\overline{u'^2} + \overline{v'^2} + \overline{w'^2}}{3}\right)^{\frac{1}{2}}}{U} \quad , \tag{1.4}$$

where primes denote perturbed quantities. In recent years there has been a growing awareness of the importance of other measures of turbulence such as the velocity and

direction of disturbance propagation as well as the frequency and wavelength of the disturbance. MEIER et al. (1987), for example, have shown that the onset of transition correlates better with the spectral density of the free-stream turbulence in the frequency range of the T-S waves than the total intensity.

The effect of Tu on transition location as observed by DRYDEN (1959) is shown in Fig. 1.13. There appears to be no significant effect of external turbulence on Re_t for turbulence levels of less than ~ 0.1 %. With further increase in Tu, there is a continuous decrease in Re_t. The experimental results of BLAIR (1982) and GOSTELOW and BLUNDEN (1988) show a similar decrease in Re_t with increasing Tu above a turbulence intensity of 0.1%. VAN DRIEST and BLUMER (1963) and McDONALD and FISH (1973) have predicted theoretically the same trends. HALL and GIBBINGS (1972) and ABU-GHANNAM and SHAW (1980) have provided further experimental data and empirical predictions accounting for free-stream turbulence intensity and pressure gradient. EDWARDS and FURBER (1956) and JUNKAN and SEROVY (1967) have found no significant influence of Tu on convective heat transfer from a flat plate, apart from that due to an advancement of transition location.

Empirical correlations currently provide the best prediction of transition location with variations in turbulence intensity and pressure gradient. Figure 1.13, for example, shows that the semi-empirical prediction formulated by MACK (1977) fits DRYDEN's data quite well at moderate turbulence levels. At very low turbulence levels (i.e. $Tu < 0.1\%$), however, contemporary empirical methods fail to fit the

experimental data well. Recently, GOVINDARAJAN and NARASIMHA (1991) have postulated that, at these turbulence levels, the dominant factor influencing the onset of transition is no longer free-stream turbulence, but residual disturbances (e.g. noise, and vibration) specific to the each facility and, perhaps, each operating condition. This is consistent with the experimental observations of DRYDEN mentioned previously. The implication is that the mysterious 'unit Reynolds number effect' may disappear provided adequate allowances are made for variations in these sort of parameters. GOVINDARAJAN and NARASIMHA propose an 'equivalent turbulence intensity', q_0, to represent these residual facility-dependent disturbances. Their correlation employing q_0 is presented in Fig. 1.14 against a range of experimental data.

1.2.2.3 *Surface Roughness*

Surface roughness above a certain scale is know to move transition forward. Two critical excrescence heights, denoted $k_{crit,1}$ and $k_{crit,2}$, are of interest. Transition is unaffected by excrescences of heights, k, where $k < k_{crit,1}$. If $k > k_{crit,1}$, increasing k moves transition forward until, at $k = k_{crit,2}$, transition occurs just aft of the excrescence. The values of $k_{crit,1}$ and $k_{crit,2}$ for a given flow depend on the fluid viscosity and external velocity distribution as well as the shape and location of individual excrescences.

YOUNG and PATERSON (1981) provide a detailed account of the effects of excrescences on transition as well as calculation procedures. The only theoretical study known to the author which attempts to include the influence of surface roughness on transition location is that of McDONALD AND FISH (1973).

1.2.2.4 *Heating and Pressure Gradient*

It is well established that heat transfer to or from a surface influences boundary layer transition. LINKE (1942) observed that heating a body in air increased its drag, and he correctly surmised that the transition location had been moved upstream. The destabilising influence of heating in air is chiefly due to the variation of viscosity with temperature. As discussed below, higher viscosity near the hot surface leads to an inflection in the velocity profile (Fig. 1.15a), as confirmed experimentally by LIEPMAN and FILA (1947). Cooling leads to 'fuller' velocity profiles and, therefore, greater stability and a delay of transition location in an air boundary layer (see MACK, 1975). As STRAZISAR et al. (1977) observed, the trends are reversed in water. A number of theoretical investigations, such as those performed by WAZZAN et al. (1968), NAYFEH and EL-HADY (1980) and LEKOUDIS (1980), have predicted the same trends. WAZZAN et al. have noted that there exists a critical heating rate for water flows. Above this critical heating rate, the stabilising influence of 'fuller' velocity profiles is overcome by the destabilising influence of reduced viscous damping and a further increase in heating *reduces* the Re_{crit}.

The influence of pressure gradient on transition is also well documented. For example, VAN DRIEST and BLUMER (1963), HALL and GIBBINGS (1972), ABU-GHANNAM and SHAW (1980) and BLAIR (1982) dealt with pressure gradient and free-stream turbulence effects on the transition process. A favourable pressure gradient leads to delayed transition and an adverse gradient to early transition. These effects, like those due to heating, may be explained by reference to velocity profiles and the point of inflection criterion (see Fig. 1.15b).

Neglecting buoyancy effects, but accounting for the temperature dependency of the viscosity of the fluid, μ, the two-dimensional boundary layer momentum equation (Eqn. 13.6 in SCHLICHTING (1979)) may be written as

$$\rho\left(u\frac{\partial u}{\partial x} + v\frac{\partial u}{\partial y}\right) = -\frac{dp}{dx} + \frac{\partial}{\partial y}\left(\mu\frac{\partial u}{\partial y}\right) \quad , \tag{1.5}$$

where x is distance along the surface, y is distance normal to the surface, p is the mean static pressure and u and v are components of the velocity in the x and y directions respectively.

Evaluated at the wall, $u = v = 0$. Hence,

$$\frac{dp}{dx} = \frac{\partial}{\partial y}\left(\mu\frac{\partial u}{\partial y}\right) \quad . \tag{1.6}$$

Expanding,

$$\frac{dp}{dx} = \left(\frac{\partial \mu}{\partial y}\right)_w\left(\frac{\partial u}{\partial y}\right)_w + \mu_w\left(\frac{\partial^2 u}{\partial y^2}\right)_w \quad , \tag{1.7}$$

where w denotes values evaluated at the wall. Rearranging Eqn 1.7,

$$\left(\frac{\partial^2 u}{\partial y^2}\right)_w = -\frac{1}{\mu_w}\left(\frac{\partial \mu}{\partial y}\right)_w\left(\frac{\partial u}{\partial y}\right)_w + \frac{1}{\mu_w}\frac{dp}{dx} \quad , \tag{1.8}$$

where the LHS of Eqn 1.8 represents the curvature of the velocity profile, $u(y)$, at the wall. If the wall is heated, the temperature of the fluid at the wall will be greater than the temperature of the fluid in the free stream. The viscosity of air increases with temperature and, therefore, $(d\mu/dy)_w < 0$ for a heated surface in air. Since $(du/dy)_w > 0$ in a boundary layer, the curvature of the velocity profile at the wall is positive when

$dp/dx = 0$. The curvature at the edge of the boundary layer, however, is negative. It follows that a point of inflection exists within the boundary layer velocity profile.

When a favourable pressure gradient ($-dp/dx$) is combined with surface heating the sign of the velocity profile's curvature at the wall depends on the relative magnitudes of the terms on the RHS of Equation 1.8. The boundary layer is expected to be *more stabile* in relation to the boundary layer on an unheated flat plate with zero pressure gradient when

$$\left| \left(\frac{\partial \mu}{\partial y} \right)_w \left(\frac{\partial u}{\partial y} \right)_w \right| < \left| \frac{dp}{dx} \right| . \tag{1.9}$$

Conversely, the boundary layer is relatively *less stable* when

$$\left| \left(\frac{\partial \mu}{\partial y} \right)_w \left(\frac{\partial u}{\partial y} \right)_w \right| > \left| \frac{dp}{dx} \right| . \tag{1.10}$$

To the author's knowledge, there are no studies in the literature which have quantitatively examined the combined effects of heat transfer and favourable pressure gradient on transition location in an air boundary layer. CEBECI and SMITH (1968) unsuccessfully attempted to do so while endeavouring to use heating as a boundary layer trip. BLAIR (1982) examined the influence of pressure gradient on transition on a heated surface but did not examine the influence of varying heating rates. LAUCHLE and GURNEY (1984) examined the effects of heating on an underwater axisymmetric body with a nearly-uniform favourable pressure gradient. The temperature distribution was nearly constant, and transition location was plotted versus heating as shown in Fig. 1.16. However, due to the aforementioned competing

influences of viscosity on the stability of a water boundary layer, quantitative agreement on the movement of transition with heating for air and water boundary layers seems unlikely. The results presented herein represent an investigation to examine quantitatively the effects of heating on transition location with both zero and favourable pressure gradients in the incompressible air boundary layer.

1.2.3 *Techniques for Transition Detection*

The wholesale change in the characteristics of the boundary layer flow during transition lends itself to a number of detection techniques. Some of the most common will be discussed here. A study of the velocity distribution in the boundary layer, for example, offers a convenient means of detecting transition. Fig. 1.17 shows that transition involves a significant change in the shape of the mean velocity distribution curve through the boundary layer. It is also apparent from this figure that the boundary layer suddenly thickens in the region of transition. The flat plate boundary layer, for example, changes from a laminar growth rate proportional to $x^{1/2}$ to a turbulent growth proportional to $x^{4/5}$. The shape factor, $H = \delta_1/\delta_2$ also decreases from ≈ 2.6 in the laminar region to ≈ 1.4 in the turbulent region (Fig. 1.18). Here, δ_1 is the displacement thickness and δ_2 the momentum thickness. Hot wires, hot films and Pitot tubes offer convenient means of measuring the boundary layer velocity distribution.

The higher velocity gradient at the wall associated with turbulent boundary layers is responsible for increased shearing stress, τ according to the formula,

$$\tau = \mu \left(\frac{\partial u}{\partial y} \right)_w \quad . \tag{1.11}$$

The characteristic rise in the coefficient of skin friction through the transitional region is amenable to detection by a number of techniques including surface shear stress gauges and shear sensitive liquid crystals (on which more will follow).

In the transition region, turbulent mixing leads to a rise in heat transfer and mass transport which is analogous to the rise in skin friction. This increased mass transport is utilised by sublimating chemicals to indicate transition location. The chemical sublimes first at the point of highest mass transport (transition end) and last at the point of lowest mass transport (transition start). Thermocouples or temperature sensitive liquid crystals (on which more will be said later) may be employed to detect temperature variations on a uniformly heated surface in unheated flow, or an unheated surface in heated flow. DEOM (1989), CROWDER (1990) and HORSTMAN et al. (1990) have recently reported on thermo-imaging as a non-intrusive means of mapping surface temperature. Given a knowledge of the flow characteristics and the temperature distribution, transition start and end may be determined.

As noted in Section 1.2.1, intermittency also provides a means of measuring the transition location. Fig. 1.19 shows hot film traces at various locations through an intermittent (transitional) boundary layer. Intermittency increases from a value of $\gamma \approx 0.0$ in the laminar region to $\gamma \approx 1.0$ at the end of transition. An 'intermittency meter' such as that constructed by KIM et al. (1989), may be used to translate hot

film intermittency traces into quantitative values of γ.

Intermittency is generally recognised as providing the best indication of the location of the transitional region since, physically, the location at which turbulent spots first appear is represented by $\gamma = 0.0$, and $\gamma = 1.0$ corresponds to the location at which the spots coalesce to form a fully turbulent boundary layer. OWENS (1970) and BLAIR (1982) have noted, however, that other methods of detecting transition may not provide the same transition start and end locations as those indicated by intermittency. This is to be expected if, as NARASIMHA (1958) suggested, mean flow characteristics in the transitional region may be considered to be a combination of fully laminar and fully turbulent flows, each proportionally weighted by the intermittency factor. At low intermittency factors, the turbulent contribution to the mean flow characteristics will be small. Skin friction, for example, will continue to fall for a short period after $\gamma > 0$. Hence, the transition location as indicated by minimum τ will be downstream of the location at which the value of γ has begun increasing.

Nevertheless, the difference between transition locations as derived from heat transfer distributions, for example, and those determined from intermittency is small. GOVINDARAJAN and NARASIMHA (1991) tentatively suggest

$$Re'_t \sim 0.9\, Re_t \quad , \tag{1.12}$$

where Re'_t is the Reynolds number at which turbulent spots first appear and Re_t is that indicated from the heat transfer or skin friction distribution.

1.3 *Liquid Crystals*

Liquid crystals (LC's) are a highly anisotropic state of matter which exists between the solid and liquid phases of some compounds. Although they appear as liquids, they exhibit optical properties characteristic of a crystalline (solid) state. In particular, LC's scatter light very selectively.

This behaviour is traced to their molecular arrangement. Each LC has a helical structure whose characteristic pitch length fortuitously coincides with the wavelength of the visible spectrum. When the helix is subjected to certain physical influences (the two primary influences being temperature and surface shear stress), the helix pitch changes and the wavelength of reflected light is altered accordingly. Since the LC's fundamental chemical structure is unaffected by these changes, its responses are theoretically rapid, continuous and reversible indefinitely.

Measurements of a particular physical mechanism are made by ensuring that the LC's sensitivity to other stimuli is either reduced to a negligible level or accounted for. For these tests, encapsulated chiral nematic LC's were used for temperature indication. The gel-like capsule enveloping each LC consists of polyvinyl alcohol and is approximately 10 μm in diameter. In this form, the LC's sensitivity to shear is negligible and surface temperatures can be measured to within 0.2 °C. IRELAND and JONES (1987) report response times of ~ 3 ms for these encapsulated LC's. A neat (unencapsulated) cholesteric liquid crystal which has a temperature insensitive selective colour reflection was used for shear indication.

Over the past 20 years LC coatings have found various uses in aerodynamic and aerothermal studies. JONES (1991) discusses the various properties of LC's which may be useful to research engineers. Only those liquid crystal techniques which are relevant to the present experiments are addressed here. OKER and MERTE (1976), HIPPENSTEELE et al. (1983), BAUGHN et al. (1985, 1986), and FISHER and EIBECK (1990) have used *temperature sensitive* LC coatings to measure the surface temperature in steady-state convective heat transfer experiments. IRELAND and JONES (1985,1986), JONES and HIPPENSTEELE (1988), BYERLEY et al. (1988) and WANG et al. (1990) have utilised temperature sensitive LC's to measure convective heat transfer using a transient technique. In the steady-state tests, a knowledge of the power being supplied to a heated strip and the surface and free-stream temperatures enables a heat transfer coefficient to be determined. In transient tests, the heat transfer coefficient is found from the free-stream temperature and the surface temperature history as indicated by the LC. For temperature indication, cholesteric liquid crystals which have a narrow colour play temperature band (typically 1 °C) are chosen. The temperature level at which this colour play occurs can be adjusted over a wide range of temperatures by modifying the composition. A direct comparison of the steady-state and transient techniques by BAUGHN et al. (1989) concluded that the former was simpler and provided lower uncertainties, while the latter was better suited to complex geometries. The present work is intended to assess the suitability of the steady-state technique specifically for transition detection.

The use of *shear sensitive* liquid crystals in aerodynamic measurements has been a more recent innovation. Two different processes can be employed to indicate

shear level with this form of LC. In the first process, the LC layer starts with a Grandjean texture, displaying colour, and shearing produces a colour change. This process is reversible as the material will assume its original colour when shearing ceases. GALL and HOLMES (1986), HOLMES and OBARA (1987), and JOHNSON (1988) have used the neat cholesteric LC coatings to indicate shear stress by this *reversible colour play* technique in flight tests. REDA (1991) utilised shear sensitive LC's to study unsteady fluid physics on an oscillating airfoil, reporting a response time of < 30 ms. BONNET et al. (1989) note that the reversible technique gives a qualitative measure of relative shear stress but is not useful for quantitative measurements due to the strong dependence of illumination and viewing angles on the colours seen.

In the second process, that used in the present experiments, the material is applied to the surface and heated in order to drive it into the isotropic phase. The model and LC film are then allowed to cool, the LC adopting the colourless focal conic texture. If this is then sheared, the movement of the film aligns the cholesteric helices and the layer displays the colourful Grandjean texture (see Bonnet et al. (1989)). This texture change from focal conic to Grandjean is irreversible. Such a texture change method, relying on the time to change from a colourless to a colourful texture, is not dependent on viewing angle or illumination and, therefore, may be calibrated to give a quantitative measure of shear stress. In these experiments, the *irreversible texture change* technique has been used for the first time to obtain quantitative measurements of surface shear stress in a transitional boundary layer.

Liquid crystals offer a number of potential advantages over other transition detection techniques. Liquid crystals are simple and inexpensive to use. Unlike Pitot tubes, hot wires, and hot films, they offer full surface mapping of temperature and shear stress. Reversible LC techniques also overcome some of the limitations of sublimating chemicals by providing continuous indications of transition rather than only one transition pattern per flight. Low ambient temperatures confine sublimating chemicals to in-flight tests below 20000 ft., while HOLMES et al. (1986) have used shear LC's up to 50000 ft. Thermo-imaging is relatively expensive and restricted by surface material, surface emissivity and conduction effects due to non-uniform substrates.

Liquid crystals also have a number of limitations. The heating associated with temperature sensitive LC techniques is known to influence the transition location. The steady-state heat transfer technique is unsuited for use on complex geometries, may be time consuming, and has an element of subjectivity, although AKINO et al. (1989) have developed a promising means of alleviating the latter two difficulties by employing band-pass colour filters and a black and white video camera in conjunction with the LC's. Damage to the LC layer due to ultraviolet light and moisture has previously presented an obstacle to flight tests involving temperature sensitive LC's. WALTON (1990), however, has recently reported progress on an ultraviolet blocking agent as well as a waterproof coating for temperature sensitive LC's. As for shear sensitive LC's, the reversible colour play technique offers only a qualitative indication of surface shear stress. While the irreversible texture change technique provides quantitative measures of shear stress, the crystal layer must be prepared anew for each

test condition. Except for the irreversible shear sensitive LC technique, LC's offer little directional flow visualisation.

Chapter 2: *Experimental Techniques*

2.1 *Test Facilities*

2.1.1 *Tunnel*

All experiments were carried out in a low speed wind tunnel (0 to 40 m/s) which drew in air at ambient pressure and temperature (Fig. 2.1). The test section of the tunnel measured 500 mm wide (nominally) by 300 mm in height. For each metre advanced downstream, the test section widened by approximately 20 mm to allow for boundary layer growth along the tunnel walls. One wall of the test section consisted of perspex and was, therefore, particularly suited for viewing liquid crystals. Removable sections in the tunnel roof were also replaced with 12 mm perspex in order to better accommodate viewing and photographing the test surface. Holes were drilled in these replacement panels to facilitate various probes and securing mechanisms for a pressure gradient fairing.

The tunnel was not particularly 'clean'. Smoke and shear-sensitive liquid crystal flow visualisation techniques suggested that some cross-flow was present on a flat plate inserted in the test section. Free-stream turbulence measurements using a constant temperature hot wire indicated that free-stream turbulence intensity was approximately 0.2 to 0.5 %. Electrical interference generated by the tunnel motor precluded more accurate measurements of free-stream turbulence.

2.1.2 *Flat Plate*

A symmetrical flat plate served as the measurement surface. It was machined from 12 mm perspex and measured 0.9 metres in length. The plate was secured to two aluminium channels which were bolted to the tunnel floor. The apparatus was designed to produce symmetrical flow on either side of the plate. Tunnel conditions could be adjusted to allow natural transition to occur over the length of the model. In order to avoid laminar flow separation, a leading edge involute was chosen on the basis of experimental evidence compiled on flat plates under similar flow conditions by MOSS (1991) and DAVIS (1980). The taper from the leading edge expanded to the thickness of the plate at 50 mm downstream. The span of the plate increased slightly in accordance with the downstream expansion of the tunnel width. Machining of the plate's leading edge was performed on an NC milling machine. A seal was formed between the edges of the plate and the tunnel wall using a foam sealing strip. Three such perspex plates were made: the first on which to adhere an aluminium heating strip, a second with pressure tappings of 0.5 mm diameter placed at 150 mm intervals along its centre-line in order to assess pressure gradients along the surface of the perspex plate, and a third in which to mount a carbon-fibre heater. A fourth plate with a slightly different leading edge was used for the shear sensitive LC tests.

2.1.3 *Pressure Fairing*

Favourable pressure gradients were applied to the plate using an adjustable flat fairing above the measurement plate as shown in Figure 2.2. The fairing consisted of two sections (the aft- and fore-fairings) and was designed to produce a uniform pressure gradient on the test surface. Both sections of the fairing assembly were

constructed of 12 mm perspex secured to the tunnel ceiling and hinged at a downstream location corresponding to the leading edge of the measurement surface. Thus, the aft-fairing could be lowered while the fore-fairing remained stationary. The aft-fairing extended downstream slightly past the trailing edge of the measurement surface. The leading edge of the fore-fairing tapered into the tunnel contraction. A pressure tapping in the fore-fairing provided a means of measuring oncoming velocity. Curved sections attached to the upper surface of the aft-fairing protruded through the tunnel roof and were clamped to its exterior, locking the aft fairing in position. Markings on the curved sections facilitated accurate positioning of the fairing. The edges of the fairing were sealed with foam sealing strip.

2.2 *Temperature Sensitive Liquid Crystal Experiments*

In the steady state convective heat transfer experiments, ohmic heating was used to supply a uniform surface heat flux to the flat plate. Liquid crystals on the surface of the plate were then used to measure the surface temperature and, given a knowledge of flow conditions and the power being input to the plate, the coefficient of heat transfer, h, was determined.

Transition start and end were identified by the characteristic rise in mean heat transfer coefficient in the transition region (Fig. 2.3a). As the surface of the plate was heated, the LC would display contours of constant temperature. Qualitatively, transition start was found by the first appearance of liquid crystal (LC) colour (lowest h and highest surface temperature) as shown in Fig. 2.3b. As the current flowing to the heater was increased, the isotherm moved upstream in the laminar region and

downstream in the transitional region. An isotherm also moved upstream through the turbulent region until it eventually merged with the isotherm moving downstream through the transitional region (Fig 2.3c). This merger was taken to indicate the end of the transitional region (highest h and lowest surface temperature).

As noted in Section 1.2.3, this technique does not necessarily give the same transition locations as those determined using boundary layer shape factors or intermittency techniques. However, this method of identifying transition *does* give a consistent set of data on transition with heat transfer and pressure gradient.

For these experiments, two types of heating strip were used. An aluminium heater was employed to validate the measurement technique and establish the data reduction procedures. A carbon heater was then used to simulate that which is to be installed on the NLF nacelle.

2.2.1 *Aluminium Heater*

2.2.1.1 *Experimental Apparatus*

A 127 mm wide heater strip was adhered along the centre-line of the flat plate as shown in Fig. 2.4. The heater strip extended from the downstream end of the plate around the leading edge and back to the rear on the other side of the plate. Electrical connections were made at each end of the strip at the rear of the plate. A current was passed through the strip, which had uniform resistance, to supply a uniform surface heat flux to both sides of the plate.

The heater, of 50 μm overall thickness, consisted of a polymer film metallised with aluminium and was supplied by Goodfellow ltd. of Cambridge, England. Resistance measurements using a four-wire technique showed that the film had a resistance of 0.46 Ω/square at 18.5°C. The film's temperature coefficient of resistance, α, was measured to be 8.4×10^{-4} Ω/°C by placing a sample of the film in a bath of de-ionised water and measuring its resistance over a 40°C temperature range. This α was estimated to lead to maximum variations in surface heat flux of < 0.26% for the transitional boundary layers of the present experiments. OKER and MERTE (1981) have reported that the resistance of thin films as deposited generally changes with age as the strains within the film are relieved. This annealing process is accelerated by heating the thin film. However, no measurable change in resistance was recorded for the aluminium film.

A qualitative measure of the uniformity of the heater's resistance was made by passing a current through the heater under zero flow and checking for uniformity in the colour play of the LC's on the surface of the heater. Such a test indicated that the resistance was quite uniform, provided the section of aluminium was selected with care. Due to the manufacturing process, resistance was found to decrease near one edge of the roll and this section was, therefore, avoided. No quantitative measurement was made of the uniformity of the heater's resistance. BAUGHN et al. (1985) have reported, however, that the non-uniformities in resistance of polyester metallised with vapour-deposited *gold* were found to be less than 5% and introduced errors in measurements of local heat transfer coefficient of 2-4%. Using similar materials, HIPPENSTEELE et al. (1983) have estimated the non-uniformities in resistance to

cause maximum errors in local heat flux of ± 8%, although this estimate could be significantly reduced by 'careful selection' of the heater sheet.

The metallised film was attached, polymer side up, to the plate with impact adhesive. This method proved simple, produced few bubbles between the substrate and the film, and made for an adequate bond while still allowing for re-positioning when necessary. Care was taken to avoid damaging the metal side of the film as any imperfections quickly caused the heater to fail when a current was applied.

Good electrical contact with the heater was found to be imperative as points of high contact resistance quickly burned through the heater. Adequate contact was achieved by using a metal clamp on either side of the plate. A thin strip of rubber was sandwiched between the polymer side of the heater and a stiff metal strip. Similarly, a copper strip was placed between the metal side of the heater and the perspex substrate. Screws then ran through the entire assembly and were threaded into the perspex. By tightening the screws, the aluminium was forced securely against the copper strips. The rubber piece between the aluminium strip and the heater made for a reduced and more uniform contact resistance between the aluminium heater and copper strip. Wire leads soldered onto the copper strips carried electrical current to the assembly. Figure 2.5 illustrates the arrangement of the electrical contacts.

A very thin (125 μm) type T thermocouple, attached to the surface of the heater film near the rear of the plate (see Fig. 2.4), was used to determine the temperature at which the LC changed colour (i.e. to calibrate the crystal). The LC

displays a series of colours corresponding to various temperatures. However, only the yellow isotherm was calibrated as it was most easily identifiable and had the narrowest temperature band. The yellow isotherm was estimated to define a temperature to within 0.2 °C. The upper surface of the heater film was sprayed with a thin coating (approximately 5 μm) of a matt black paint to provide a dark background against which the coloured light reflected by the LC layer was easily viewed. The painted surface was smoothed with 1200 grade emery paper. It was imperative that the painted surface be allowed to dry completely before applying the LC as the trichloroethane solvent contained within the paint is damaging to encapsulated LC.

Thermochromic encapsulated liquid crystals were supplied by B.D.H. ltd. of Poole, England. The LC's are in liquid form and are combined with Mowilith binder in a mixture of 5 parts LC to one part binder. A quantity of demineralised water equal to the quantity of LC and binder was also added to make the mixture thinner and easier to air brush onto the surface in thin, uniform coats. Filtering the LC through a thin mesh screen helped prevent the air gun from developing blockages.

Three types of LC, each with a different colour play temperature range, were pre-mixed and sprayed onto the painted surface in thin layers. This resulted in a maximum of three isotherms being produced for a given heat flux from the heater strip. Individual layers were heated with a hot air gun to evaporate moisture and access the quality of the colour play (colour intensity increasing with thickness up to a limiting value). A protective layer of binder was sprayed over the LC layer. This protective layer may be sanded in order to reduce surface roughness. The LC and

binder layers were approximately 20μm thick. Maximum variations in the surface finish were estimated by WALTON (1990) to be < 6 μm. Calculations based on a review of YOUNG and PATTERSON (1981) suggest that this is well below the height at which a two-dimensional excrescence would disturb the boundary layer. The packaging arrangement of the heater and liquid crystals is shown in Fig. 2.6.

Power was supplied to the heater from a 11 amp, 240 volt A/C variac transformer. The leads to the heater were taken through the roof of the tunnel downstream of the plate. Current was measured with a Salford Selectest model 'Super 50' analog ammeter which was connected in series with the heater and power supply. Current was used to calculate the power being dissipated by the heater. These calculations were confirmed using voltage measurements from a Thurlby model 1503-HA digital multimeter which was connected in parallel with the heater. The electrical configuration is shown schematically in Fig. 2.7. Estimates of the accuracy of all instruments are listed in the uncertainty analysis, Appendix B.

Mean total and static pressures were measured using a Pitot-static tube placed at the centre-line of the tunnel at mid height approximately 10 mm downstream of the plate. The Pitot-static tube was connected to a 13 station manometer bank. When the plate used to measure surface pressure gradient was installed, no electrical connections to the plate were necessary. However, five additional static pressure lines ran from the static ports along the underside of the flat plate. The lines exited through the roof at the rear of the plate and were connected to the manometer bank.

A total temperature probe inserted through the tunnel roof alongside the Pitot-static tube assessed the mean total temperature. It consisted of a type K thermocouple attached to a ceramic rod and housed in an aspirated aluminium tube of 1.5 mm diameter. A 90° elbow held the thermocouple normal to the free stream. Temperature measurements were displayed digitally on a Comark model 6900 digital amplifier/thermometer.

2.2.1.2 *Experimental Program*

2.2.1.2.1 *Flat Plate, Zero Pressure Gradient*

The objectives of the tests using temperature sensitive liquid crystals on a flat plate at zero incidence were three-fold: (1) to ensure that natural transition would occur on the measurement surface, (2) to verify that transition could be detected and analyzed, and develop procedures to do so, and (3) examine the effects of heating on transition location under a zero pressure gradient.

Pressure tappings placed at 150 mm intervals indicated that, due to leakage in the tunnel doors, an adverse pressure gradient existed along the plate in the stream-wise direction. This was corrected by sealing the joints of the tunnel with foam tape and clamping the tunnel at approximately the centre of the test section with a C-clamp. At zero incidence, the test surface then had a zero pressure gradient.

Static pressure measurements on the test surface, when compared with those of the Pitot-static tube, indicated that the free-stream flow speed increased slightly in

the region of the flat plate (see Fig. 2.8). Therefore, measurements of actual free-stream velocities in the region of the plate were obtained by correcting the velocity measurements provided by the Pitot-static tube according to the formula,

$$u = 1.017\,u_i + 0.39 \tag{2.1}$$

where u is the velocity over the test surface and u_i is that indicated by the Pitot-static tube.

An AC current was passed through the heater strip. The width and resistance of the strip being uniform, the current produced a uniform ohmic heat flux along the length of the strip. The system was left to reach a steady state, which was considered to be the point at which surface temperature indications provided by the thermocouple attached to the heater strip stabilised. Stabilisation times were typically between 10 and 15 minutes (this could be longer for large temperature changes and/or low speed flows). Section 3.1.1.1 details a method by which better estimates of stabilisation times were obtained. Heat was transferred from the strip via three mechanisms--conduction into the perspex plate, radiation from the surface to the surroundings and convective heat transfer to the air stream.

The geometry of the plate was such that conduction into the perspex was negligible once steady state was obtained. This was achieved with a flat plate and heater arrangement in which flows on either side of the plate were assumed symmetrical. Transition locations were assumed to be identical on either side of the plate. Transverse conduction into the surrounding perspex at the edges of the heater strip was estimated to be a maximum of 8% (for a fully laminar boundary layer).

However, results were only taken at the centre-line of the strip, where estimates suggested lateral conduction to be negligible. Conservative estimates found conduction in the longitudinal direction to be a maximum of 0.8% of the convective heat transfer for the perspex plate (see Appendix C).

Due to the uncertainty associated with the emissivity of the LC layer no radiation correction has been made. BAUGHN et al. (1985) suggest that emissivity varies considerably with the thickness of the LC layer. Infrared measurements made (under the assumption of a grey body) on a body similar to the perspex model, but with *ink* (rather than matt black paint) lying *over* the crystal layer (rather than under it), gave an emissivity of 0.96. This agrees roughly with typical emissivities given by BAUGHN et al. Estimates based on these emissivities indicate that radiation could amount to a maximum of 7% of the convective heat transfer.

Only the upper surface of the plate was sprayed with black paint, while the aluminium was left exposed on the lower surface. Therefore, owing to the relatively lower radiation on the lower surface, a small temperature gradient will develop between the upper and lower surfaces. However, estimates suggest that the additional heat flux into the upper surface is less than 0.5%.

Markings were placed alongside the heater in 10 mm increments from the leading edge. The locations of liquid crystal isotherms and gas temperature were noted and a local heat transfer coefficient, h, was calculated from

$$h = \frac{\frac{i^2\theta}{w^2} - \sigma e (T_c^4 - T_g^4)}{T_c - T_g} \quad , \tag{2.2}$$

where i, is the current, w is the width of the heater, T_C is the calibrated temperature of the liquid crystal, T_g is the gas temperature, σ is the Stefan-Boltzman constant, ε is the emissivity (which was set to zero for the present tests) and Θ is the resistance per square of the heater. Local Θ was corrected for temperature variations in resistance using,

$$\theta = \theta_{ref} [1 + \alpha (T_c - T_{ref})] \quad , \tag{2.3}$$

where α is temperature coefficient of resistivity and the subscript *ref* indicates values at a reference condition. This was repeated for a number of current settings. Isotherms appeared in different locations for each power setting, thereby allowing h to be determined at a number of locations along the length of the plate. Transition start and end were identified as described in Section 2.2.

2.2.1.2.2 *Flat Plate, Constant Pressure Gradient*

In many practical applications in which the steady-state heat transfer technique employing temperature sensitive LC's may be used to detect transition location or map Stanton number contours, there exists a *non*-zero pressure gradient. The NLF project is particularly relevant. The geometry of the NLF nacelle is such that a favourable pressure gradient exists over a large portion of the heater. Therefore, temperature sensitive liquid crystal experiments were performed under a favourable pressure gradient with the aims of (1) simulating the NLF environment, (2) determining

whether present experimental techniques are suitable for detecting transition location in a favourable pressure gradient, (3) investigating the influence of surface heating on boundary layer transition in favourable pressure gradients and (4) determining whether a Stanton number could be used to correlate the movements of transition with variations in heating in a manner similar to that used when no pressure gradient was present.

Favourable pressure gradients were applied to the plate using an adjustable flat fairing as described in Section 2.1.3. This produced an approximately uniform pressure gradient on the test surface. An approximately zero pressure gradient was achieved with the fairing in the most upright position. Details of the pressure gradient are given in Section 3.1.1.2.

The perspex plate and aluminium heater used for the favourable pressure gradient tests were the same as those used for the zero pressure gradient tests. However, the means of gathering data was slightly different. Previously, the input current was varied arbitrarily in order to produce a series of constant temperature contours (refer to Section 2.2.1.2.1). In the pressure gradient tests, however, the current was increased until the LC just began to show colour (indicating the transition start location). The current was then incrementally reduced as the plate stabilised such that, when the plate had reached the fully stabilised condition, the surface was being heated just enough to provide an indication of transition start. Similarly, the transition end location and its associated heating rate were established by varying the current such that, when the plate was stabilised, the contours of constant temperature moving

downstream and those moving upstream just touched. The process was repeated for each of the three LC's at each fairing setting. This method gave three transition start and end locations and the heating rate associated with each for a range of pressure gradients. Previously, these data had to be interpolated from plots of h versus x such as shown in Fig. 2.3a. and were, therefore, less accurate.

Since the plate with the aluminium heating element did not contain pressure tappings, it was not possible to directly evaluate the local pressure gradient and flow speed when the aluminium heater was in the tunnel. Therefore, the plate with static pressure tappings was used to directly measure the pressure gradients and flow speeds. These results were noted and related to the heated plate through the oncoming flow speed and pressure fairing setting as described in the next paragraph.

With the pressure plate in the tunnel, the pressure fairing was run through a series of settings labelled settings 0-10. Setting zero corresponded to the fairing being drawn fully up (zero pressure gradient). At each successive setting, the downstream support was lowered 5 mm. The upstream support was adjusted so as to make the pressure gradient as uniform as possible. The position of each support, the oncoming speed, total pressure and local static pressures were then recorded. This procedure was repeated for each tunnel speed setting of interest. The positions of the supports which provided the most uniform pressure gradient for a given fairing setting were found to be independent of tunnel speed setting. At each fairing setting, local velocities on the surface of the plate were related to oncoming speed by fitting a first order least-squares curve fit to a plot of distance along the plate, x, versus the ratio

of local to oncoming velocities. Hence, when the heated plate was installed in the tunnel, the oncoming speed was measured directly and local speed was found from

$$u_l = u\,(A + Bx) \quad , \tag{2.4}$$

where u_l is the local velocity, u is the velocity at the leading edge of the plate (oncoming velocity corrected according to Eqn 2.1), and A and B are constants. Values of A and B for all conditions of interest to these tests, as well as the corresponding positions of both supports, are provided in Table 2.1.

Table 2.1 Pressure Fairing Schedule

Fairing Setting	Support 1 (mm)	Support 2 (mm)	Oncoming Speed (m/s)	A	B
0	0	0	20.8	1.00	0.00
1	2	4	20.7	1.00	0.02
2	4	9	20.5	0.99	0.04
0	0	0	26.4	1.00	0.00
1	2	4	26.3	1.00	0.01
2	4	9	26.1	0.99	0.03
3	5	14	25.8	0.98	0.06
0	0	0	32.4	1.00	0.01
1	2	4	34.2	0.94	0.02
2	4	9	31.9	0.99	0.04
3	5	14	31.6	0.98	0.06
4	9	19	31.2	0.98	0.09

Note that the oncoming speed tended to decrease as the pressure fairing was lowered, contracting the test section and thereby increasing the drag on the motor (which was held at a constant power setting). The constants A and B are dependent on fairing setting, but show little dependence on oncoming flow speed. Nevertheless, *A* and *B* were only employed when the oncoming flow over the heated plate was within 2 m/s of that for which the constants were determined. This led to estimated errors in local velocity of < 1%.

2.2.2 *Carbon Heater*

2.2.2.1 *Experimental Apparatus*

Oxford University is to perform in-flight heat transfer experiments on the surface of an NLF nacelle. Experimental heat transfer distributions will be used to determine the location of transition from laminar to turbulent flow for a range of test conditions. A heater is to be incorporated into the skin of the nacelle and isolated from the surrounding carbon structure. The heater will consist of a strip of unidirectional carbon fibres with uniform resistance along its length. A uniform surface heat flux will be created by passing a current through the fibres. The present experiments are, to the author's knowledge, the first to attempt to locate transition and make quantitative heat transfer measurements employing part of the aircraft structure (the carbon fibre) as a heating element.

A flat model of the carbon heater which is to be incorporated into the NLF nacelle was manufactured to the specifications of Oxford University by Hurel-Dubois

(UK) ltd., of Burnley, England. Incompressible steady state convective heat transfer tests similar to those performed on the aluminium foil were carried out on the carbon sample. These experiments were intended to test the thermal and mechanical properties of the carbon sample, and to ensure that the methods of detecting transition which were developed on the aluminium plate remained valid for the carbon sample.

The upper surface of the carbon structure is shown mounted in the perspex plate in Figure 2.9. The carbon model measured 0.203 m x 0.518 m, with a 0.100 m x 0.565 m heating element centred in the model. The model was mounted in a perspex plate identical to the one described in Section 2.1.2 with the heating element down the centre-line of the plate. After smoothing with plastic padding, the step from the perspex to the carbon plate was < 50 μm at a position 65 mm downstream of the leading edge. The unheated starting length was 115 mm. There was no detectable step from the heater to the surrounding carbon-fibre structure.

The heating element consisted of a single layer of high tensile strength (HTS) unidirectional PAN fibres with a nominal thickness of 0.125 mm. The unidirectional fibres were insulated on the underside by two layers of 0.3 mm woven glass cloth (weave style 7781) with a thermal conductivity, k, of 0.03 W/(m·K) (refer to TOULOUKIAN et al. (1970)). Both the heater and glass cloth were set into a woven carbon cloth. The entire assembly was impregnated with epoxy resin which is also an insulator, $k \approx 0.23$. The nominal thickness of the composite was ~ 3 mm, and the fibre volume fraction was 57 % (reference CLAYTON (1991)).

The unidirectional carbon fibres which composed the heating strip had a uniform resistance in the longitudinal direction of 0.22 Ω/square. A qualitative measure of the uniformity of the heater's resistance was made by passing a current through the heater under zero flow conditions and checking for uniformity in the colour play of the LC's on its surface. Resistance was found to be extremely uniform. The carbon heater's temperature coefficient of resistance, α, was measured to be ~ 0.0 by placing a sample of the carbon fibre in a bath of de-ionised water and measuring its resistance over a temperature range of 22-70°C.

Three temperature sensitive liquid crystals were applied to the surface of the carbon structure in the manner which was detailed in Section 2.2.1.1. Figure 2.10 shows the complete packaging arrangement of the heater and LC's. As the surface of the carbon composite is already black, painting was unnecessary. A type K thermocouple of 125 μm thickness was mounted on the surface of the heater for use in calibrating the LC's.

RHODES and MOSES (1991) have noted that, due to its anisotropic nature, both thermal and electrical resistance in unidirectional carbon fibres are higher in the transverse direction than in the longitudinal direction by a factor of approximately 10. Therefore, poor electrical contact was found to produce non-uniform heating on the test surface, in addition to contact heating. In order to allow for electrical contact without disturbing the finish on the upper surface, the unidirectional fibres were fed through a slit in the insulating glass cloth and in the woven carbon cloth and extended out the bottom of the structure. Fig. 2.11 shows the underside of the carbon

composite mounted in the perspex plate. The best electrical connection was made after removing the resin from the ends of the fibres. These were then clamped onto a metal frame which was glued to the underside of the carbon-fibre structure. The free carbon fibres were clamped with a strip of rubber which deformed, allowing all fibres to come into contact with the metal base. Fig. 2.12 shows a cross-section of the electrical contact. A photo of the contact is provided in Figure 2.13a.

It is desirable to minimise the length of fibre which extends from the heater to the electrical contact. Upon leaving the connection, the fibres are generating heat. This could lead to overheating in the nacelle if the heat is not dissipated. Therefore, the amount of heat generated along the length of the carbon fibre leads was reduced by soaking the fibres in electrically conducting paint, see Figure 2.13b. This effectively increased the length of the contacts down to the point where the fibres remain coated with epoxy.

A silver loaded conducting paint based on acetone and xylene was chosen to reduce the resistance of the free fibres. The paint was supplied by RS Components of London, England. The fibres were soaked in the conducting paint which was diluted with acetone in order to allow the paint to better penetrate between the fibres. The acetone then evaporated, leaving the conducting paint.

The effective reduction in overall heater length was apparent from the reduction in the carbon heater's total resistance. The silver loaded paint was applied to ~ 45 mm of the fibre leads and reduced the heater's total resistance by 0.10 Ω.

Thus, given a heater resistance of 0.22 Ω/square, the heater's length was effectively reduced by the length of the carbon that was treated with the conducting paint.

2.2.2.2 *Experimental Program*

Current was passed through the heating strip, creating a uniform surface heat flux. As with the perspex plate, heat was transferred from the heated surface via radiation from the surface to the surroundings, conduction to the surrounding carbon structure and convection to the air stream. Radiation was ignored due to the uncertain emissivity of the LC layer (refer to Section 2.2.1.2.1).

An effort was made to minimise the thermal conductivity of the carbon structure through careful selection of the carbon fibres from which it was constructed. Nevertheless, thermal conduction was found to be much more significant in the carbon model than in the perspex model.

A number of studies have investigated the thermal conductivity of unidirectional carbon fibres in both the longitudinal and transverse directions. The thermal conductivity of some woven fabrics, such as Kevlar, has also been studied (TOULOUKIAN et al. (1970)). However, to the author's knowledge there are no studies addressing the conductivity of woven carbon fabrics. Therefore, a model was constructed which assumed that conduction in the woven carbon fibres occurred solely in the longitudinal direction of the fibres. As the fibres in the woven cloth run at 45 degree angles to the heater's unidirectional fibres, this effectively reduced the longitudinal thermal conductivity, k, by $1/\sqrt{2}$ in the direction perpendicular to the

heater.* The longitudinal thermal conductivity of the fibres was estimated to be 9.5 W/(m·K) at 300°K based upon the estimates of CLAYTON (1990) as well as the work of AGARWAL and BROUTMAN (1980) and RHODES and MOSES (1991).

Lateral thermal conduction from the heater to the surrounding carbon structure was found to be significant in relation to convective heat transfer. However, measurements were taken only on the centre-line of the heater, where errors due to conductive losses were estimated to be 2-8% of the convective heat transfer rate. This estimate assumed a linear temperature gradient from the centre-line to the edges of the heater. In reality, the temperature gradient is nearly zero at the centre-line of the heater. Hence, lateral conductive losses will be much less near the centre-line. Conductive losses will be further reduced on the NLF nacelle where the thermal conductivity of the carbon structure will be reduced by ~ 20% due to the reduced thermal conductivity of unidirectional fibres at lower temperatures. Fig. 2.14 shows the variation of thermal conductivity with temperature for unidirectional fibres. This plot was constructed from the results of RHODES AND MOSES (1991).

The underside of the carbon plate was insulated with 25 mm of styrofoam. Conduction to the underside of the plate was, therefore, considered negligible. It was

* Note that longitudinal thermal conductivity of the carbon plate is largest for the case in which the fibres within the layered cloth run at 45° angles to the unidirectional fibres. As the carbon cloth is rotated in relation to the unidirectional fibres, the effective k of the cloth is continuously reduced. When the cloth has been rotated a full 90°, so as to place successive layers of the woven carbon fibre parallel and perpendicular to the unidirectional fibres, the k of the carbon structure in the longitudinal direction has been effectively reduced to 1/2 the value of the longitudinal thermal conductivity of the carbon fibres.

also found to be important to insulate the contacts and the area surrounding them. If left uninsulated, heat was rapidly convected away from this area, particularly as the free-stream air flowed through the exposed carbon fibre leads. This resulted in conduction from other sections of the plate, producing spurious heat transfer results.

A worst case analysis of *longitudinal* conduction is presented in Appendix C. The regions where errors due to conduction are expected to be the greatest are those in which d^2T_f/dx^2 is at a maximum or minimum. These regions correspond roughly to the start and end of transition. Results indicate that the calculated values for Stanton number at the start of transition may be as much as 13% high. Again, this may be reduced to ~ 11% for the NLF nacelle due to the drop in the thermal conductivity of the carbon fibre with decreasing temperature (refer to Fig. 2.14). Conversely, at transition end, calculated values of Stanton number may be as much as 13% percent *too low* on the carbon model. There will be little error in areas where the temperature gradient is small (such as in the turbulent region). Conduction does not affect the location of transition as indicated by the LC's. However, as noted in Appendix C, the calculated location of adiabatic Reynolds number may be slightly affected.

Current was supplied to the heater and the carbon model was allowed to reach thermal stability (typically taking on the order of 4 minutes). The distribution of heat transfer coefficients along the length of the plate was found using the method described in Section 2.2.1.2.1.

2.3 *Shear Sensitive Liquid Crystal Experiments*

Experiments to measure surface shear stress were performed using a shear sensitive, temperature insensitive, unencapsulated cholesteric liquid crystal. Previous uses of shear sensitive crystals for aerodynamic studies (e.g. HOLMES et al. (1986) and REDA (1991)) have employed the *reversible colour play* technique discussed in Section 1.3. This study represents the first experimental study implementing the *irreversible texture change* method, first introduced by BONNETT (1989), to measurements in transitional boundary layers. Using this technique, the LC is applied to the test surface and is driven into the colourless focal-conic texture. If this is then sheared, the movement of the film aligns the cholesteric helices and the layer displays the colourful Grandjean texture (see BONNETT et al. (1989)). This process of changing texture is irreversible unless the LC is heated to drive it back into the focal conic texture. However, unlike the conventional reversible technique, there is no dependence on illumination or viewing angle. Therefore, the LC may be calibrated to give a *quantitative* measure of shear stress.

2.3.1 *Experimental Apparatus*

A flat plate, similar to that used for heat transfer measurements, was utilised for the shear stress measurements. The back surface of the plate was sprayed with a matt black paint to clarify the colour change of the LC layer. The neat cholesteric liquid crystal, designated TI511, was supplied by BDH Ltd. of Poole, England.

The cholesterics can be deposited on the surface by spraying, silk-screening or painting. Using the latter technique it was difficult to obtain a film of uniform

thickness. In order to spray the coating onto the surface the liquid crystal is first dissolved in a suitable solvent, typically trichloroethane. After spraying, the solvent evaporates leaving a thin film of cholesteric LC on the surface. This technique of application has been used successfully by REDA (1991) and HOLMES et al. (1986) in aerodynamic flight tests in which a thin coating (~ 10μm) of LC was desirable, such that the film changed colour but did not run under aerodynamic loading. The texture change technique, however, requires that the LC layer be thick enough to allow the crystal layer to flow. This thickness was difficult to achieve when spraying. Furthermore, when sprayed on, each coating could be used only once and it was difficult to ensure that all of the solvent had evaporated.

Silk-screening was found to be the best technique for the present experiments. This produced a film of uniform thickness which could be re-used by re-screening the same mixture after it had flowed during an experiment. The results presented in Section 3.2 were obtained with a silk-screened layer approximately 40 μm thick.

It was found to be important to avoid dust contamination of the surface. Dust particles on the LC film sometimes moved under the action of aerodynamic drag resulting in the formation of streaks of Grandjean texture in the film. Any imperfections or bubbles in the LC film were manually removed, and the LC was re-screened.

The cholesteric LC was deposited along a strip 60 mm wide and 700 mm long down the centre of the plate. The film started 60 mm from the leading edge of the plate. This was done to prevent the LC layer from disturbing the boundary layer at

the front of the plate where the boundary layer was thin and thereby inducing early transition. Calculations based on the review of YOUNG and PATTERSON (1981) indicate that a two dimensional excrescence of height less than 70 μm at 60 mm from the leading edge will not disturb the boundary layer for any of the conditions of the present tests.

2.3.2 *Experimental Program*

After silk screening, most of the LC layer was in the Grandjean texture and the layer was a dull red colour. The film was driven back to the colourless focal conic state by heating it into the isotropic phase (approximately 50°C for the TI511 mixture used) with a hot air gun and allowing it to cool back to the cholesteric phase.

The tunnel was started when the plate had returned to ambient temperature, applying steady shear stress to the measurement surface. After the shear has been applied, it takes some time for the film to show a dull red colour. As the cholesteric helices align with increased displacement of the film surface (i.e. as the mesophase progresses from the focal-conic to the Grandjean texture) the viscosity of the layer rapidly decreases. Eventually the liquid crystal film flows and displays a deep red colour.

Markings were placed alongside the LC film at 10 mm increments from the leading edge. The location at which the LC began to flow and the length of time for which the shear stress had been applied were noted. The location at which the LC film first begins to show colour (region of highest shear stress) provides a *qualitative*

indication of transition end. With time, the location at which the crystal begins to flow moves forward through the transitional region, and downstream through the turbulent region. The time that is required to induce flowing in the LC film is used to *quantify* the surface shear stress as discussed in Section 3.2.

Chapter 3: *Results and Discussion*

3.1 *Temperature Sensitive Liquid Crystals*

3.1.1 *Aluminium Heater*

3.1.1.1 *Flat Plate, Zero Pressure Gradient*

Basic results from the heat transfer experiments are presented for a range of flow speeds in Fig 3.1. Results are shown for all three liquid crystals at each condition and, for comparison, laminar and turbulent predictions from the well established boundary layer code STAN5 (CRAWFORD and KAYS (1976)). In the regions of fully laminar and fully turbulent flow, the levels of Stanton number indicated by each of the crystals are in good agreement. In general, the levels of heat transfer are lower than would be expected from standard correlations and predictions of STAN5, particularly in the region of fully turbulent flow. This is also apparent in the results of KIM et al. (1989) in fully turbulent regions.

Experimental uncertainty alone does not account for the low levels of heat transfer in the turbulent region. Uncertainties in measured values of heat transfer coefficient are estimated to be maximum of ± 8.7% in the turbulent region for these experiments. There are at least two other possible explanations for unexpectedly low measurements of the coefficient of heat transfer. First, as mentioned in Section 2.1.1,

flow visualisation indicated that there may be some secondary flows generated at the tunnel contraction resulting in a non-two-dimensional boundary layer on the plate. Therefore, a section of the heater may have experienced a relatively low mass flow rate over its surface. The second possibility is that an area of relatively high resistance existed within the heater. Either possibility would cause a local 'hot spot' to develop. As a result, the local coefficient of heat transfer would be unexpectedly low. Such a 'hot spot' *was* apparent on the heating strip at ~ 350-550 mm from the leading edge. Nevertheless, the results suggest that the arrangement was suitable for the present purposes.

The results clearly show the influence of heating on transition location. The lowest temperature LC consistently shows a later start and end of transition. This is because the lower temperature LC displays colour at a lower heating rate than the higher temperature LC's. As the heating rate is increased, both start and end of transition are moved forward.

The shape of the heat transfer rise through the transitional region and the length of transition are distorted when presented as in Fig. 3.1. For a given LC, the heating required to produce colour change at the start of transition is less than that required to produce change at the end of transition. Thus, when the Stanton number is being measured at the end of transition, the transition start location will have moved further upstream because of the forward movement of transition with increased heating. It is possible, therefore, to see a maximum Stanton number upstream of the minimum in these plots.

The apparent length of transition can also appear distorted. For example, when coefficient of heat transfer is plotted so as to indicate the heat transfer distribution along the plate as in Fig. 3.2, the length of transition appears misleadingly short. At any given heating rate, the start and end of transition would be further apart and the rise through transition more gradual than is indicated in these figures.

As previously mentioned (Section 1.2.2.4), it is well established that a surface heat flux destabilises a laminar boundary layer leading to early transition. The magnitude of this effect for a given flow and heat flux is of importance if the technique is to be used in an attempt to determine where transition would occur on an unheated surface (as is its intended use for the NLF program). By using three liquid crystals on the heater simultaneously, this effect was examined by observing the change in transition location with different surface heat fluxes.

Dimensional analysis (see Appendix A) for this incompressible flow indicates that the Reynolds numbers at start and end of transition should be a function of Stanton number in the form

$$\frac{\dot{q}}{\rho u C_p T_g} \quad , \tag{3.1}$$

where $\dot{q}$ is the convective heat transfer rate, ρ, u and T_g are the density, speed and temperature of the free-stream fluid, respectively, and C_p is the specific heat of the fluid. From the experimental results, the Reynolds numbers at the start and end of transition for each LC at each flow speed were determined. This gave transition Reynolds numbers at three heating rates at each speed. An equation for critical

Reynolds number, Re_{crit}, as a function of the heating parameter of the form

$$Re_{crit} = A\, e^{-B \frac{\dot{q}}{\rho u C_p T_s}} \quad , \tag{3.2}$$

was least-squares fitted to each set of three points, and an extrapolation to zero heat transfer rate was used to determine an adiabatic transition Reynolds number, $Re_{crit,ad}$, for each speed. The results for both start and end of transition at all speeds are plotted in Fig. 3.3. These suggest that the Stanton number parameter used correlates the data quite well. The reduction in transition Reynolds number is shown to be an exponential function of Stanton number. The maximum heating effect is roughly a halving of the adiabatic critical Reynolds number at Stanton numbers greater than ~ 0.3×10^3. At a given speed, transition end appears to be less effected by the heating than is transition start. However, the difference is slight and the effect on both transition end and start may reasonably be related by a single curve. A least-squares curve fit to the data has the form

$$\frac{Re_{crit}}{Re_{crit,ad}} = 1 - 0.50\,(1 - e^{-10.4 \times 10^3 \frac{\dot{q}}{\rho u C_p T_s}}) \quad . \tag{3.3}$$

The results shown in Fig. 3.3 agree qualitatively with the experimental results of LAUCHLE and GURNEY (1984). Their plot of transition Reynolds number versus heating (Fig. 1.16) is, qualitatively, a mirror image of the results obtained in this experiment. This is to be expected since their experiments were carried out in water (refer to Section 1.2.2).

The time required for the perspex plate to reach thermal stability was estimated

by setting the power which was being input to the heater and observing how the temperature on the surface of the plate varied with time. The locations of LC contours were noted every 60 seconds. For the first power setting, the plate was heated from a cooled condition. Subsequent readings were taken by changing the power setting on the already heated plate. Calculated heat transfer distributions for a transitional boundary layer at times ranging from 3-20 minutes are shown in Fig. 3.4. The results suggest that ~ 15 minutes are required for the perspex plate to reach full thermal equilibrium. Five minutes are adequate for obtaining both qualitative and quantitative results (to within ~ 2%) in regions of high temperature gradients, where a relatively large change in the plate's surface temperature results in small changes to the stream-wise location of the LC contour.

In the turbulent boundary layer, where dT/dx is modest, a relatively small change in surface temperature moves the LC contours a significant distance. However, dh/dx is also small in the turbulent regions, such that the resulting errors in the calculated level of heat transfer are small (within ~ 8%) after 10 minutes.

3.1.1.2 *Flat Plate, Constant Pressure Gradient*

Favourable pressure gradients were applied to the plate using the adjustable fairing described in Section 2.1.3. This produced an approximately uniform pressure gradient on the test surface. An approximately zero pressure gradient was obtained with the fairing in its most upright position. A typical series of pressure distributions measured on the surface for various fairing settings is presented in Fig. 3.5. where

$$C_p = 1 - \frac{P_0 - P_s}{P_0 - P_{s_{ref}}} \quad . \tag{3.4}$$

Here, P_0 is the total pressure, P_s is the static pressure at a given distance along the plate and P_{sref} is a reference static pressure. The static pressure at the first tapping was used for P_{sref} for these tests.

The results of tests intended to assess the repeatability of the pressure gradients are shown in Figs. 3.6 and 3.7 for (nominal) flow speeds of 35.0 and 28.7 m/s respectively. Each figure shows a comparison of two tests performed on different days, but at the same nominal speed. The results show excellent repeatability.

Dimensional analysis (Appendix A) suggests that the appropriate pressure gradient parameter for the present experiments is the *acceleration parameter*, K, where

$$K = \left(\frac{\nu}{u_l^2}\right)\frac{du_l}{dx}. \tag{3.5}$$

Here, ν is the kinematic viscosity and u_l is the local velocity. This acceleration parameter has been used previously by a number of researchers including BLAIR (1982), JONES and LAUNDER (1972), and GAUGLER (1984).

The conditions for the experiments are summarised in Table 3.1. The oncoming speed is the flow speed at the start of the test plate. At higher values of K and at lower flow speeds transition measurements could not be made on the test surface. While these acceleration parameters are small, they are of the same order as

Table 3.1 Favourable pressure gradient test conditions.

Flow Condition	Oncoming Speed (m/s)	$K \times 10^8$	Air Temperature, T_g (°C)
1a	22.3	0.2	17
1b	22.3	1.1	17
1c	21.9	2.6	17
2a	28.7	0.0	13
2b	28.4	0.6	13
2c	27.8	1.9	13
2d	27.3	3.5	13
3a	35.0	0.2	16
3b	35.0	0.8	16
3c	34.1	2.7	14
3d	33.3	4.1	11

those expected on the NLF nacelle.

At a given condition, there was a variation in K along the length of the plate due to U_l increasing with distance from the leading edge. However, the variation was small (a maximum of 3.7% at condition 3d), and assuming K to be constant at each condition provided a consistent set of results. The pressure fairing could have been designed to create a constant K rather than a constant dP/dx, but this would have increased the complexity of the testing.

At each test condition, the Reynolds numbers at the start and end of transition (based on the local flow speed) were determined for three different heating rates.

These were used to extrapolate to zero heat flux in order to obtain the adiabatic transition Reynolds numbers, $Re_{crit,ad}$. The method is described in Section 3.1.1.1.

Fig. 3.8 shows values of $Re_{crit,ad}$ normalised with the value of $Re_{crit,ad}$ at zero pressure gradient ($K = 0$) and plotted as a function of K. The results for both start and end of transition fall on a single curve and show a strong dependence of transition location on pressure gradient in the present arrangement. An exponential curve of the form,

$$\frac{Re_{crit,ad}}{Re_{crit,ad}(K=0)} = 1 + 1.07\,(e^{0.33\times10^{-8}K} - 1) \quad , \qquad (3.6)$$

fits the data well. The fact that the data fall neatly onto a single curve provides confidence in the method of obtaining adiabatic transition locations.

Figs. 3.9-3.13 show Re_{crit} normalised with $Re_{crit,ad}$ and plotted as a function of Stanton number for each flow condition. Plots are provided for both transition start and transition end at each condition (except condition 3, where transition end did not occur on the measurement surface). Surface heating is shown to have a relatively greater destabilising influence upon the normalised transition Reynolds number as the pressure gradient becomes increasingly favourable.

In Section 3.1.1.1, it was shown that $Re_{crit}/Re_{crit,ad}$ could be correlated with a Stanton number. Experiments performed with the pressure fairing in place produce results which agreed with the previous correlation at zero pressure gradient but deviate from it for the $K > 0$ cases. Fig. 3.14 shows a comparison of results taken at $K = 0$,

with and without the pressure fairing in place. A curve fit to *all* of the data at K = 0 had the form

$$\frac{Re_{crit}}{Re_{crit,ad}} = 1 - 0.50\left(1 - e^{-9.3\times10^{3}\frac{q}{\rho u C_p T_e}}\right) \tag{3.7}$$

This is very similar to the curve which was fitted to results with the pressure fairing absent (Equation 3.3). Uncertainty analysis suggested that the accuracy to which Stanton number and $Re_{crit}/Re_{crit,ad}$ could be measured was dependent on the flow speed and the power required for a given crystal to show colour. The error bars shown in Fig. 3.14 are for measurements of transition end for each LC at a flow speed of 24.2 m/s. They are characteristic of typical uncertainties. Also shown is a 95% confidence interval for the correlation (Eqn. 3.7). Details of the uncertainty analysis are given in Appendix B.

In Figure 3.15, all results taken with the pressure fairing in place ($K \geq 0$) are superimposed on the results taken with the fairing absent. Note that *all* zero pressure gradient results, whether taken with the fairing in place or not, are given the symbol '+' in this figure. Under a favourable pressure gradient, heating moves transition forward a proportionally greater distance than an equivalent heating with zero pressure gradient. As K is increased the influence is larger.

Figure 3.15 suggests, however, that the destabilising influence of heating upon the boundary layer is not strictly a function of K, but also varies with oncoming speed (lower oncoming speeds showing a greater influence due to heating). Hence, heating

is shown to have the greatest effect on the normalised transition location at condition 1c (the lowest speed), although K was greater for conditions 2d, 3c and 3d.

For $K = 0$, normalised Reynolds numbers at transition start and end effectively collapsed onto a single curve plotting against Stanton number. However, the results do show a trend towards a smaller proportional change in $Re_{crit}/Re_{crit,ad}$ for a given Stanton number at transition end than at transition start. This trend is accentuated for $K > 0$.

The length of transition, η could not be measured directly using this heat transfer technique. As discussed in Section 3.1.1.1, the amount of heat required to identify transition end is greater than that required to identify transition start. Therefore, the transition start location and associated heating rate for each of the LC's was recorded. Then for each LC, the Reynolds number at transition end was determined for the same heating rate as that used to determine the location of transition start by interpolation from plots of transition end Reynolds number versus Stanton number, such as those in Figures 3.9-3.13. The transition length at the designated heating rate was then determined.

Transition length was found to increase with increasing K as shown in Fig 3.16. This is consistent with the findings of others, such as GAUGLER (1984). Heating had no discernible effect upon η in these experiments.

Transition lengths, normalised with the distance to the start of transition, are plotted as a function of the heating rate in Fig. 3.17. Because of the technique used to find transition length, the uncertainty in η/X_t was found to be quite large (a maximum of ± 24.0%). Appendix B describes the uncertainty analysis.

These results indicate that there is little variation in the normalised transition length with either heating rate or pressure gradient. However, the results are for quite small values of K (maximum 2.7×10^{-8}). Influences may be larger at higher pressure gradients.

3.1.2 *Carbon-Fibre Heater*

Figures 3.18 and 3.19 show heat transfer results from the carbon plate at flow speeds of 34.3 and 7.9 m/s respectively. The lines on these plots represent the following boundary layer heat transfer correlations, corrected for unheated starting length, from KAYS and CRAWFORD (1980) for flow over a flat plate with a constant heat flux and zero pressure gradient:

$$St = \frac{0.453\, Pr^{-2/3}\, Re^{-1/2}}{[1-(\xi/x)^{3/4}]^{1/3}} \qquad (\textit{laminar}) \quad , \tag{3.8}$$

$$St = \frac{0.030\, Re^{-0.2}\, Pr^{-0.4}}{[1-(\xi/x)^{9/10}]^{1/9}} \qquad (\textit{turbulent}) \quad . \tag{3.9}$$

The unheated starting length, ξ, was measured as 0.115 m. Although INCROPERA and DeWITT (1985) note that these expressions may be in error by as much as 25% due to variations in surface roughness and free-stream turbulence, in tests similar to

these SOHN et al. (1989) and KIM et al. (1989) have had results which agree with these correlations quite well. The corrections for unheated starting length may be expected to break down near the origin of the thermal boundary layer (see KAYS and CRAWFORD, and TAYLOR et al. (1990)).

The level of Stanton numbers and their distributions suggest that the boundary layer flow over the heated section of the plate was fully turbulent for the tests presented in Figs. 3.18 and 3.19. Tests using the aluminium heater, however, showed the boundary layer to be transitional and fully laminar at free-stream speeds of 34.3 and 7.9 m/s respectively. Experiments using shear sensitive liquid crystal were used to investigate the state of the boundary layer. The strip of shear sensitive liquid crystal was 60 mm wide and began 45 mm downstream of the leading edge. It was applied down the centre-line of the carbon heater using the technique discussed in Section 2.3.1. The tests indicated that the boundary layer may have been disturbed by the 50 μm step where the perspex plate joined the carbon sample. The sequence of photographs presented in Fig. 3.20 shows the shear sensitive LC flowing first at the juncture between the carbon and perspex plates. However, the results also show the shear sensitive LC flowing ahead of the junction shortly afterward. If the boundary layer had been laminar ahead of the junction, the shear stress should not have been high enough to cause the LC to flow.

Tests were also performed with a roughness trip near the leading edge in order to ensure that the boundary layer *was* fully turbulent. The trip consisted of a 10 mm by 240 mm strip of P40 emery cloth which was secured 4 mm downstream of the

leading edge using double-sided tape. Figures 3.21 and 3.22 show heat transfer results at flow speeds of 28.9 and 7.9 m/s respectively. Measurements of the coefficient of heat transfer were generally insensitive to the presence of the boundary layer trip. This indicates that the untripped boundary layer was also turbulent on the measurement surface.

This turbulent boundary layer was attributed to blockage on the underside of the carbon plate. At a distance 90 mm downstream of the leading edge, the electrical contacts protruded 28 mm into the free-stream. As a result of this obstruction, the plate was effectively placed at incidence to the free-stream. Thus, the boundary layer separated at the leading edge, reattaching as a turbulent boundary layer.

Although the boundary layer was not transitional for these tests, the results suggest that the carbon heater may provide a suitable means of obtaining transition locations and heat transfer measurements. The carbon heater was clearly capable of sustaining temperature gradients in the longitudinal direction, as shown by the contours of constant temperature which were present during tests taken on the fully turbulent boundary layer (see Fig. 3.23). Furthermore, the levels of Stanton numbers indicated by each of the three liquid crystals are in good accord and show acceptable agreement with standard correlations for fully turbulent flows.

In order to obtain transition on the carbon heater, the disruption to the flow on the underside of the plate was minimised by placing a streamlined jacket over the electrical contacts. The plate was also elevated 45 mm at the leading edge and 57 mm

at the trailing edge, effectively creating an angle of attack of -1°. As a result, transition was achieved on the heating element (see Figure 3.24). The acceleration parameter, K, was estimated to be 2.9×10^{-6} based on measurements from three static pressure ports which were in the perspex plate downstream of the carbon insert.

Results obtained using this configuration are shown in Fig. 3.25 for an oncoming flow speed of 28.3 m/s. Also presented is a STAN5 prediction with transition start set upstream of the heated section. The levels of Stanton number indicated by each of the three crystals are in good agreement. Calculated Stanton numbers at transition end are ~ 15% high in comparison to the prediction but approach the prediction in the turbulent region. Results from a number of other studies (e.g. BLAIR and WERLE (1981), BLAIR (1982), SOHN et al. (1989) and TAYLOR et al. (1989)) show a similar discrepancy between predicted and experimental Stanton numbers at transition end. However, experiments on the aluminium heater displayed no such trend. This result is, therefore, most likely a consequence of the unheated starting length. TAYLOR et al. (1990) have found that neither integral nor numerical boundary layer heat transfer solutions accurately predict Stanton numbers in the heated region immediately downstream of an unheated starting length. They report that,

> ... a step in wall temperature has a large effect on the Stanton number in the heated region near the step. But as the thermal boundary layer develops, the Stanton numbers approach the results for the constant wall temperature boundary layers.

Further confirmation that the boundary layer was transitional was obtained by placing a spherical excrescence 2 mm in diameter on the surface of the plate at a

location 120 mm from the leading edge. Figure 3.26 shows a turbulent wedge which formed behind the surface roughness in the otherwise laminar boundary layer. The wedge extended downstream, eventually merging into the turbulent boundary layer at the position of natural transition.

The time required for the carbon plate to reach thermal stability was estimated using the method detailed in Section 3.1.1.1. This is particularly relevant to flight testing of the NLF nacelle as experimental time will be limited. Calculated heat transfer distributions for fully turbulent boundary layers at speeds of 28.9 and 7.9 m/sec are shown in Figs. 3.27 and 3.28 at times ranging from one to ten minutes. These results suggest that ~ four minutes are required for the carbon plate to reach full thermal equilibrium, but that quite accurate results can be obtained after as little as two minutes. Similar testing on the aluminium heater (Section 3.1.1.1) indicated that this period may be reduced when taking data in regions in which the temperature gradient is high (i.e. in transitional regions).

3.1.3 *Preliminary Results from a Curved Carbon-Fibre Heater*

Figure 3.29 shows a carbon-fibre heater set into a curved carbon substrate representative of a section of the NLF nacelle. The carbon structure, the heater and electrical contacts were all manufactured by Hurel-Dubois ltd. to the specifications of Rolls-Royce plc. and Oxford University in the same manner as discussed in Section 3.1.2. The heater is 100 mm x 625 mm and begins 70 mm from the leading edge of the nacelle section. The model expands slightly in width with distance from the leading edge, measuring 283 mm (nominally) x 930 mm. The carbon substrate curls

under to create a rounded leading edge in accordance with the design of the NLF nacelle. Except for the heater (which remains black), the nacelle section is white (as required for the thermal imaging transition detection technique to be performed by DLR). The white coating is feathered out at the edges of the heater such that no detectable step exists between the heater and the surrounding carbon structure. Resistance temperature detectors (RTD's) 25mm x 70 mm were mounted along the underside of the heater at 100 mm increments. For these tests, the underside of the heater was shielded from the free-stream flow by a loose plastic covering, thus providing an insulating region of dead air. The model was mounted vertically in the tunnel such that it was flush with the upper and lower surfaces of the tunnel test section (refer to Fig. 3.29). The angle of attack of the nacelle section was adjusted by rotating it about a mounting screw attached midway along its length and extended through the tunnel floor.

The heater conformed well to the double curvature of the nacelle section. An imperfect contact at the upstream end of the heater led to a hot-spot there. This did not preclude a qualitative test of the heater performance. Figure 3.30 shows the nacelle section with a fully laminar boundary layer along the length of the heater. A turbulent wedge formed downstream of an excrescence attached to the surface of the heater, thereby confirming the laminar nature of the boundary layer. The RTD's attached to the backside of the heater acted as small heat sinks (as shown in Figure 3.30). However, their presence is not thought to offer a significant impediment to heat transfer tests.

By varying the angle of attack of the nacelle section, it was also possible to cause the boundary layer to undergo transition along the test surface. Figure 3.31 shows the location of transition start as indicated by an LC. The hot-spot due to the imperfect contact is apparent at the upstream electrical contact. No heating was detected at the downstream contact.

These qualitative results represent only preliminary investigations. Quantitative measurements of transition and heat transfer on the nacelle section are currently under way at Oxford University.

3.2 *Shear Sensitive Liquid Crystal*

3.2.1 *Natural Transition*

Shear sensitive liquid crystal was used qualitatively to determine the end of transition by noting the location at which the liquid crystal film first changed colour. A direct comparison of transition end location as determined from the heat transfer experiments and transition location as determined from the shear stress experiments was obtained by placing a 60 mm strip of shear sensitive LC alongside the aluminium heating strip. This necessarily placed the shear sensitive LC towards the side of the plate where experiments indicated that cross-flow was present in the boundary layer. The location of transition end as determined by extrapolating the heat transfer results to adiabatic conditions, agreed with the location of transition end determined from the shear experiments to within 15% over the range of speeds at which the shear LC could be used.

More detailed tests using the shear sensitive LC were performed on a plate with a slightly different leading edge. The tests were conducted at the high end of the tunnel's speed range, where the surface shear stress was relatively high (but less than 5 Pa). At lower tunnel speeds the shear stress indication was influenced to a greater extent by non-uniformities in the layer of shear sensitive LC. For levels of shear stress < 2 Pa the LC film changed colour in patches, thereby rendering the method unreliable for quantitative measurements. Reliable results were obtained at 36.5 and 33.4 m/s. BONNETT et al. (1989) have reported that it may be possible to obtain results at lower shear stresses by reducing the viscosity of the LC.

A sequence of photographs showing the LC layer at different times at the highest flow speed is presented in Figure 3.32. The first photograph after the flow starts, $t = 19$ sec., shows the location of the end of transition (highest shear stress) at about 250 mm from the leading edge of the plate. At greater times, the location at which the layer starts to flow moves downstream rapidly and upstream slowly. This is associated with the small gradient in shear stress in the turbulent boundary layer compared with that in the transitional region.

BONNETT et al. show that the type of cholesteric liquid crystal used has a calibration of the form

$$\ln(\tau) = A + B\ln(t) \quad , \tag{3.10}$$

where τ is the surface shear stress, t is the time for the LC to show colour and A and B are constants found by calibration. An attempt to calibrate this LC has been made by fitting the experimental data in the turbulent region for the highest speed runs to

a prediction from STAN5. The result of such a procedure is shown in Fig. 3.33, where the values determined for A and B are 1.9 and -0.18 respectively. Also shown are the experimental results from the lower speed runs plotted using that calibration and compared with another prediction. In both cases, the experimentally determined transition location has been used for the prediction. The results are encouraging, but further tests over a wider range of shear stress are required for validation.

At present the technique requires the observer to assess the locations at which the layer of LC has started to move at a given point in time. This requires some subjective judgement if the layer is not uniform. However, the form of the calibration (Eqn. 3.10), is such that a 30% error in t typically leads to only a 6% error in τ. Experiments also indicate that the time required for the LC to show colour is influenced by temperature. This is associated with the temperature dependence of the viscosity of the mixture.

The influence of temperature is apparent in Figs. 3.34 and 3.35, which show the repeatability of measurements using shear sensitive LC. The same calibration constants were used for all tests presented regardless of the operating temperature. Repeated tests at a given speed consistently indicated the same location for transition end.

Some tests were performed by WALTON (1991) with a fully developed turbulent flow in a duct of cross-section 3 mm x 75 mm in an attempt to independently calibrate the same cholesteric liquid crystal of the same thickness. Preliminary results

from these tests indicate that the form of the calibration is as in Eqn 3.10. Slightly different values of A and B were indicated (1.75 and -0.175), but the values of shear stress obtained with this calibration were within 15% of those in Fig. 3.33.

The method of using shear sensitive liquid crystal will not be suitable for use in regions with large negative gradients of shear stress in the direction of flow. The LC flows much more rapidly once it has entered the Grandjean texture, which it will do at earlier times in regions of higher shear stress. The LC will, therefore, flow downstream over parts of the LC layer where shear stress is low and the layer remains in the focal conic texture. Thus, results will be masked in areas of low τ.

3.2.2 *Induced Transition*

In order to insure that the shear sensitive liquid crystal was performing as expected, small excrescences were attached to the plate 55 mm from the leading edge to produce turbulent wedges in an otherwise laminar boundary layer. Sequences of photographs showing the development of the wedges at two flow speeds are presented in Figures 3.36 and 3.37. For these tests, the flow was started without any excrescences and the LC was allowed to change colour in the transition region. The flow was then stopped. The excrescence was attached to the surface of the plate and the tunnel was restarted. For the higher speed test, the excrescence height was 0.3 mm. This was found to be insufficient to generate a wedge at the lower speed, and the height of the excrescence was increased to 0.5 mm.

These tests, particularly that at the lower speed, show the variation of shear

stress within the wedge. Contours of shear stress are presented in Figure 3.38. As would be expected, the shear is higher close to the excrescence where the hydrostatic boundary layer is thinner. The semi-angle of the wedge increases with distance downstream as has been observed previously for small excrescences by SCHUBAUER AND KLEBANOFF (1955). The magnitude of the semi-angle (approximately 6°) suggests that the shear LC has changed colour only in the fully turbulent region of the wedge where the shear stress will be highest (see Fig. 3.39). The results also indicate that the shear stress is higher towards the edges of the wedge than near the centre. Considering the variation of shear stress along a span-wise line it is noted that the level of shear stress rises from the laminar value outside of the wedge and increases through an intermittent region at the edge of the wedge (although the full extent of this rise has not been captured in the present experiment). The shear stress attains a maximum value at the edge of the fully turbulent region of the wedge but decreases toward the centre.

These results are in general agreement with those of CLARK and JONES (1991) who obtained contours of heat transfer in a turbulent wedge using the steady-state heat transfer technique and temperature sensitive liquid crystals. They have noted that the level of heat transfer rises from the laminar value outside the wedge and increases through an intermittent region at the edge of the wedge (see Fig. 3.40). However, CLARK and JONES have not taken data for semi-angles of < 5° (the fully turbulent portion of the wedge). Therefore, they have not reported the decreasing rate of heat transfer along a span-wise line in the fully turbulent section of the wedge, which was indicated by the shear crystal.

Longitudinal streaks are also apparent in the LC film, especially early in the sequence of photographs at the lower speed. These appear to be associated with the presence of stream-wise vortices. THOMSON (1988) has reported that stream-wise vortices wrap around the protuberance and trail downstream. The location in planform of six vortex legs can be distinguished in the LC film (first photograph of Fig 3.37). Similar flow visualisation has been achieved using sublimation of acenaphthene on a flat plate, as shown in Fig. 3.41. THOMSON suggests that the induced velocities associated with these vortices is responsible for flow breakdown to turbulence. Hence, turbulence appears to occur first directly downstream of the surface roughness in the vicinity of the innermost vortex legs which are the strongest. Transition occurs in the proximity of the other vortex legs further downstream. The LC film's capability to detect stream-wise vortices suggests that the shear sensitive LC is quite sensitive to variations in surface shear stress.

These results show the possible usefulness of shear sensitive liquid crystals for full coverage measurement of surface shear stress in transitional boundary layer flows.

Chapter 4: *Conclusions and Recommendations*

The present study is primarily directed at developing a steady state heat transfer technique employing temperature sensitive liquid crystals for transition detection. Conclusions related to the technique itself are presented here, followed by those related to the development of a constant heat flux heater constructed of unidirectional carbon-fibres. Finally, conclusions are presented from experiments employing liquid crystal to measure surface shear stress.

4.1 *Heat Transfer Measurements*

Tests performed on a flat plate in incompressible flow suggest that the steady state heat transfer technique employing encapsulated temperature sensitive liquid crystals provides a suitable means for obtaining high resolution heat transfer measurements and detecting boundary layer transition. Self-consistent measurements of heat transfer are obtained from a multiple LC layer and agree well with standard correlations in the laminar boundary layer. Results fall below the correlations in the turbulent portion of the boundary layer (particularly near transition end) by a maximum of 15%, but approach the correlations further downstream.

Measured coefficients of heat transfer in the laminar and turbulent regions of the boundary layer were found to be unaffected by the level of heat transfer from the surface. However, results clearly indicate that heating the surface significantly hastens

transition and must, therefore, be considered when inferring the point of transition for an unheated surface. By using three liquid crystals, each with a different colour-play temperature, it is possible to plot the movement of transition as a function of heating for a given condition. An exponential extrapolation to zero heating then provides a measure of the adiabatic transition Reynolds number. Plotted against a normalised transition Reynolds number, a Stanton number of the form $\dot{q}/(\rho u C_p T_o)$ correlates the movement of transition with heating. Uncertainties in measurements of Stanton numbers and normalised transition Reynolds numbers are a maximum of 9.5% and 6.9% respectively in the present tests.

The destabilising influence of heating on the flat plate boundary layer is counteracted by the stabilising influence of a favourable pressure gradient. Under adiabatic conditions, the transition Reynolds number increases rapidly with favourable pressure gradient and a single 'acceleration' parameter, K, is found to correlate Reynolds number at transition start and end. With favourable pressure gradients, heating has a greater influence on transition location than in zero pressure gradient. As K increases, the influence of heating increases. The present results suggest that a single acceleration parameter alone does not correlate the movement of transition with heating. With zero pressure gradient, normalised Reynolds numbers at transition end effectively collapse onto a single curve plotting against Stanton number. With favourable pressure gradient, results show a trend towards a smaller change in normalised Reynolds numbers with heating at transition end than at transition start.

Using the present technique with narrow-band liquid crystals, transition length

can not be measured directly, but can be extracted indirectly. Transition length is found to increase with increasing K, and heating has no discernible effect on transition length. *Normalised* transition length varies little with heating or the small pressure gradients of the present experiments. The method of obtaining transition length introduces significant uncertainties (a maximum of ± 24% in the normalised transition length). Theses uncertainties could be reduced significantly by using a wide-band LC for transition detection (as discussed below).

4.1.1 *Future Work*

Narrow-band temperature sensitive liquid crystals have been used in the present heat transfer experiments. These enable surface temperatures to be accurately measured which, in turn, allows heat transfer coefficients to be found. However, this work is primarily a background study into using the steady state heat transfer technique to measure *transition*. This requires only that the positions of *minimum* and *maximum* surface temperatures be located for a number of heating rates in order to infer the adiabatic transition location. This may be more efficiently accomplished by using a wide-band LC which is capable of indicating the location of transition start and end at a single heating rate and (unlike narrow-band LC's) will not require the heating rate to be adjusted so as to position a particular isothermal band at the location of minimum or maximum surface temperature.

A proposed technique is to use a wide-band LC (to locate transition) accompanied by a narrow-band LC (to obtain accurate values of heat transfer coefficients). Accurate surface temperature measurements can be supplemented by

resistance temperature detectors (RTD's) but, of course, these will only provide measurements at discrete locations. Tests with combined wide- and narrow-band LC coatings are under way at O.U.E.L.

4.2 *Unidirectional Carbon-Fibre Heater*

A constant heat flux heater constructed from unidirectional carbon fibres was also tested in a wind tunnel is proposed for use in in-flight transition detection experiments. The heater is to be integrated into the load-bearing structure of an aircraft engine nacelle. To the author's knowledge this represents the first attempt, to locate transition and make heat transfer measurements employing part of the aircraft structure as a heating element. Such an experimental technique may prove very useful in a variety of future flight test applications.

The unidirectional carbon fibres produce an extremely uniform surface heat flux. There is no detectable step between the heater and the surrounding carbon structure. The heater is capable of sustaining the lateral and longitudinal temperature gradients necessary for detecting transition and making heat transfer measurements using the present technique. Measurements of heat transfer in a turbulent boundary layer obtained using the carbon heater agree well with standard correlations. Limited tests in transitional boundary layers found measurements of heat transfer near the end of transition to be a maximum of ~ 15% higher than STAN5 predictions. This is attributed to boundary layer conditions. Further downstream (in the well-developed portion of the turbulent boundary layer), heat transfer measurements approach predictions. The carbon plate requires approximately four minutes to reach full

thermal equilibrium in the present tests, although quite accurate results can be obtained after as little as two minutes.

Good electrical contact to the carbon heater is essential, as poor contact results in non-uniform heating of the test surface and contact heating. Suitable electrical contacts have been devised and successfully tested. Resistance in the exposed carbon fibres leading to the electrical contacts may be effectively eliminated by soaking the fibres in a mixture of silver-loaded conducting paint and xylene, then allowing the xylene to evaporate.

The thermal conductance of the carbon-fibre matrix is estimated to be 6.7 $W \cdot m^{-1} \cdot K^{-1}$. Due to this relatively high thermal conductivity, adequate thermal insulation on the underside of the carbon heater (to include the contacts and the area surrounding them) is very important. Conservative estimates suggest that lateral and longitudinal conduction may amount to a maximum of 2-8% and 13% respectively for these tests.

Preliminary tests on a carbon-fibre heater set into a curved section representative of that proposed for the NLF nacelle indicate that transition can be detected using temperature-sensitive liquid crystals.

4.3 *Surface Shear Stress Measurements*

In related experiments, shear sensitive liquid crystal is used for the first time

to obtain *quantitative* measurements of surface shear stress in a transitional boundary layer. The technique relies upon calibrating the time required for an LC layer to change from the focal-conic texture to the Grandjean texture when subjected to a shearing force.

There is a lower limit of shear stress (2 Pa) below which reliable results can not be obtained using the present materials. Therefore, measurements could not be obtained in the laminar portion of the boundary layer with the flow speeds available in the present tunnel.

The shear sensitive LC calibration, obtained in the test rig using a STAN5 prediction, was found to lead to results at another test condition in good agreement with another STAN5 prediction. Independent calibrations produced results within 15% of those which used the calibration from the test rig.

Repeated runs at similar conditions provide consistent indications of transition end location. Transition end Reynolds numbers as given by shear sensitive LC agree with the (adiabatic) transition end Reynolds numbers obtained using the heat transfer technique to within 15% when both tests are performed on the same plate.

Shear sensitive LC was also used to obtain contours of shear stress within a turbulent wedge induced by a surface excrescence. Results were obtained in the fully turbulent region of the wedge and partially in the intermittent regions on either side of the wedge. In the span-wise direction the level of shear stress rises from the

laminar value outside the wedge and is shown to increase through the intermittent region at the edge of the wedge until reaching a maximum value at the start of the fully turbulent region. Shear stress then decreases toward the centre of the wedge. Stream-wise vortices downstream of the excrescence were also visible in the LC film.

These results show the potential usefulness of shear sensitive LC's for full coverage measurement of surface shear stress in transitional boundary layers. While results are encouraging, further tests over a wider range of shear stress levels are required for validation. Shear sensitive LC will not be suitable for use in regions of large negative gradients of shear stress in the flow direction.

Appendix A: *Dimensional Analysis*

Consider the flow of an incompressible fluid past a uniformly heated flat plate on which a boundary layer forms and undergoes transition (see Fig. A.1). The physical quantities which determine the location of transition are: the free stream velocity, u, the viscosity, μ, the density of the fluid, ρ, the gas temperature, T_g, the specific heat of the fluid at constant pressure, C_p, a length scale, l, the distance to the start of transition, x_t, the thermal conductivity of the fluid, k, the acceleration of the flow, du/dx, and the heat flux from the plate, $\dot{q}$.

The fundamental dimensions required to describe these 10 physical variables are

$$M = \text{dimensions of mass} \quad ,$$

$$L = \text{dimensions of length} \quad ,$$

$$T = \text{dimensions of time} \quad ,$$

$$\Theta = \text{dimensions of temperature} \quad ,$$

$$Q = \text{dimensions of heat} \quad .$$

The physical variables and their dimensions are

$$[u] = LT^{-1} \quad ,$$

$$[\mu] = MT^{-1}L^{-1} \quad ,$$

$$[\rho] = ML^{-3} \quad ,$$

$$[T_g] = \Theta \quad ,$$

$$[C_p] = QM^{-1}\Theta^{-1} \quad ,$$

$$[l] = L \quad ,$$

$$[x_t] = L \quad ,$$

$$[k] = QT^{-1}L^{-1}\Theta^{-1} \quad ,$$

$$[du/dx] = T^{-1} \quad ,$$

$$[\dot{q}] = QT^{-1}L^{-2} \quad .$$

The resulting indicial matrix follows.

quantity	M	L	T	Θ	Q
u	0	1	-1	0	0
μ	1	-1	-1	0	0
ρ	1	-3	0	0	0
T_g	0	0	0	1	0
C_p	-1	0	0	-1	1
l	0	1	0	0	0
x_t	0	1	0	0	0
k	0	-1	-1	-1	1
du/dx	0	0	-1	0	0
$\dot{q}$	0	-2	-1	0	1

Note that rows associated with the physical variables k, μ, q, l, and du/dx are linearly dependent. Therefore, the rank of the indicial matrix is five.

Following the Buckingham pi theorem as presented in ANDERSON (1984),

let N equal the number of physical variables and R equal the rank of the indicial matrix. Let $P_1, P_2, \ldots, P_N$ represent the physical variables in the relation

$$f_1(P_1, P_2, \ldots, P_N) = 0 \quad . \tag{A.1}$$

Then, the physical relation in equation A.1 may be re-expressed as a relation of (N - R) dimensionless Π products,

$$f_2(\Pi_1, \Pi_2, \ldots, \Pi_{N-R}) = 0 \quad ,$$

where each Π product is a dimensionless product of an arbitrarily selected set of R physical variables plus one other physical variable. Let $P_1, P_2, \ldots, P_R$ be the arbitrarily selected set of R physical variables. Then

$$\Pi_1 = f_3(P_1, P_2, \ldots, P_R, P_{R+1}) \quad ,$$

$$\Pi_2 = f_4(P_1, P_2, \ldots, P_R, P_{R+2}) \quad ,$$

$$\vdots$$

$$\Pi_{N-R} = f_5(P_1, P_2, \ldots, P_R, P_N) \quad .$$

Since $N = 10$ and $R = 5$, equation A.1 may be expressed as a relation of five Π products. Using ρ, u, x_t, k, and Tg as repeating variables the following dimensionless quantities emerge:

$$\Pi_1 = \frac{\rho\, u\, x_t\, C_p}{k} \quad ,$$

$$\Pi_2 = \frac{\mu}{\rho\, u\, x_t} \quad ,$$

$$\Pi_3 = \frac{l}{x_t} \quad ,$$

$$\Pi_4 = \frac{x_t \dot{q}}{k T_g} \quad ,$$

$$\Pi_5 = \frac{x_t}{u} \frac{du}{dx} \quad .$$

These dimensionless quantities may now be combined in various manners in order to produce other more useful dimensionless products. Reynolds number is already represented by Π_2. Multiplying Π_1 by Π_2 produces a Prandtl number. The product of $1/\Pi_2$ and Π_3 is a unit Reynolds number. A dimensionless heating parameter, or Stanton number, is created by multiplying Π_4 by $1/\Pi_1$. Finally, a convenient acceleration parameter, K, is formed by combining Π_2 and Π_5. The new Π quantities, then, are

$$\Pi_1 = \frac{\rho u x_t}{k} \quad ,$$

$$\Pi_2 = \frac{\mu C_p}{k} \quad ,$$

$$\Pi_3 = \frac{\rho u l}{\mu} \quad ,$$

$$\Pi_4 = \frac{\dot{q}}{\rho u C_p T_g} \quad ,$$

$$\Pi_5 = \frac{\nu}{u^2}\frac{du}{dx} \quad .$$

$$\therefore \; Re_t = f_6(Pr, Re_p, St, K) \quad .$$

Appendix B: *Uncertainty Analysis*

An analysis of the uncertainties in measurements of transition length and Reynolds and Stanton numbers at transition start and end was performed. The measurements which were analyzed were obtained using the aluminium heater with zero pressure gradient conditions. Since the resistance of the carbon-fibre heater is more uniform than that of the aluminium heater, uncertainties in results obtained using the former are expected to be smaller. The experimental arrangement was the same regardless of which heater was employed.

Following KLINE and McCLINTOCK (1953) and BAINES et al. (1991), let an experimental result F be a linear function of n independent variables, $\phi_1, \phi_2, \ldots \phi_n$, each of which is normally distributed and possesses the same level of odds

$$F = F(\phi_1, \phi_2, \ldots \phi_n) \quad . \tag{B.1}$$

Each ϕ_i may be written as

$$\phi_i = \hat{\phi}_i + \delta\phi_i \quad , \tag{B.2}$$

where $\hat{\phi}_i$ is the true value and $\delta\phi_i$ is the uncertainty. The component of uncertainty of F due to an uncertainty in ϕ_i is then

$$(\delta F)_i = \left(\frac{\partial F}{\partial \phi_i}\right)\delta\phi_i \quad . \tag{B.3}$$

The expression for the uncertainty of the result which gives the same odds as each of the variables is

$$\delta F = \sqrt{\left[(\delta F)_1^2 + (\delta F)_2^2 + \ldots + (\delta F)_n^2\right]} \quad . \tag{B.4}$$

Uncertainties in measurements of the following variables were considered:

(1) electrical current, i,

(2) total temperature, T_0,

(3) calibrated temperature at which the liquid crystal shows colour, T_c,

(4) location of isothermal line, x

(5) free-stream velocity, u,

(6) local resistance of the heater, R.

Uncertainty in each individual variable may derive from:

(1) limitations in the precision to which an instrument can be read,

(2) unsteadiness or non-uniformities,

(3) instrument calibration inaccuracies.

Values of the current being fed to the heater were read from a Salford Selectest model 'Super 50' analog ammeter. Uncertainties in measurements of i were due to minimum resolution of the analog meter (± 0.02 amps), fluctuations in current provided by the variable voltage source (± 0.03 amps) and the calibrated accuracy of the ammeter (0.3% of full scale ± 2.5% of the reading).* A 10 amp scale was used for these experiments.

*Published accuracy for the Salford Selectest is ± 2.5% of full scale. However, experiments showed that, when the Selectest was mounted horizontally and was monitoring current in the same arrangement as for the experiment, its measurements of current agreed with measurements from a Thurlby 1503-HA digital multimeter within the accuracy of the latter instrument throughout the range of current settings employed in these experiments. Therefore, uncertainty analysis was performed using the published accuracy of the 1503-HA.

Measurements of mean free-stream total temperature were made using an aspirating total temperature probe containing a type T thermocouple. A Comark model 6900 digital thermometer was used to monitor the temperature of the thermocouple. Estimated δT_0 was ± 0.2°C. This contributed < 0.3% uncertainty to measured Stanton numbers and was, therefore, neglected.

Uncertainties regarding the temperature at which a specific colour band of a given LC shows colour were due to the limited accuracy of the Comark model 6900 thermometer (± 0.2°C), uncertainty in ascertaining the location of the isothermal line in relation to the calibrating thermocouple (± 0.2°C) and drifting in the response temperature of the LC (± 0.2°C). Total δT_c was ± 0.3°C. This typically contributed < 0.1% uncertainty to measurements of Stanton numbers. Consequently, δT_c was neglected.

The degree of certainty to which the location of an isothermal contour could be measured varied depending on whether the contour designated the location of transition start or end. Temperature gradients are sharper in the region of minimum heat transfer than in the region of maximum heat transfer. Consequently, the colour contours are sharper near transition start. Near x_s the location of the contour could be determined to ± 3 mm, while resolution was ± 7 mm near x_T.

The resistance of the metallised polymer was 6.29 Ω, as measured by a Thurlby model 1503-HA digital multimeter. The 1503-HA is calibrated to an accuracy of 0.05% f.s. ± 0.15% of the reading. Uncertainty in the value of the local

resistance due to non-uniformities was assumed to be ± 5% (ref. Sect. 2.2.1). Therefore, δR was ± 0.36 Ω.

Free-stream velocity was calculated from measurements of total and static pressure in the free-stream. The measurements were made using a Pitot-static tube and a manometer bank inclined at 30 deg. Total pressure could be read to within ± 0.5 mm of manometer fluid. Fluctuations in tunnel speed added uncertainty to static pressure measurements, which could be read to within ± 1 mm of manometer fluid. Total uncertainty amounted to ± 1.1 mm of manometer fluid.

In transitional boundary layers, the largest uncertainties in measurements of *Re* and *St* occur at low speeds where the relative uncertainty in *i* and *u* is maximal. The lowest speed at which measurements of transition start and end were available was 22.3 m/s (designated flow condition 1a in Section 3.1.1.2). Table B.1 shows

Table B.1 Transition locations and Reynolds numbers, and their associated heating rates, at 22.3 m/s. Flat plate, zero pressure gradient.

	Transition Start			Transition End		
	x_t (m)	Re_t (x 10^{-5})	St_t (x 10^5)	x_T (m)	Re_T (x 10^{-5})	St_T (x 10^5)
23.7°C crystal	.210	3.04	3.39	.330	4.78	5.91
29.7°C crystal	.200	2.87	5.94	.290	4.16	10.7
37.1°C crystal	.165	2.35	9.23	.225	3.20	17.4

measurements of transition start and end locations and Reynolds numbers, and their associated heating rates, for each LC at this speed.

B.1. *Uncertainty in Reynolds and Stanton Numbers at Transition End*

Using Eqns. B.3 and B.4, uncertainties in Reynolds and Stanton numbers were calculated from the uncertainties associated with measurements of i, R, x and u. Results are shown in Table B.2 for transition end, where uncertainty is expected to be highest (since $\delta x_T > \delta x_t$).

Table B.2 Uncertainty in Reynolds and Stanton numbers at transition end on a flat plate with zero pressure gradient. Speed = 24.2 m/s.

		Variable (ϕ)				Total
		i	R	x_T	u	
23.7°C crystal	δRe_T (± %)	-----	-----	2.1	1.3	2.5
	δSt_T (± %)	6.6	5.8	-----	1.4	8.9
29.7°C crystal	δRe_T (± %)	-----	-----	2.4	1.4	2.8
	δSt_T (± %)	6.5	5.6	-----	1.0	8.6
37.1°C crystal	δRe_T (± %)	-----	-----	3.1	1.6	3.5
	δSt_T (± %)	6.3	5.7	-----	1.1	8.6

B.2. *Uncertainty in Transition Length*

Measurements of transition length at a given heating rate were complicated by the fact that the indication of transition start, as given by an LC, occurs at a different heating rate than does the indication of transition end (see Sect. 3.1.1.1). Therefore, a number of extrapolations were required in order to determine the locations of transition start and end for a single heating rate. The procedure is described in detail in Section 3.1.1.2. Briefly, the use of three LC's provided Reynolds numbers at transition end for three different heating rates. These were used to determine the Reynolds number at transition end for zero heating, $Re_{T,ad}$. The values of Re_T and St_T for each liquid crystal were then varied individually by an amount equal to δRe_T and δSt_T respectively (as shown in Table B.2) and the effect on $Re_{T,ad}$ was observed. This provided a measure of $\partial Re_{T,ad}/\partial Re_T$ and $\partial Re_{T,ad}/\partial St_T$ such that the uncertainty in $\delta Re_{T,ad}$ could be found using Eqns. B.3 and B.4. Given the heating rate at transition start and $Re_{T,ad}$, Eqn. 3.10 could then be used to determine the location of x_T at the same heating rate as x_t. The difference between x_T and x_t is the transition length, η, at a given heating rate. Transition length was normalised with the distance to transition start.

Uncertainty in the correlation which quantifies the effect of heating on transition (Eqn 3.10) was estimated based on a 95% confidence interval constructed with the aid of Student's t-distribution. Figure 3.14 shows Eqn. 3.10 superimposed on all experimental measurements of transition Reynolds number versus heating rate at zero pressure gradient. The vertical difference between the correlation and the experimental data was calculated for each point and the resulting data set was assumed to be normally distributed. Student's t-distribution (with 41 degrees of freedom) could

then be used to construct a 95% confidence interval for the correlation.

Fig. B.1 is a schematic illustration of the means by which uncertainties compound when this technique is applied. The numerical uncertainties included in this figure represent those for a speed of 22.3 m/s with a heating rate of $St = 9.23 \times 10^{-5}$ (that at which the 37.1°C LC indicated the location of x_t). The relative uncertainties in the calculated values of normalised transition lengths for the 23.7, 29.7 and 37.1°C LC's at this condition were ± 24.0, 22.0 and 21.9% respectively. Bars representing these uncertainties are superimposed on measurements of normalised transition length in Figure 3.17.

Figure 3.14 illustrates uncertainties in plots of Re/Re_{ad} v. St at the same conditions as discussed above. For an LC mixture with response temperatures of 23.7, 29.7 and 37.1°C, uncertainties in $Re_T/Re_{T,ad}$ are, respectively, 6.4, 6.5 and 6.9%. Values of δSt_T have been provided in Table B.2.

The relative uncertainty in u is slightly larger in favourable pressure gradients since local velocity was not measured directly. However, as the distance to transition start also increases in favourable pressure gradients (transition is delayed), the smaller relative uncertainty in x_t more than compensates for the additional uncertainty in u. Therefore, the uncertainties in Re, St, Re/Re_{ad} and η/x_t discussed here are a worst-case illustration.

Appendix C: *Estimates of Longitudinal Conduction*

Estimates of longitudinal conduction due to stream-wise surface temperature variations on the heated plate are provided in this appendix for both the aluminium and carbon heaters.

Consider an infinitesimal element of a heated flat plate (representing both heater and substrate) of unit width as shown in Fig C.1. Assume that the plate is in steady-state and that the longitudinal temperature distribution is uniform in the span-wise direction. Also assume that, at a given stream-wise location, the temperature within the element does not vary with y (i.e. $T_s = T_s(x)$). The heat generated within the element is

$$\dot{q}_g = i^2 \, \theta \, dx \quad , \tag{C.1}$$

where i is the current and Θ is the local resistance/square of the heater. Heat is conducted into the left face and out the right face of the element. Heat is also convected out the upper surface. The lower surface is assumed to be perfectly insulated.

$$\dot{q}_g = \dot{q}_{conv} + \dot{q}_{cond,out} - \dot{q}_{cond,in} \quad . \tag{C.2}$$

According to Fourier's law, the heat flowing into the left face of the lattice can

be expressed as

$$\dot{q}_{cond,in} = -k\,t\,\frac{dT_s}{dx} \quad . \tag{C.3}$$

Similarly, conduction out the right side of the lattice is

$$\dot{q}_{cond,out} = -k\,t\left(\frac{dT_s}{dx} + \frac{d^2T_s}{dx^2}\,dx\right) \quad . \tag{C.4}$$

Convection may be represented as

$$\dot{q}_{conv} = h\,dx\,dT = h\,dx\,(T_s - T_g) \quad . \tag{C.5}$$

Replacing Eqn. C.2 with Eqns. C.1, C.3 and C.4,

$$i^2\,\theta\,dx = h\,dx\,(T_s - T_g) - k\,t\left(\frac{dT_s}{dx} + \frac{d^2T_s}{dx^2}\,dx\right) + k\,t\,\frac{dT_s}{dx}. \tag{C.6}$$

Simplifying,

$$\underset{(1)}{i^2\,\theta = h\,(T_s - T_g)} \underset{(2)}{- k\,t\,\frac{d^2T_s}{dx^2}} \quad . \tag{C.7}$$

Thus, a ratio of (2) to (1) should provide a measure of the relative importance of conduction for these experiments. A negative value of (2) represents a net heat loss from the element under consideration due to conduction, while a positive value of (2) indicates a net gain in heat. Given the high surface temperature characteristic of transition start, negative values of (2) are expected in this region. Conversely, (2) should be positive near transition end.

Conduction will be largest (in relation to convection) in transitional boundary

layers at low speed. At reduced flow speeds, convective heat transfer is relatively low, and temperature gradients are highest in transitional boundary layers. Figure C.2 shows the stream-wise surface temperature distribution along a flat plate with a constant heat flux surface and a transitional boundary layer at 24.2 m/s as predicted by STAN5. For this prediction, experimental evidence was used to obtain the input parameters of $x_t = 0.16$ m, $x_T = 0.22$ m and $\dot{q}_g = 1060$ W·m^{-2}.

Attempts to analytically differentiate a polynomial fitted to the line in Fig. C.2 did not produce consistent results. Therefore, a numerical second derivative of the temperature distribution, d^2T_s/dx^2, was determined from the data . Results are shown in Figure C.3. Conductive losses are highest slightly downstream of transition start, while gains due to conduction are largest at approximately the location of transition end.

Using Eqn. C.7, longitudinal conductive losses were found to be a maximum of 13.0% of convection for the *carbon* plate. Maximum conductive gains amounted to 12.6% of convection. The measured thickness of the carbon heater (t) was 3 mm, and the estimated thermal conductivity of the carbon fibres was 6.7 W·m^{-1}·K^{-1} (see Section 2.2.2.2). Note that the relative importance of longitudinal conduction should be much less in the nacelle flight tests where the convective heat transfer coefficient will be higher, and the thermal conductivity of the carbon-fibre matrix reduced.

Relative longitudinal conduction in the perspex plate was considerably smaller than in the carbon plate for the same conditions. Maximal values of $\dot{q}_{cond,out}$ and

$\dot{q}_{cond,in}$ were 0.8 and 0.7% of convective heat transfer respectively. The effective thickness of the perspex plate for these calculations was 6 mm. The thermal conductivity, k, of the perspex was assumed to be 0.2 $W \cdot m^{-1} \cdot K^{-1}$, as listed by TOULOUKIAN, et al. (1970).

Conduction does not affect the location of transition as indicated by the temperature-sensitive LC's in these experiments. Nevertheless, conductive losses (or gains) will introduce errors into local heat transfer measurements. Specifically, measurements of heat transfer coefficients are expected to be spuriously high in areas where heat is being lost through conduction (transition start). The reverse is true in areas where heat is gained via conduction (transition end). Since the adiabatic Reynolds number is determined with the aid of measurements of heat transfer at transition start and end, its accuracy may suffer as a result of conduction. A 1.5% error in measurements of convective heat transfer is estimated to result in an error of 6.2% in adiabatic Reynolds number in these tests.

References

Abu-Ghannam, B.J. and Shaw, P. (1980), "Natural transition of boundary layers -- the effects of turbulence, pressure gradient and flow history". *J. Mech. Eng. Sci.*, Vol. 22, p. 213.

Agarwal, B.D. and Broutman, L.J. (1980), *Analysis and Performance of Fiber Composites*. John Wiley and Sons, Inc., New York.

Akino, N., Kunugi, T., Ichimiya, K., Mitsushiro, K., and Ueda, M. (1989), "Improved liquid-crystal thermometry excluding human color sensation". *Trans. ASME, J. Heat Trans.* Vol. 111, p. 558.

Anderson, J.D. Jr. (1984), *Fundamentals of Aerodynamics*. McGraw-Hill, New York.

Baines, N.C., Mee, D.J. and Oldfield, M.L.G. (1991), "Uncertainty analysis in turbomachine and cascade testing". *Int. J. Eng. Fluid Mech.*, Vol. 4, No. 4.

Baughn, J.W., Hoffman, M.A. and Makel, D.B. (1986), "Improvements in a new technique for measuring and mapping heat transfer coefficients". *Rev. Sci. Instr.*, Vol. 57, p. 650.

Baughn, J.W., Ireland, P.T., Jones, T.V. and Saniei, N. (1989), "A comparison of the transient and heated-coating methods for the measurement of local heat transfer coefficients in a pin fin". *Trans. ASME, J. Heat Trans.*, Vol. 111. p. 877.

Baughn, J.W., Takashi, R.K., Hoffman, M.A., and McKillop, A.A. (1985), "Local heat transfer measurements using an electrically heated thin gold-coated plastic sheet". *Trans. ASME, J. Heat Trans.*, Vol. 107, p. 953.

Blair, M.F. (1982), "Influence of free-stream turbulence on boundary layer transition in favourable pressure gradients". *Trans. ASME, J. Eng. Power*, Vol. 104, p. 743.

Blair, M.F. and Werle, M.J. (1980), "The influence of free-stream turbulence on the zero pressure gradient fully turbulent boundary layer". United Technologies Research Center/R80-914388-12, Sept. 1980.

Blair, M.F. and Werle, M.J. (1981), "Combined influence of free-stream turbulence and favourable pressure gradients on boundary layer transition and heat transfer". United Technologies Research Center/R81-914388-17, March 1981.

Bonnett, P. (1989), "Applications of liquid crystals in aerodynamic testing". D.Phil. thesis, University of Oxford.

Bonnett, P., Jones, T.V. and McDonnell, D.G. (1989), "Shear stress measurements in aerodynamic testing using cholesteric liquid crystals". *Liquid Crystals*, Vol. 6, p. 271.

Byerley, A.R., Ireland, P.T. and Jones, T.V. (1988), "Detailed heat transfer measurements near and within the entrance to a film cooling hole". ASME Paper 88-GT-155.

Cebeci, T. and Smith, A.M.O. (1968), "Investigation of heat transfer and of suction for tripping laminar boundary layers". *J. Aircraft*, Vol. 5, p. 450.

Clark, J.P. and Jones, T.V. (1991), "On the heat transfer distribution in a turbulent wedge". Submitted for publication.

Clark, J.P., Jones, T.V., Ashworth, D.A. and LaGraff, J.E. (1991), "Turbulent spot development in a Mach 0.55 flow". *Boundary Layer Transition and Control Conference Proceedings*, Vol 1, Royal Aero. Soc., London, 1991, p. 21.1.

Clayton, P. (1990), Hurel-Dubois (UK) Ltd., Burnley. Private communication, 9 Oct.

Clayton, P. (1991), Hurel-Dubois (UK) Ltd., Burnley. Private communication, 6 Mar.

Cousteix, J., Arnal, D. and Gleyzes, C. (1991), "Recent studies on transition and turbulence at ONERA-CERT". AIAA paper 91-0332.

Crawford, M.E. and Kays, W.M. (1976), "STAN5 -- A program for numerical computation of two-dimensional internal and external boundary layer flows". NASA CR-2742, Nov. 1976.

Crowder, J.P. (1990), "Infrared cameras for detection of boundary layer transition in transonic and subsonic wind tunnels." AIAA Paper 90-1450.

Davis, M.R. (1980), "Design of flat plate leading edges to avoid flow separation". *AIAA J.*, Vol. 18, p. 598.

Dey, J. and Narasimha, R. (1990), "Integral method for the calculation of incompressible two-dimensional boundary layers". *J. Aircraft*, Vol. 27, p. 859.

Dhawan, S. and Narasimha, R. (1958), "Some properties of boundary layer flow during transition from laminar to turbulent motion". *J. Fluid Mech.*, Vol. 3, p. 418.

Emmons, H.W. and Bryson, A.E. (1951), "The laminar-turbulent transition in a boundary layer". *J. Aero. Sci.*, Vol. 18, p. 490.

Dryden, H.L. (1959), "Transition from laminar to turbulent flow". *Turbulent Flows and Heat Transfer*, ed. C.C. Lin, Princeton University Press,New Jersey, p. 1.

Edwards, A. and Furber, B.N. (1956), "The influence of free-stream turbulence on heat transfer by convection from an isolated region of a plane surface in parallel air flow". *Proc. Inst. Mech. Engineers*, Vol. 170, p. 941.

Fisher, E.M. and Eibeck, P.A. (1990), "The influence of a horseshoe vortex on local convective heat transfer." *J. Heat Trans.*, Vol. 112, p. 329.

Gall, P.D. and Holmes, B.J. (1986), "Liquid crystals for high-altitude in-flight boundary layer flow visualisation". AIAA Paper 86-2592.

Gaugler, R.E. (1984), "Review and analysis of boundary layer transition data for turbine application". NASA TM 86880.

Godard, J.L. (1989), "Reduction of transport aircraft nacelle drag by extended laminarity". *ONERA Activities, 1989*, p. A-25.

Görtler, H. (1949), "Uber ein dreidimensionale Instabilität laminarer Grenzschichten an konkaven Wänden". Nachr. Ges. Wiss., Göttingen, *Math. Phys. Kl.*, Vol. 1, p. 1. English translation NACA TM 1375.

Gostelow, J.P. and Blunden, A.R. (1988), "Investigations of boundary layer transition in an adverse pressure gradient", ASME Paper 88-GT-298.

Govindarajan, R. and Narasimha, R. (1991), "The role of residual nonturbulent disturbances on transition onset". *Trans. ASME, J. Fluids Eng.*, Vol. 113, p. 147.

Hall, D.J. and Gibbings, J.C. (1972), "Influence of stream turbulence and pressure gradient upon boundary layer transition". *J. Mech. Eng. Sci.*, Vol. 14, p. 134.

Hama, F.R., Long, J.D. and Hegarty, J.C. (1957), "On transition from laminar to turbulent flow". *J. Appl. Phys.*, Vol. 28, p. 388.

Hastings Jr., E.C., Faust, G.K., Munger, P., Obara, C.J., Dodbele, S.S., Schoenster, J.A. and Jones, M.G. (1987), "Status report on a natural laminar flow nacelle flight experiment". NASA-CP-2487, part 3.

Henke, R., Munch, F. and Quast, A. (1990), "Natural laminar flow: a wind tunnel test campaign and comparison with flight data". AIAA Paper 90-3045.

Herbert, T. (1988), "Secondary Instability of boundary layers". *Ann. Rev. Fluid Mech.*, Vol. 20, p. 487.

Hippensteele, S.A., Russell, L.M. and Stepka, F.S. (1983), "Evaluation of a method for heat transfer measurements and thermal visualization using a composite of a heater element and liquid crystals". *Trans. ASME, J. Heat Trans.*, Vol. 105, p. 184.

Holmes, B.J., Croom, C.C., Gall, P.D., Manuel, G.S. and Carraway, D.L., (1986), "Advanced transition measurement methods for flight applications". AIAA Paper 86-9786.

Holmes, B.J. and Obara, C.J. (1987), "Advances in flow visualization using liquid-crystal coatings". SAE Technical Paper Series 871017.

Horstman, K.H., Quast, A., and Redeker, G. (1990), "Flight and wind-tunnel investigations on boundary-layer transition". *J. Aircraft*, Vol. 27, p. 146.

Horstman, K.H., Redeker, G., Quast, A., Dreßler, U. and Bieler, H. (1990), "Flight tests with a natural laminar flow glove on a transport aircraft". AIAA Paper 90-3044.

Incropera, F.P. and DeWitt, D.P. (1985), *Introduction to Heat Transfer*. John Wiley and Sons, Inc., New York.

Ireland, P.T. and Jones, T.V. (1985), "The measurement of local heat transfer coefficients in blade cooling geometries". AGARD CP-390, Paper 28.

Ireland, P.T. and Jones, T.V. (1986), "Detailed measurements of heat transfer on and around a pedestal in fully developed channel flow". Proc. 8th Int. Heat Trans. Conf., San Francisco, Vol. 3, p. 975.

Ireland, P.T. and Jones, T.V. (1987), "The response time of a surface thermometer employing encapsulated themochromic liquid crystals". *J. Phys. E.: Sci. Instrum.*, Vol. 20, p. 1195.

Johnson, J.B. (1988), "Preliminary in-flight boundary layer transition measurements on a 45-degree swept wing at mach numbers between 0.9 and 1.8". NASA TM 100412.

Jones, T.V. (1991), "The use of liquid crystals in aerodynamic and heat trnasfer testing". Presented at Eurotherm Seminar no. 25, Pau, France, July 1991.

Jones, T.V. and Hippensteele, S.A. (1988), "High resolution heat-transfer coefficient maps applicable to compound-curve surfaces using liquid crystals in a transient wind tunnel". NASA TM 89855.

Junkhan, G. H. and Serovy, G.K. (1967), "Effects of free-stream turbulence and pressure gradient on flat-plate boundary layer velocity profiles and on heat transfer". *Trans. ASME, J. Heat Trans.*, Vol. 89, p. 169.

Kays, W.M. and Crawford, M.E. (1980), *Convective Heat and Mass Transfer, 2nd ed.* McGraw-Hill, New York.

Kim, J., Simon, T.W. and Kestoras, M. (1989), "Fluid mechanics and heat transfer measurements in transitional boundary layers conditionally sampled on intermittency". *ASME HTD*, Vol. 107, p. 69.

Klebanoff, P.S., Tidstron, K.D. and Sargent, L.R. (1962), "The three dimensional nature of boundary layer instability". *J. Fluid Mech.*, Vol. 12, p. 1.

Kline, S.J. and McClintock (1953), "Describing uncertainties in single-sample experiments". *Mech. Eng.*, Vol. 75, p. 3.

Lauchle, G.C. and Gurney, G.B. (1984), "Laminar boundary-layer transition on a heated underwater body". *J. Fluid Mech.*, Vol. 144, p. 79.

Lekoudis, S.G. (1980), "Stability of the boundary layer on a swept wing with wall

cooling". *AIAA J.*, Vol. 18, p. 1029.

Liepman, H.W. and Fila, G.H. (1947), "Investigation of effect of surface temperature and single roughness elements on boundary layer transition". NACA TN 1196 and NACA Rep. 890.

Liepman, H.W. (1943), "Investigations on laminar boundary-layer stability and transition on curved boundaries". NACA Adv. Conf. Rep. 3H30.

Linke, W. (1942), "Uber den stromungswiderstand einer beheizten ebenen platte". *Luftfahrtforschung*, Vol. 19, p. 157.

Mack, L.M. (1977), "Transition prediction and linear stability theory". AGARD CP-224, Paper 20.

McDonald, H. and Fish, R.W. (1973), "Practical calculations of transitional boundary layers". *Int. J. Heat Mass Trans.*, Vol. 16, p. 1729.

Meier, H.U., Michel, U. and Kreplin, H.P. (1987), "The influence of wind tunnel turbulence on boundary layer transition". *Perspectives in Turbulence Studies*, eds. H.U. Meier and P. Bradshaw, Springer-Verlag, p. 26.

Morkovin, M.V. (1969), "On the many faces of transition". *Viscous Drag Reduction*, ed C.S. Wells, Plenum Press, New York.

Morkovin, M.V. (1984), "Bypass transition to turbulence and research desiderata". *Transition to Turbulence*, NASA CP 2386, p. 161.

Moss, R. (1991), "The effects of turbulence length scale on heat transfer". D.Phil. Thesis, University of Oxford.

Narasimha, R. (1957), "On the distribution of intermittency in the transition region of a boundary layer". *J. Aero. Sci.*, Vol. 24, p. 711.

Nayfeh, A.H. and El-Hady, N.M. (1980), "Nonparallel stability of two-dimensional nonuniformly heated boundary-layer flows". *Phys. Fluids*, Vol. 23, p. 10.

Prandtl, L. (1922), "Bemerkungen über die Entstehung der Turbulenz". *Phys. Z.*, Vol. 23, p. 19.

Rayleigh, J.W.S., Baron (1913), *Scientific Papers*, Vol. VI. Cambridge University Press, Cambridge.

Reda, D.C. (1991), "Observations of dynamic stall phenomena using liquid crystal coatings". *AIAA J.*, Vol. 29, p. 308.

Redeker, G. Horstman, K.H., Köster, H. Thiede, P. and Szodruch, J. (1990), "Design of a natural laminar flow glove on a transport aircraft". AIAA Paper 90-3044.

Reshotko, E. (1976), "Boundary-layer stability and transition". *Ann. Rev. Fluid Mech.*, Vol. 8, p. 311.

Reynolds, O. (1883), "On the experimental investigation of the circumstances which determine whether the motion of water shall be direct or sinuous, and the law of resistance in parallel channels". *Phil. Trans. Roy. Soc.*, Vol. 174, p. 935.

Reynolds, O. (1895), "On the dynamical theory of incompressible viscous fluids and the determination of the criterion". *Phil. Trans. Roy. Soc.*, Vol. 186, p. 123.

Rhoades, M and Moses, W. (1991), "Thermal contact conductance between aligned, unidirectional carbon/epoxy resin composites under vacuum conditions". AIAA Paper 90-0379.

Richards, Bryan (1968), "Mechanics of boundary layer transition", AGARD-VKI Lecture series 3, Part I.

Schlichting, H. (1979), *Boundary Layer Theory, 7th ed.* McGraw-Hill, New York.

Schubauer, G.B. and Klebanoff, P.S. (1955), "Contributions on the mechanics of transition". NACA TN 3489.

Schubauer, G.B. and Skramstad, H.K. (1948), "Laminar boundary layer oscillations and stability of laminar flow". NACA TR 909.

Sohn, K.H., O'Brien, J.E. and Reshotko, E. (1989), "Some characteristics of bypass transition in a heated boundary layer". Presented at the 7th Turbulent Shear Flow Symposium, Stanford University, Aug. 1989.

Strazisar, A.J., Reshotko, E. and Prahl, J.M. (1977), "Experimental study of the stability of heated laminar boundary layers in water". *J. Fluid Mech.*, Vol. 82, p. 225.

Stuart, J.T. (1965), "Hydrodynamic Stability". *Appl. Mech. Rev.*, Vol. 18, p. 523.

Suder, K.L. and O'Brien, J.E. (1988), "Experimental study of bypass transition". NASA TM 100913.

Szodruch, J. (1991), "Viscous drag reduction on transport aircraft". AIAA Paper 91-0685.

Tani, I. (1969), "Boundary Layer Transition". *Ann. Rev. Fluid Mech.*, Vol. 1, p. 169.

Taylor, R.P., Coleman, H.W., Hosni, M.H. and Love, P.H. (1989), "Thermal boundary condition effects on heat transfer in the turbulent incompressible flat plate boundary layer". *Int. J. Heat Mass Trans.*, Vol. 32, p. 1165.

Taylor, R.P., Love, P.H., Coleman, H.W. and Hosni, M.H. (1990), "Heat transfer measurements in incompressible turbulent flat plate boundary layers with step wall temperature boundary conditions". *J. Heat Tran.*, Vol. 112, p. 245.

Thomson, K.D. (1988), "Some comments on the later stages of transition from laminar to turbulent flow in the flat plate boundary layer". *Aero. J.*, Vol. 92, p. 309.

Tollmien, W. (1929), "Uber die Entstehung der Turbulenz". English translation in NACA TM 609 (1931).

Tollmien, W. (1936), "Ein allgemeines Kriterium der Instabilität laminarer Geschwindigkeitsverteilungen. English translation in NACA TM 609 (1936).

Touloukian, Y.S., Powell, R.W., Ho, C.Y. and Klemens, P.G. (1970), *Thermophysical Properties of Matter*, Vol. 2. IFI/Plenum, New York.

van Driest, E.R. and Blumer, C.B. (1963), "Boundary-layer transition: freestream turbulence and pressure gradient effects". *AIAA J.*, Vol. 1, p. 1303.

Walker, G.J. and Gostelow, J.P. (1989), "Effects of adverse pressure gradients on the nature and length of boundary layer transition". ASME Paper 89-GT-211.

Walton, T.W. (1990), "Lifetime evaluation of encapsulated liquid crystals". Internal Rep., Dept. Engr. Sci., University of Oxford.

Walton, T.W. (1991), Dept. Engr. Sci., University of Oxford. Private communication, Dec., 1991.

Wang, Z., Ireland, P.T. and Jones, T.V. (1990), "A technique for measuring convective heat tranfer at rough surfaces". ASME Paper 90-GT-300.

Wazzan, A.R., Okamura, T. and Smith, A.M.O. (1968), "The stability of water flow over heated and cooled flat plates". *J. Heat Tran.*, Vol. 90, p. 109.

White, F.M. (1991), *Viscous Fluid Flow, 2nd ed.*, McGraw-Hill,New York.

Young, A.D. and Paterson, J.H. (1981), "Aircraft excrescence drag'. AGARDograph 264.

Young, A.D. (1989), *Boundary Layers*. BSP Profession Books, Oxford.

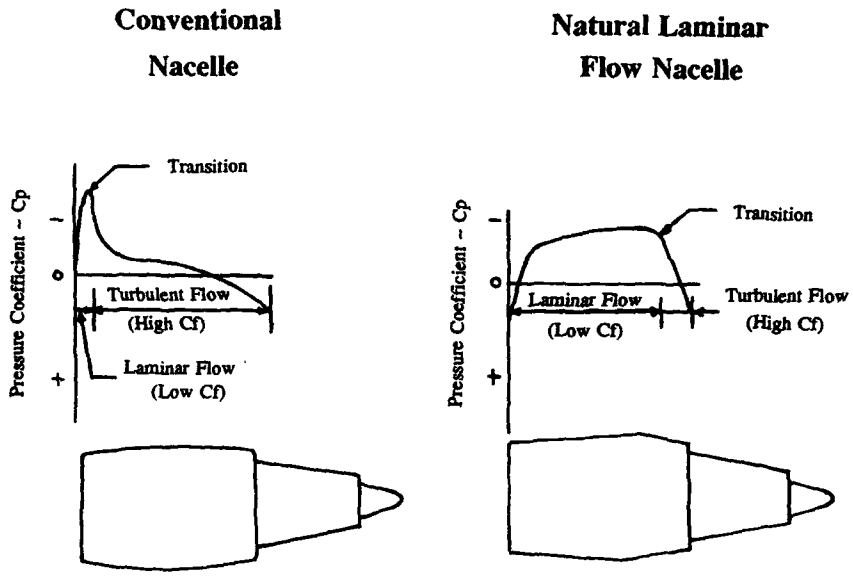

Figure 1.1 Extended laminar flow due to favourable pressure gradient on engine nacelle, after Hastings, et al. (1987).

A/C type	Range (NM)	Flights/ year	Fuel burn savings (1 A/C, 1 year)	Fuel burn savings (20 A320 or 10 A340)	Fuel burn savings (15 years)	Cost savings (M$)
A320	500	2175	70 t.	1400 t.	21000 t.	3.5 (1)
						7.0 (2)
	2000	802	84 t.	1680 t.	25200 t.	4.2 (1)
						8.4 (2)
A340	3000	657	220 t.	2200 t.	33000 t.	5.5 (1)
						11.0 (2)
	6000	4000	310 t.	3100 t.	46500 t.	7.8 (1)
						15.6 (2)

(1) 0.5 $/USG
(2) 1.0 $/USG

Figure 1.2 Savings due to 1% reduction of fuel burned, after Szodruch (1991).

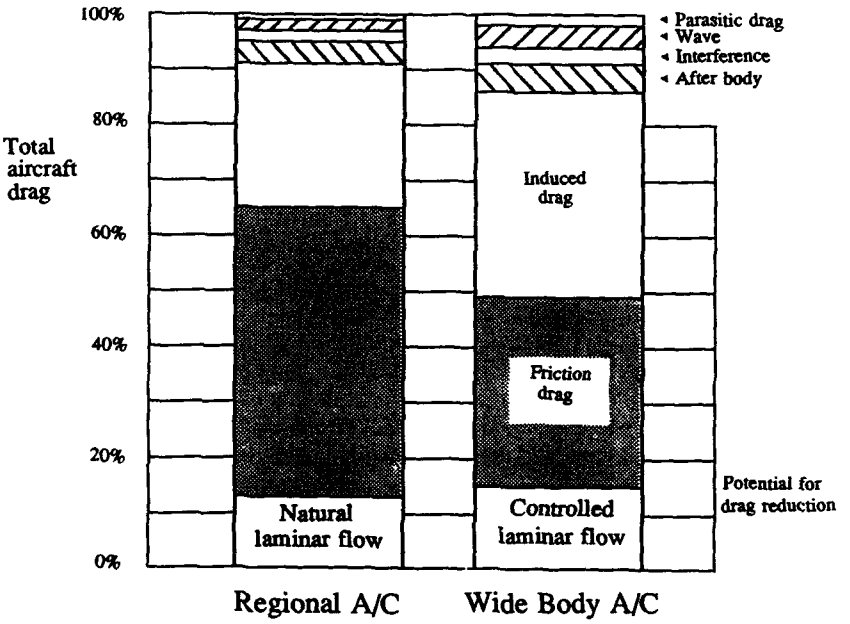

Figure 1.3 Breakdown of aircraft drag during cruise, after Szodruch (1991).

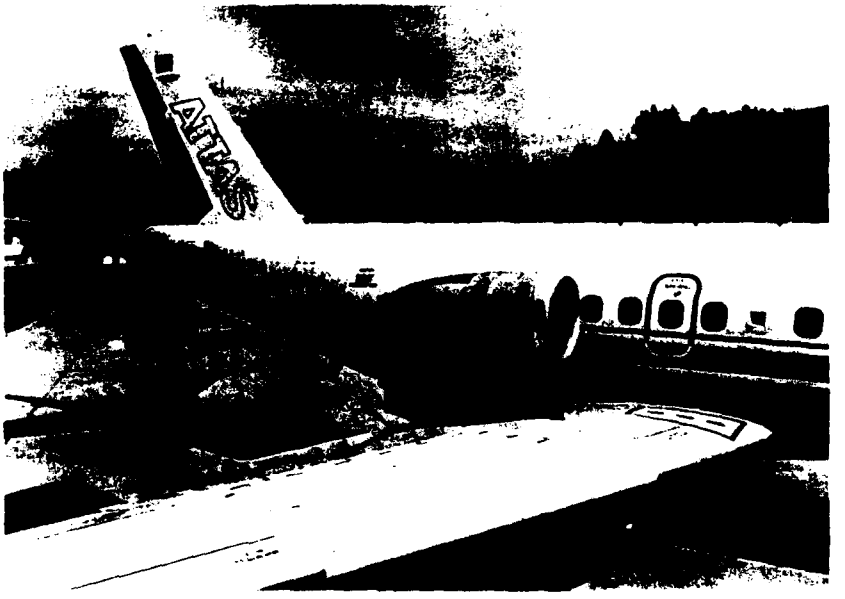

Figure 1.4 VFW-614 with Rolls-Royce M45 turbofan engines. Flight test vehicle for *natural laminar flow* nacelle.

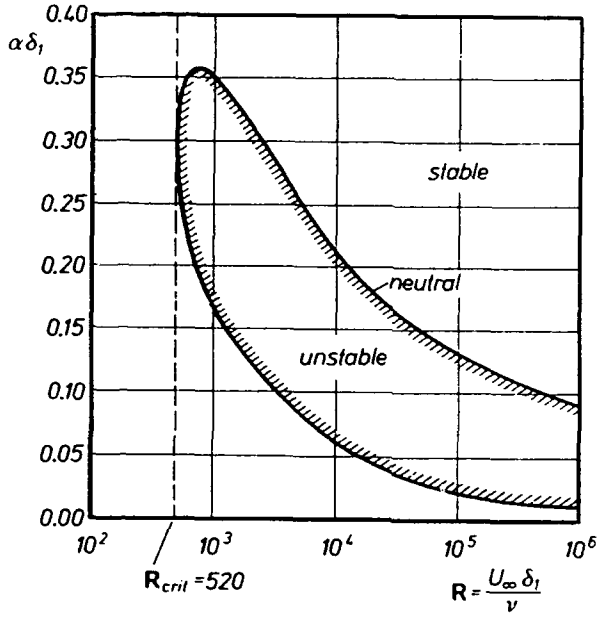

Figure 1.5 Curve of neutral stability for a boundary on a flat plate at zero incidence (Blasius profile). Figure according to Schlichting (1979); theory by Tollmien (1929).

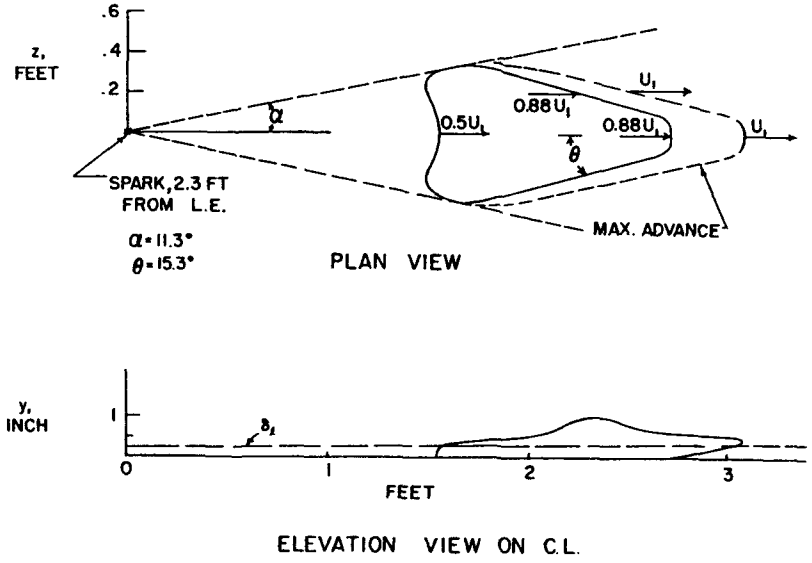

Figure 1.6 Turbulent spot initiated by electric spark between needle electrode and surface, after Schubauer and Klebanoff (1955).

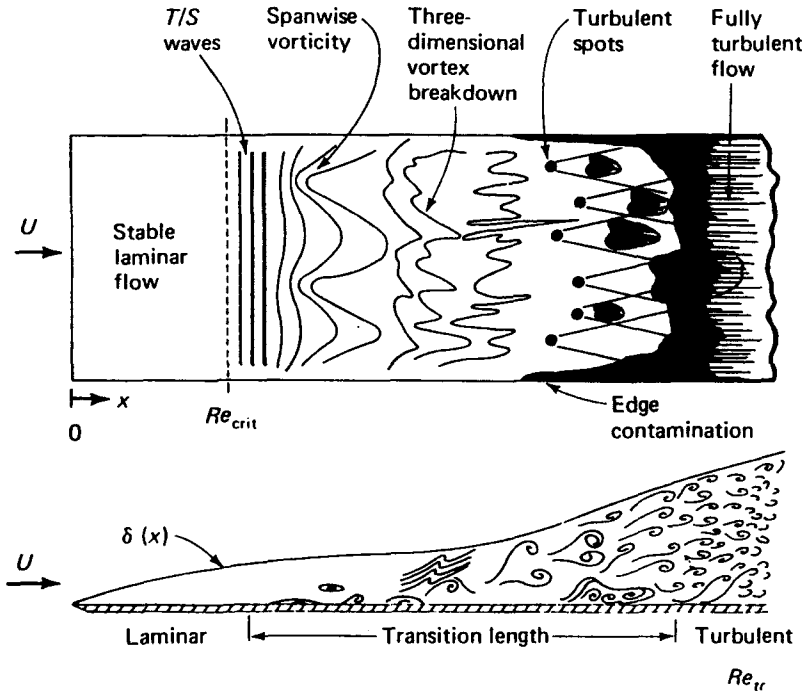

Figure 1.7 Transition via the T-S path--from White (1991)

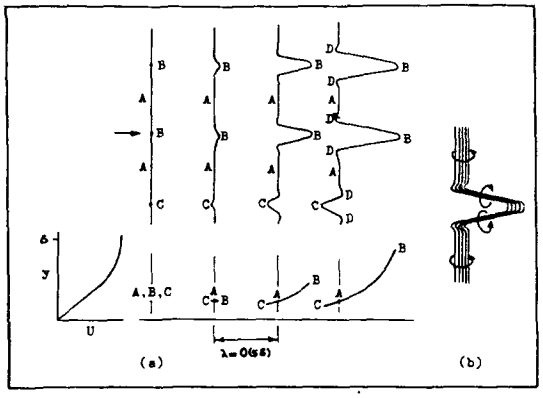

Figure 1.8 Three dimensional development of a single wage, depicted in consecutive wave periods--from Thomson (1988)

Figure 1.9 Three dimensional development of stream-wise vortices downstream of a transverse trip wire in a laminar boundary layer. Flow visualisation by dye in water, after Hama *et* al. (1957).

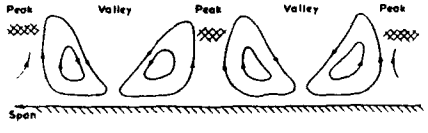

Figure 1.10 Schematic form of stream-wise vortex system, after Stuart (1965).

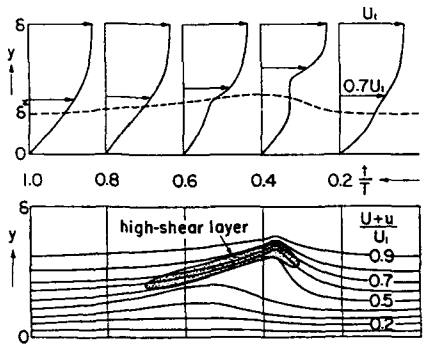

Figure 1.11 Instantaneous velocity profiles across boundary layer and contour of high-shear stress layer. Measurements of Kovasznay et al. (1962).

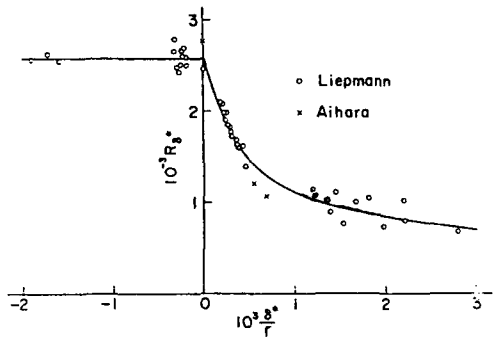

Figure 1.12 Effect of surface curvature on transition Reynolds number in zero pressure gradient flow, after Tani (1969). Negative values of δ^*/r represent convex curvature.

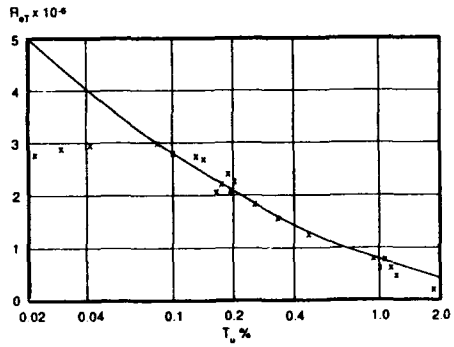

Figure 1.13 Transition Reynolds number as a function of free-stream turbulence. Experimental results by Dryden (1959). Line represents empirical correlation of Mack (1977). Figure taken from Young (1989).

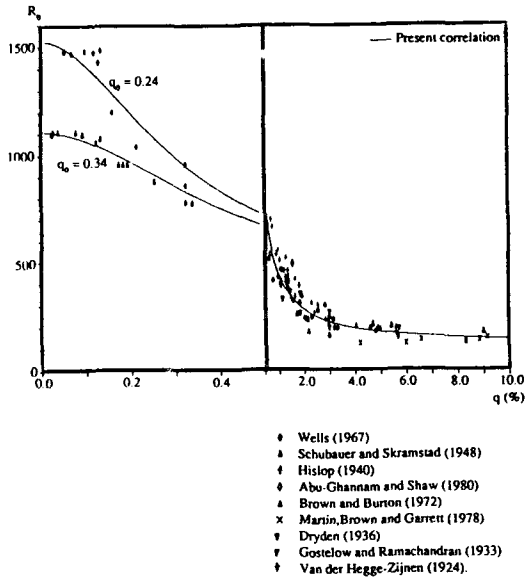

Figure 1.14 Effect of turbulence on transition Reynolds number. Correlation from Govindarajan and Narasimha (1991). Note expanded scale at low q.

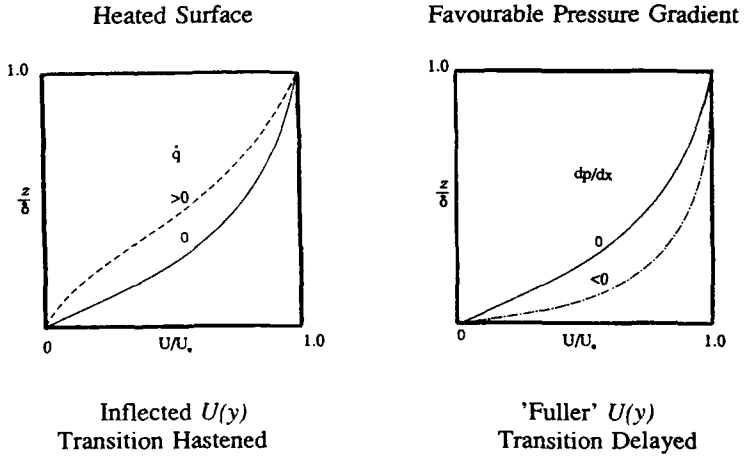

Figure 1.15 Effects of heating and favourable pressure gradient on transition in an air boundary layer.

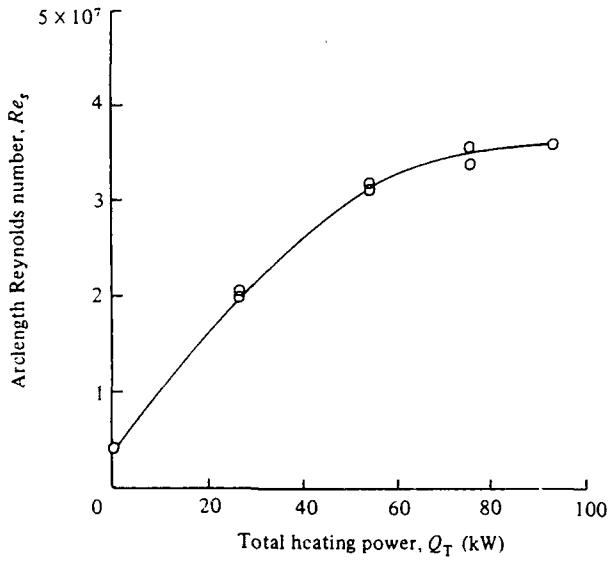

Figure 1.16 Experimentally observed influence of heating on transition Reynolds numbers, after Lauchle and Gurney (1984). Axisymmetric body in water.

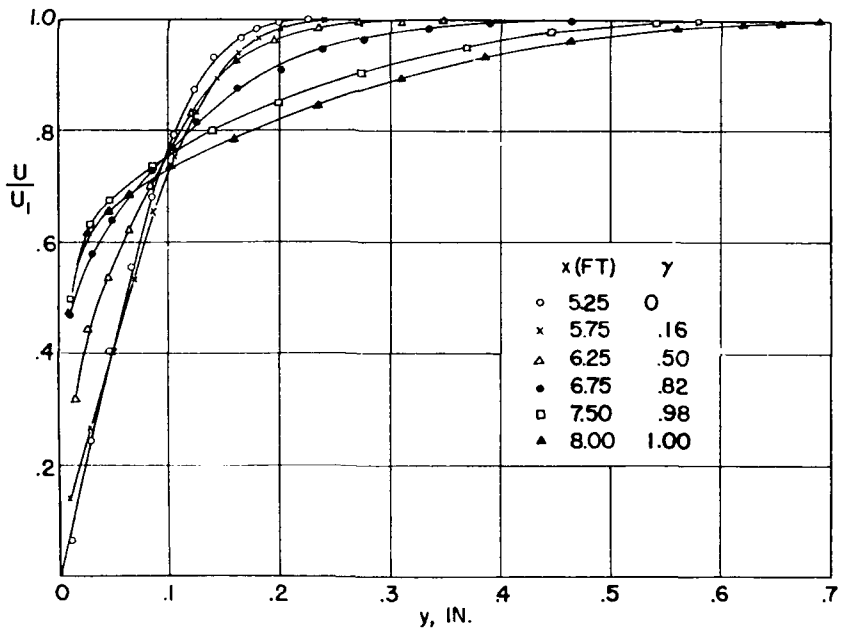

Figure 1.17 Flat plate boundary layer velocity profiles in the transition region, as measured by Schubauer and Klebanoff (1955).

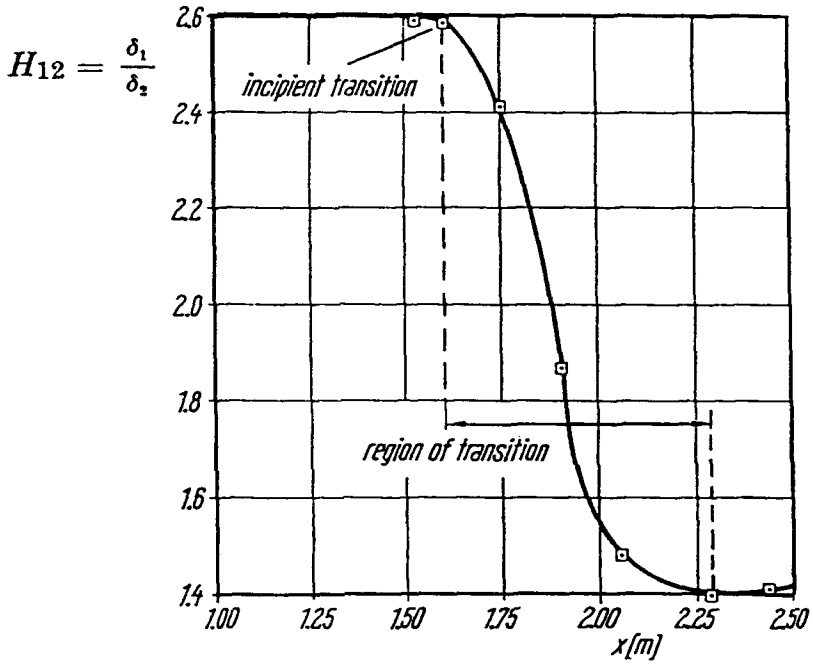

Figure 1.18 Change in the shape factor H_{12} of the boundary layer for a flat plate in the transition region as measured by Schubauer and Klebanoff (1955) and taken from Schlichting (1979).

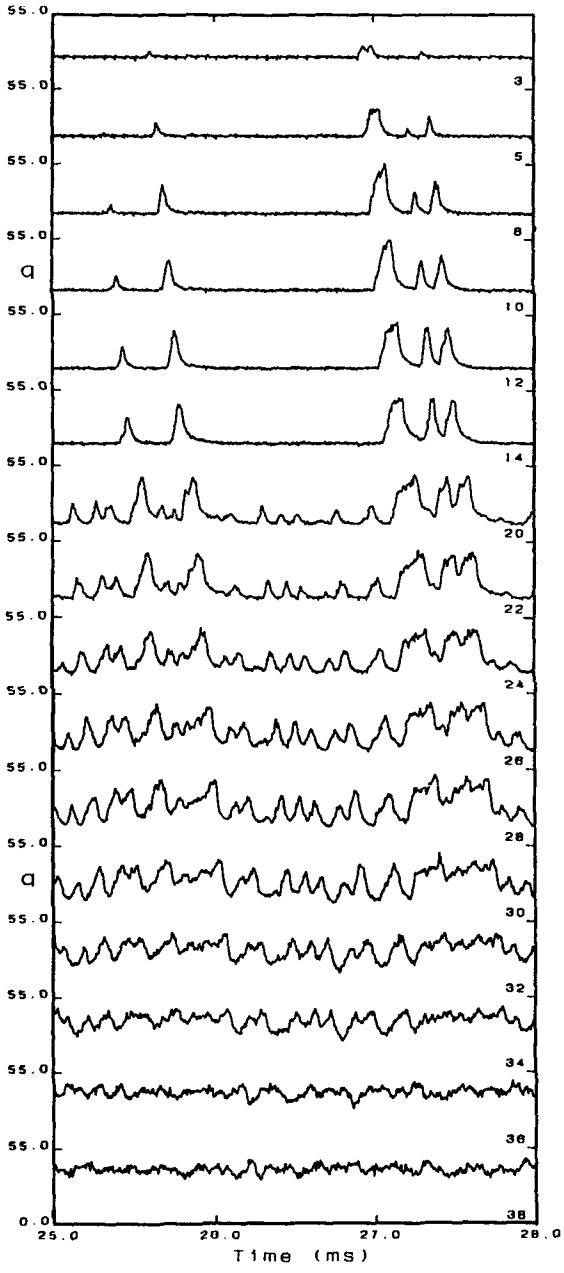

Figure 1.19 Transition from laminar to turbulent flow as indicated by successive thin films, after Clark, et al. (1991). Intermittency ≈ 0 at first gage and ≈ 1 at last gage.

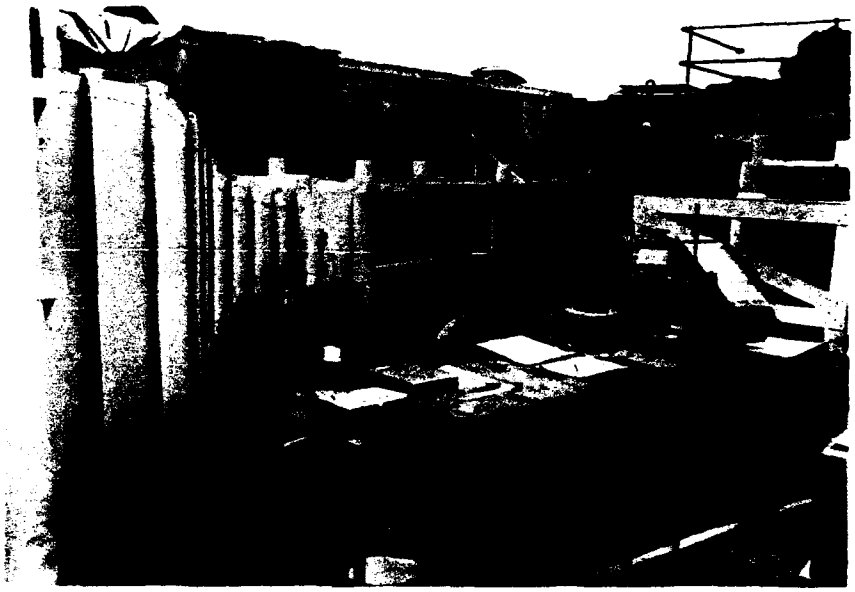

Figure 2.1 Low speed wind tunnel and general experimental apparatus.

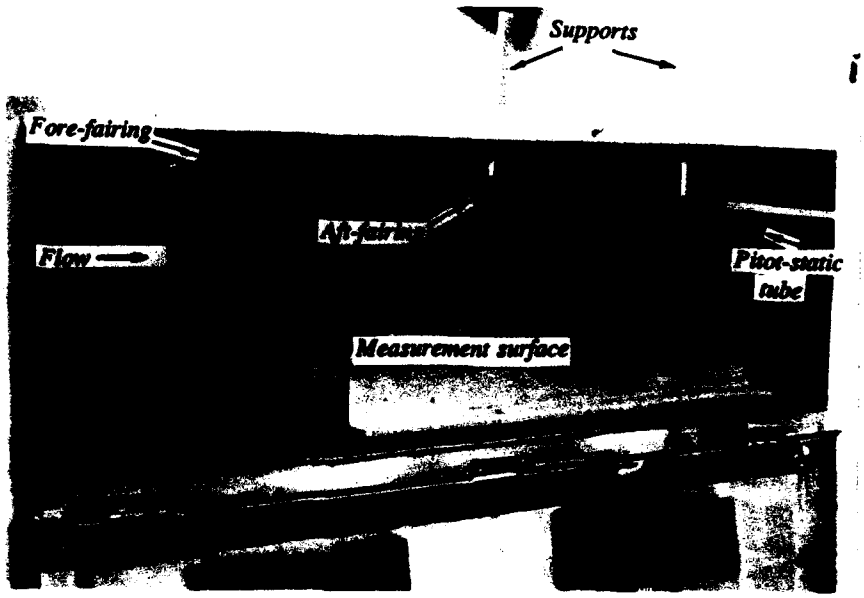

Figure 2.2 Pressure Fairing.

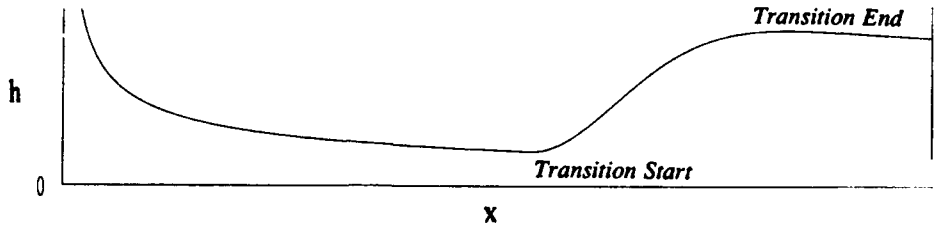

a. Typical heat transfer distribution.

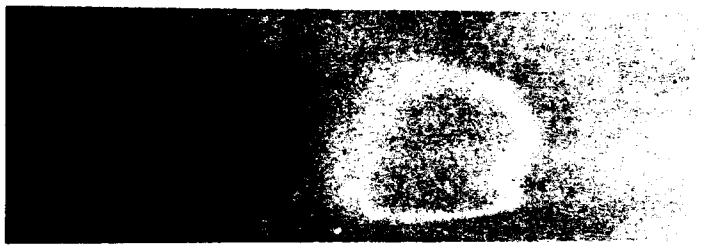

b. Low heating showing transition start.

c. High heating showing transition end.

Figure 2.3 The use of temperature sensitive liquid crystal for transition detection.

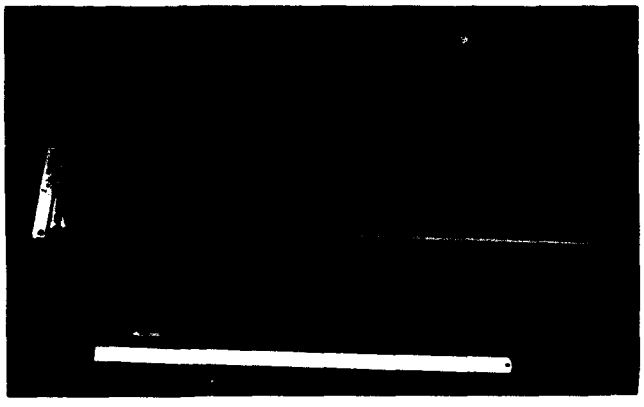

Figure 2.4 Flat plate and aluminium heater used for heat transfer experiments (flow right to left, 600 mm ruler shown).

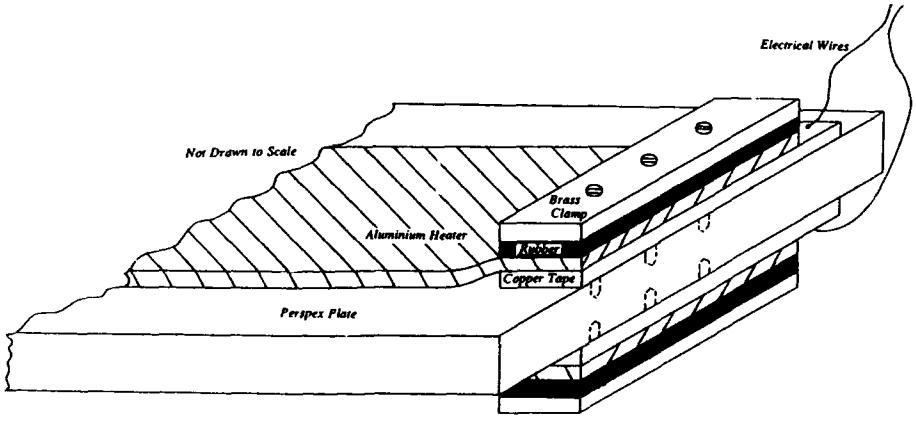

Figure 2.5 Electrical contact to aluminium heater.

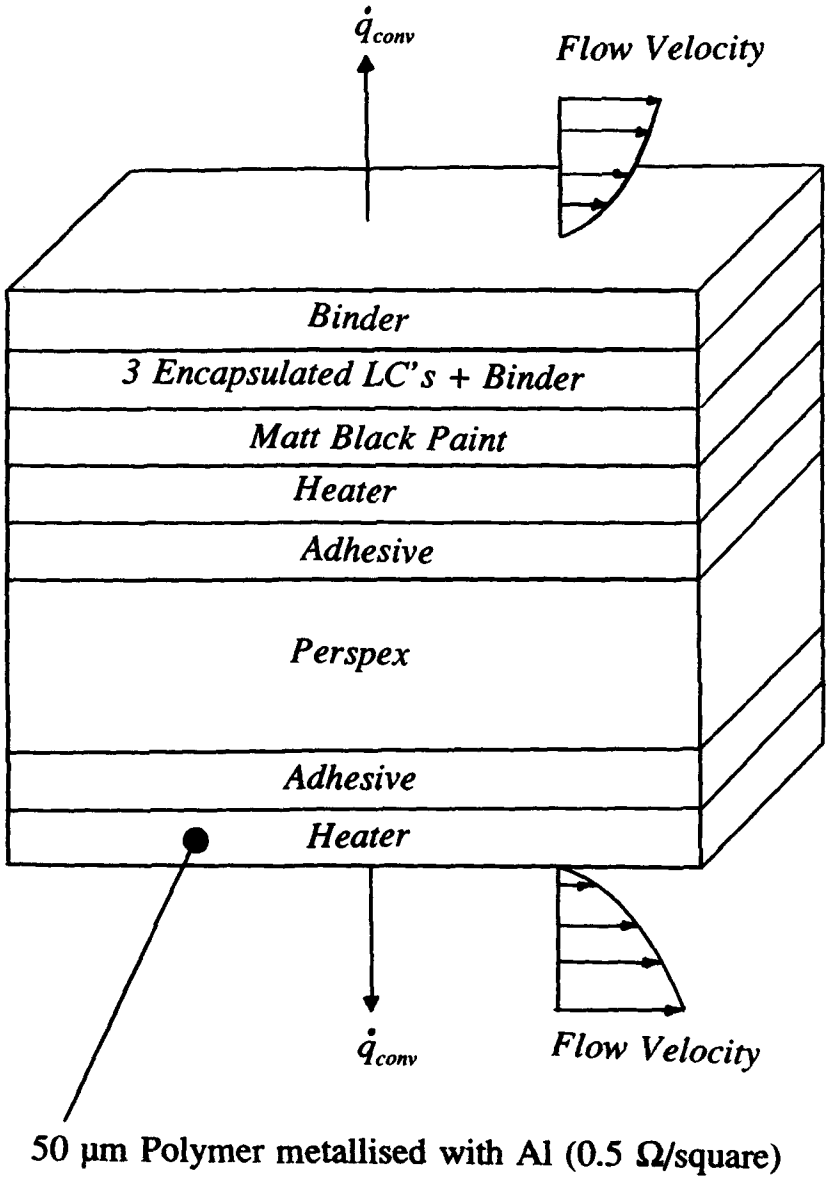

Figure 2.6 Liquid crystal/aluminium heater packaging arrangement.

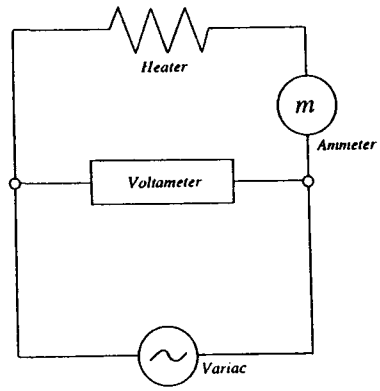

Figure 2.7 Electrical arrangement.

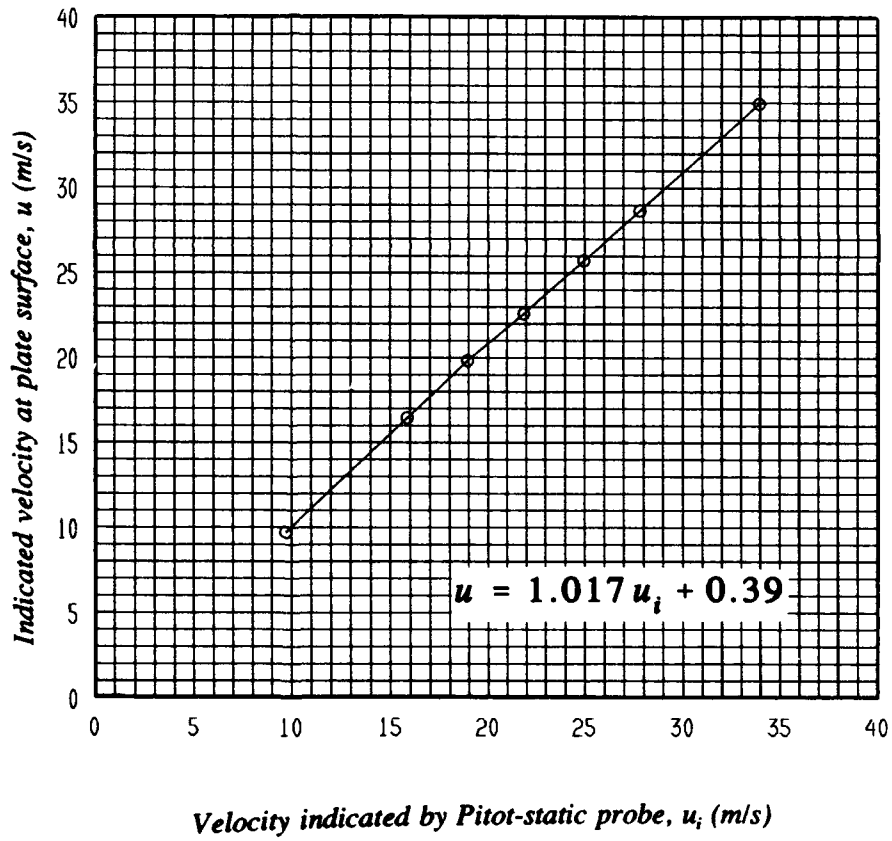

Figure 2.8 Measured vs. actual free-stream velocity.

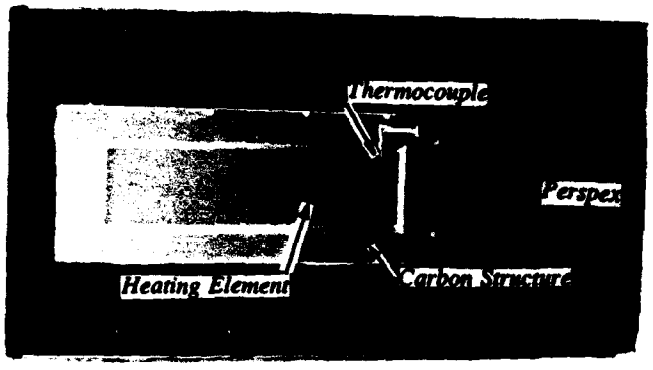

Figure 2.9 Carbon heater mounted in perspex plate (upper surface).

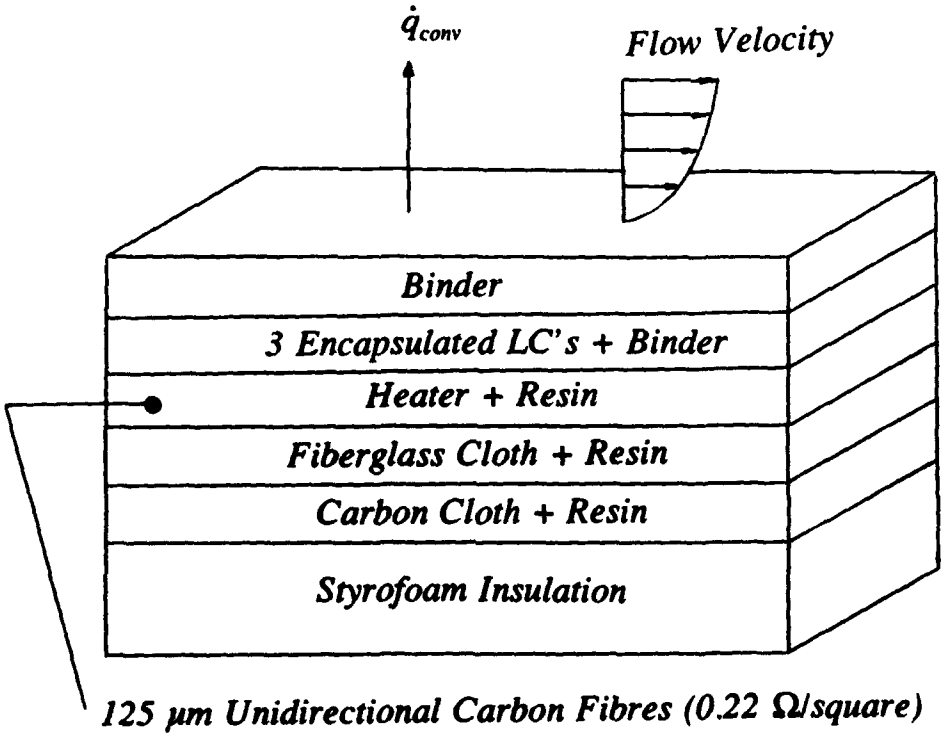

Figure 2.10 Liquid crystal/carbon-fibre heater packaging arrangement.

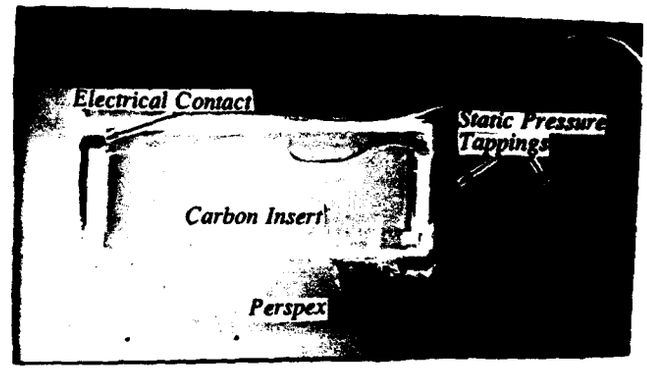

Figure 2.11 Carbon heater mounted in perspex plate (lower surface). Note: styrofoam insulation has been removed.

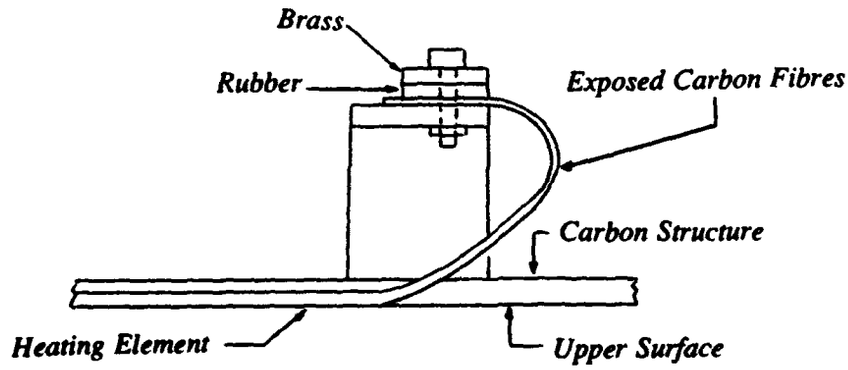

Figure 2.12 Cross section of electrical contact on carbon heater.

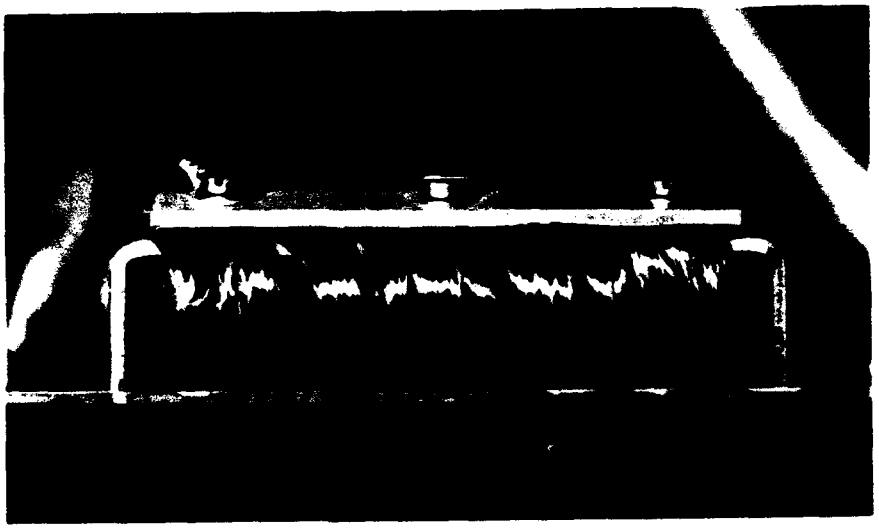

(a) *Before soaking exposed unidirectional carbon fibres in conducting paint.*

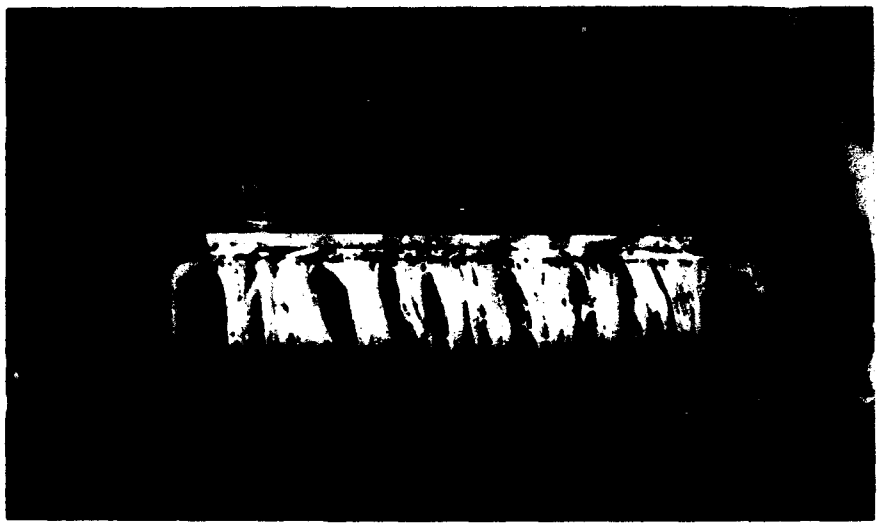

(b) *After soaking exposed unidirectional carbon fibres in conducting paint.*

Figure 2.13 Electrical contact on carbon heater.

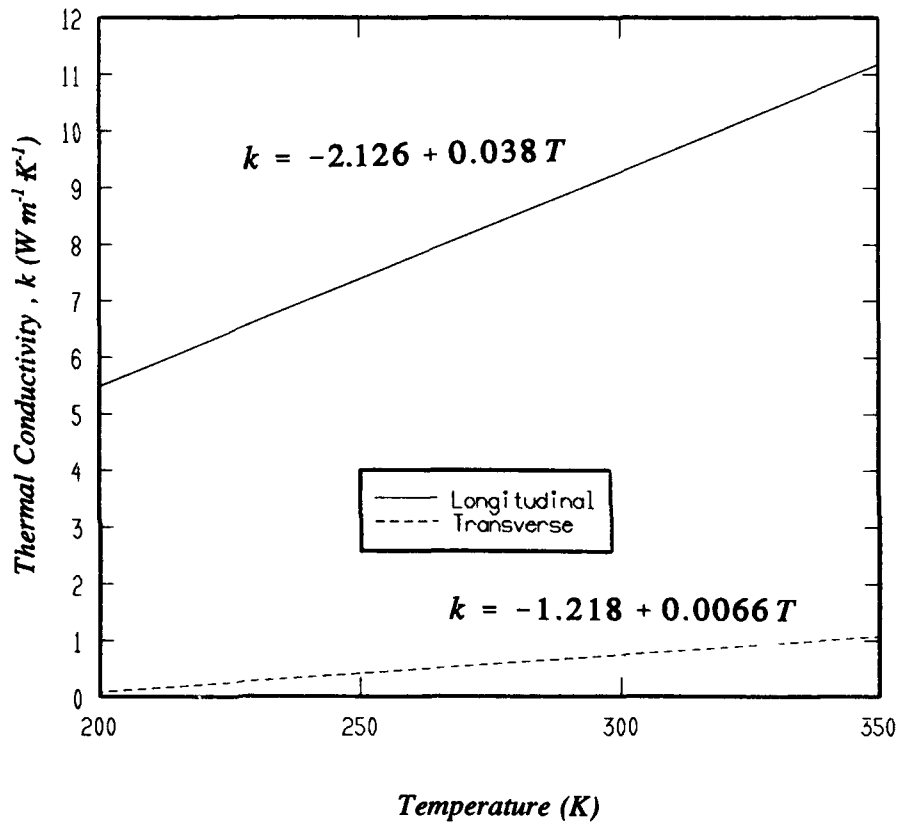

Figure 2.14 Variation of thermal conductivity with temperature for unidirectional carbon fibres, after Rhodes and Moses (1991).

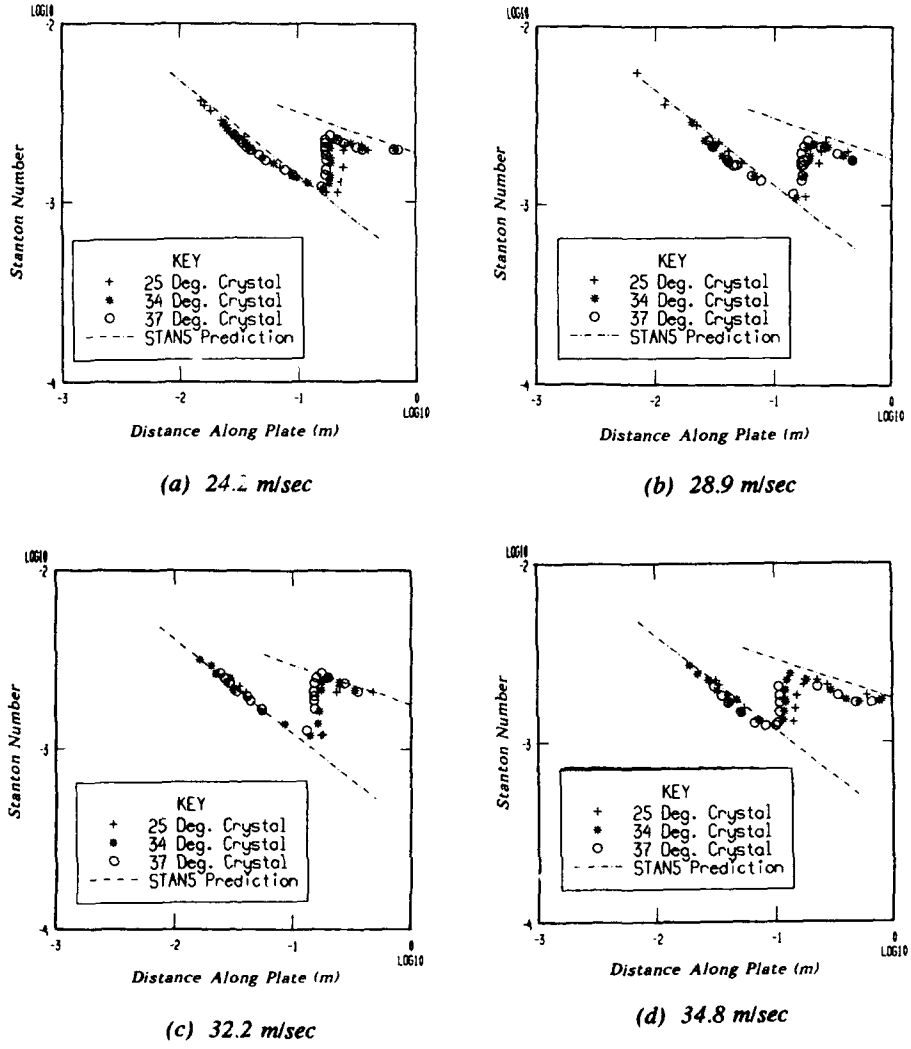

Figure 3.1 Stanton number distributions on heated plate compared with laminar and turbulent predictions.

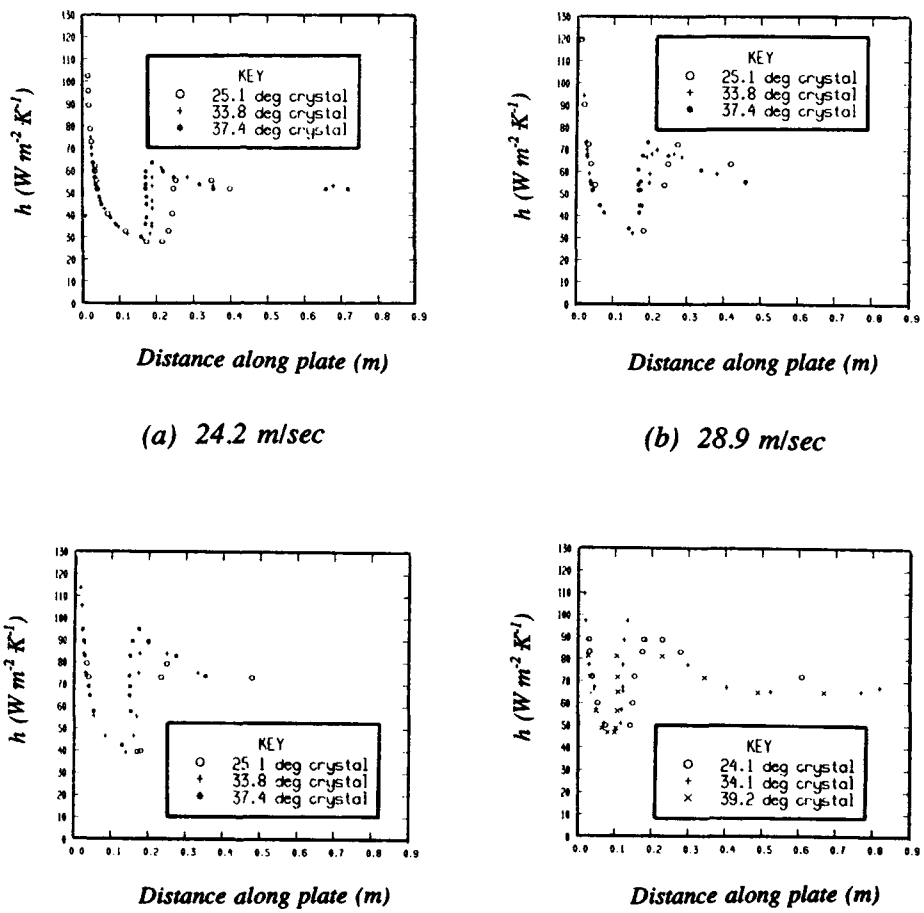

Figure 3.2 Heat transfer distribution on heated plate (aluminium heater).

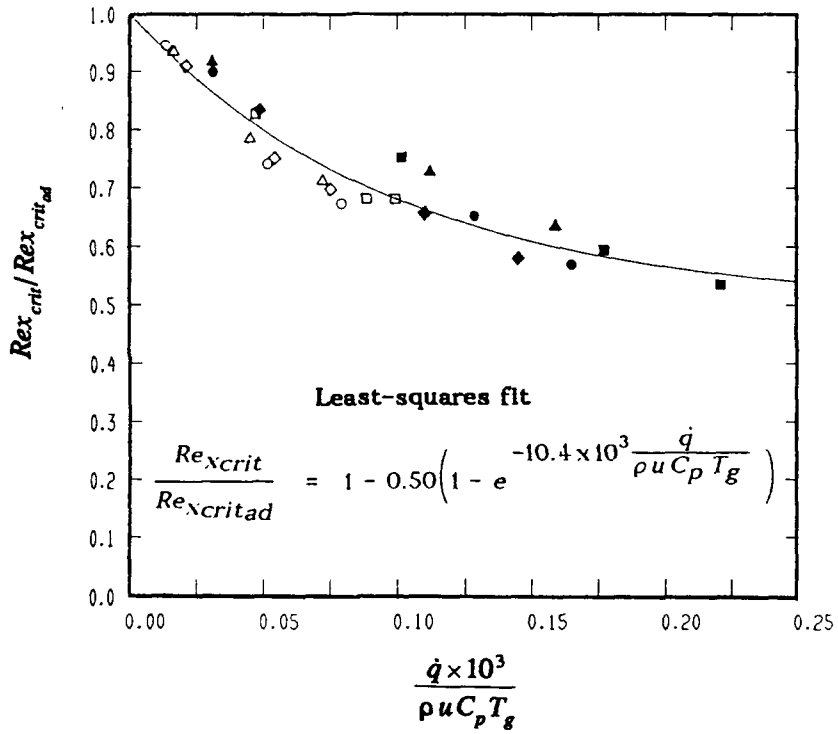

Figure 3.3 Influence of heating on transition location. □ 24.2 m/s, ◇ 28.9 m/sec, △ 32.2 m/sec, ○ 34.8 m/sec. Open symbols--transition start. Closed symbols--transition end. Solid line--least squares fit to data.

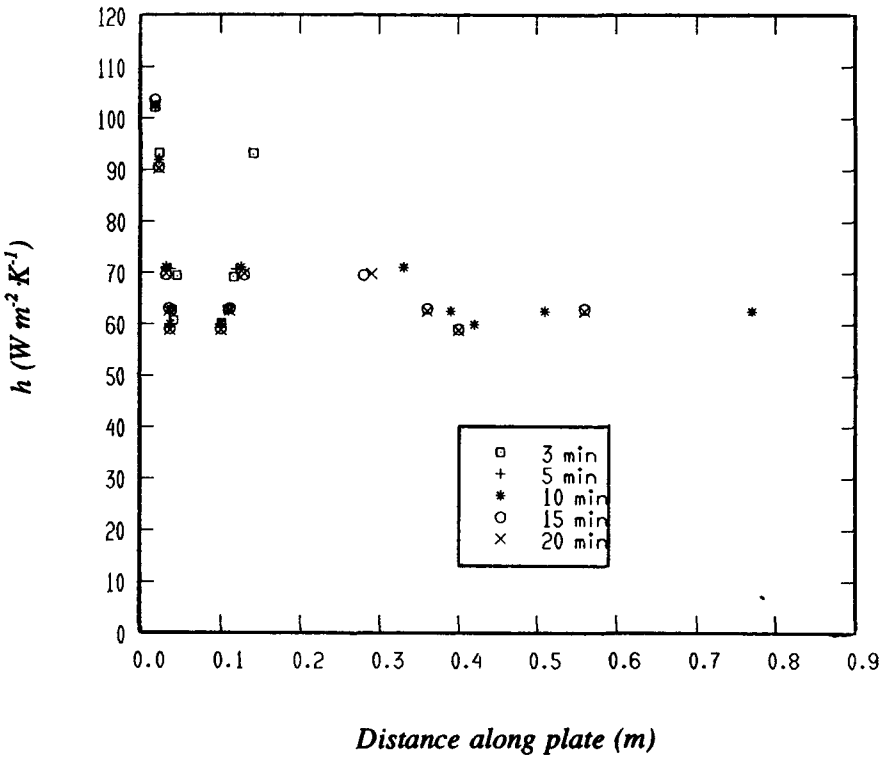

Figure 3.4 Time required for aluminium plate to reach thermal stability. Flow speed = 28.4 m/sec.

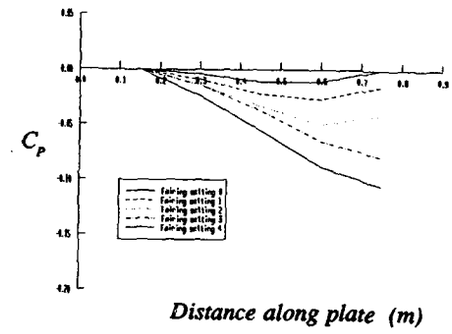

(a) Nominal speed = 22 m/sec.

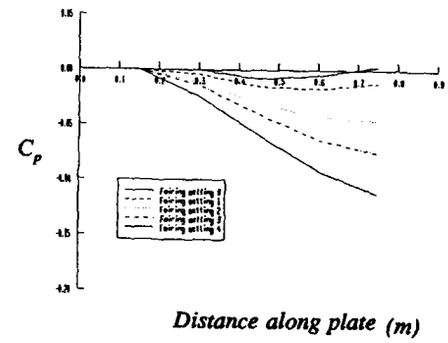

(b) Nominal speed = 28 m/sec.

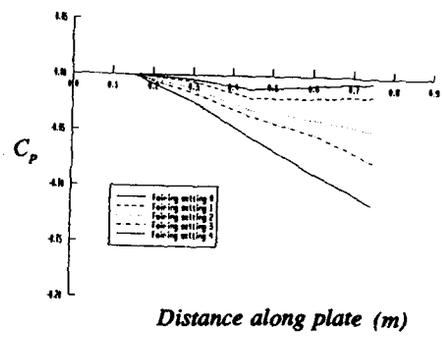

(c) Nominal speed = 35 m/sec.

Figure 3.5 Favourable pressure gradient on flat plate.

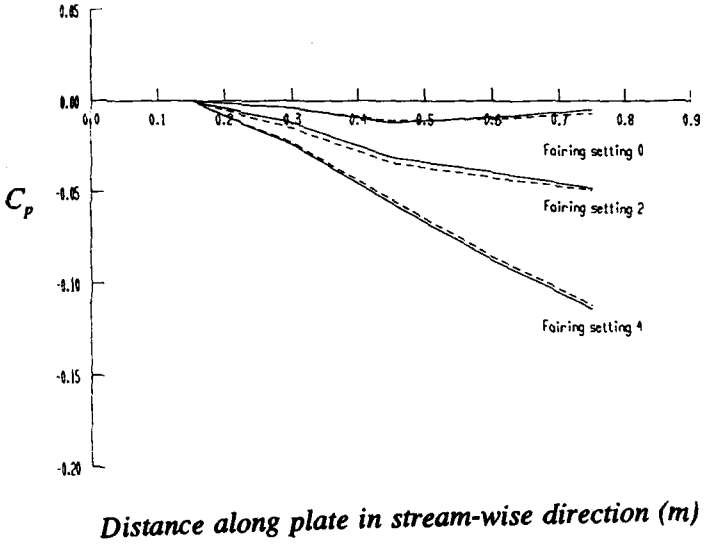

Figure 3.6 Repeatability of favourable pressure gradients. Nominal speed = 35 m/sec. Broken and solid lines represent different tests.

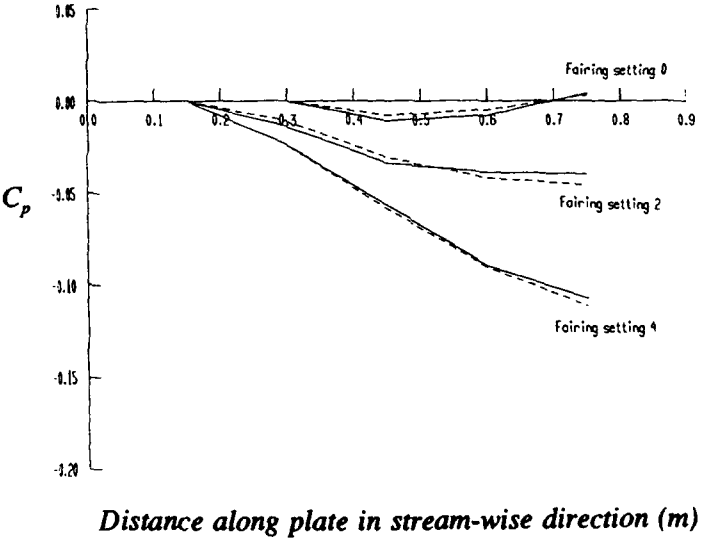

Figure 3.7 Repeatability of favourable pressure gradients. Nominal speed = 28 m/sec. Broken and solid lines represent different tests.

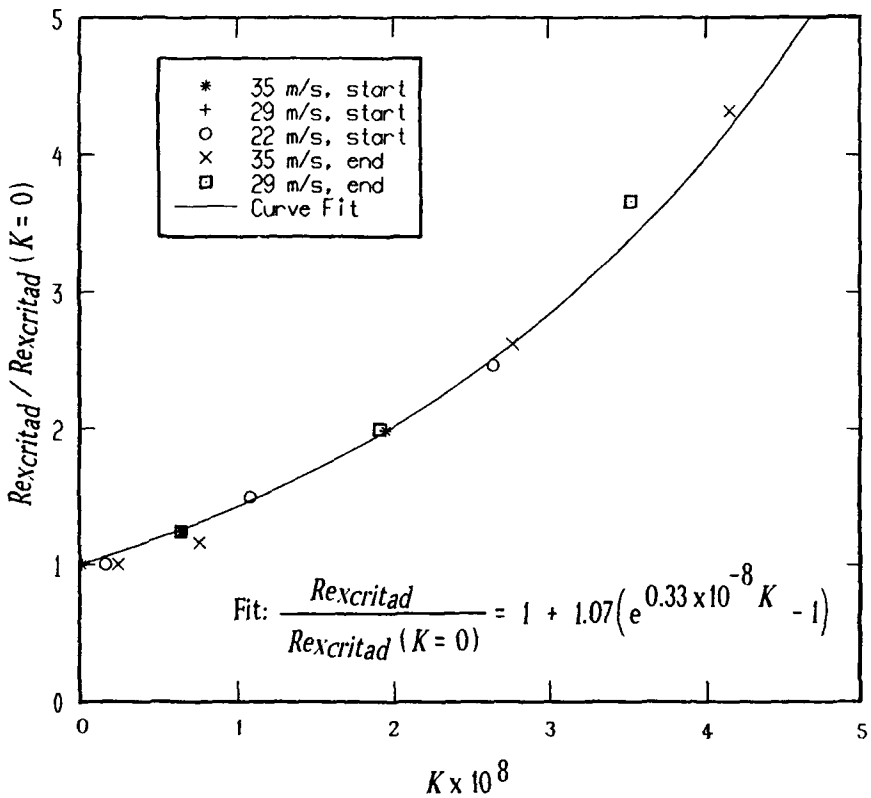

Figure 3.8 Variation in adiabatic transition location with pressure gradient.

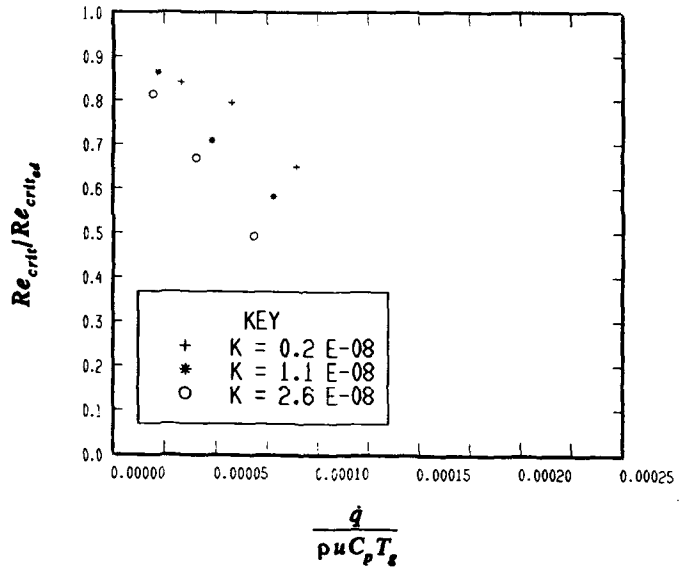

Figure 3.9 Influence of combined heating and favourable pressure gradient on transition location. Transition start, condition 1 (nominal oncoming speed = 22 m/sec).

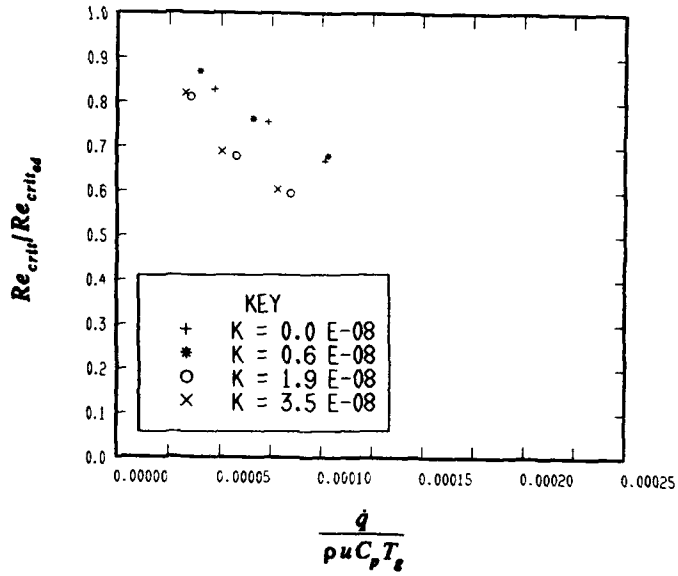

Figure 3.10 Influence of combined heating and favourable pressure gradient on transition location. Transition start, condition 2 (nominal oncoming speed = 28 m/sec).

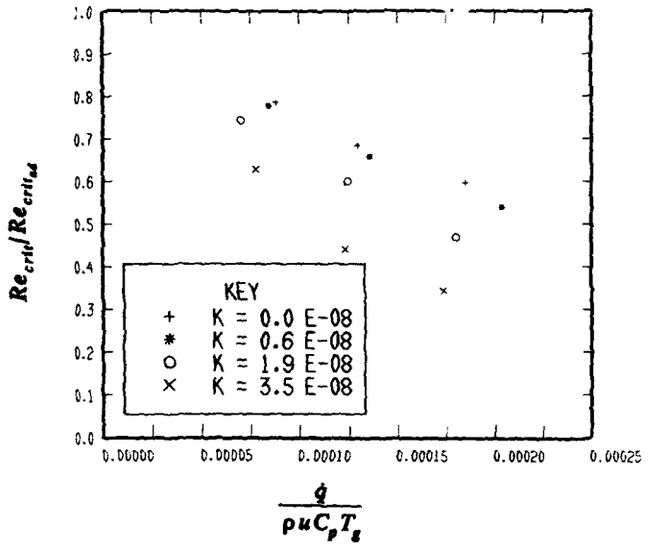

Figure 3.11 Influence of combined heating and favourable pressure gradient on transition location. Transition end, condition 2 (nominal oncoming speed = 28 m/sec).

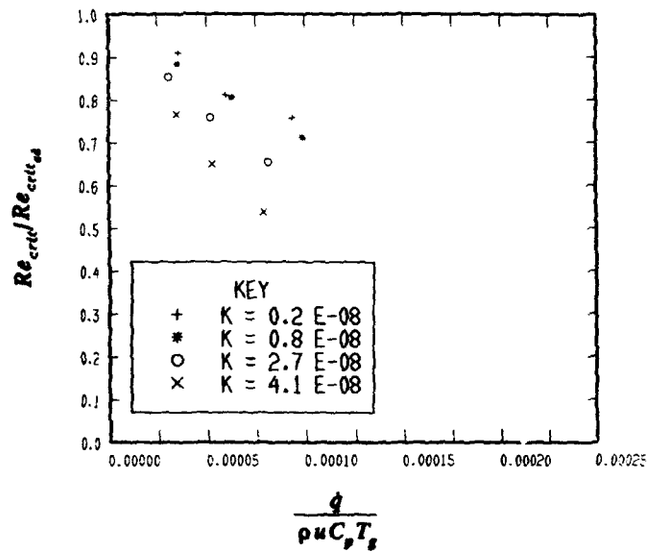

Figure 3.12 Influence of combined heating and favourable pressure gradient on transition location. Transition start, condition 3 (nominal oncoming speed = 35 m/sec).

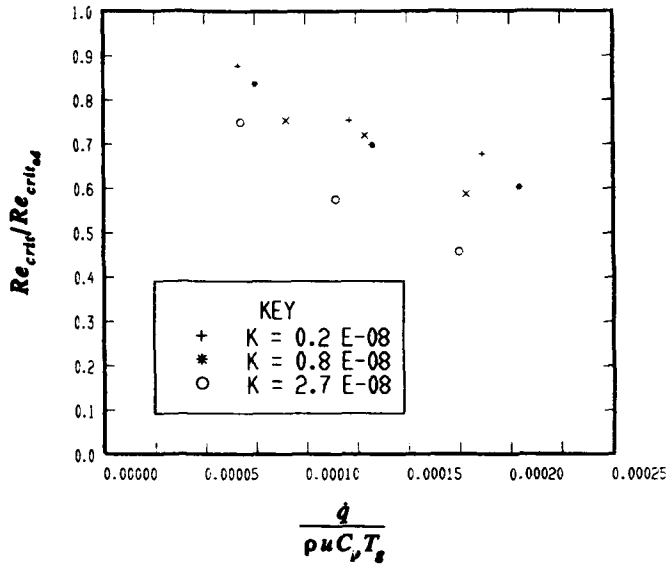

Figure 3.13 Influence of combined heating and favourable pressure gradient on transition location. Transition end, condition 3 (nominal oncoming speed = 35 m/sec).

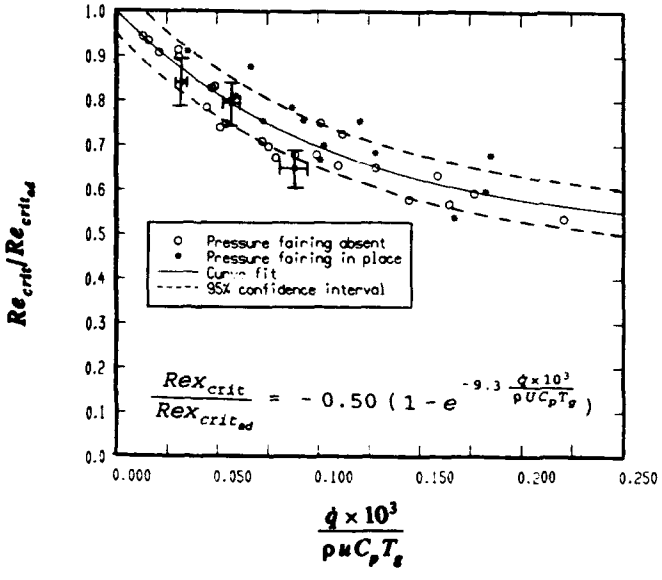

Figure 3.14 Influence of heating on transition. Zero pressure gradient.

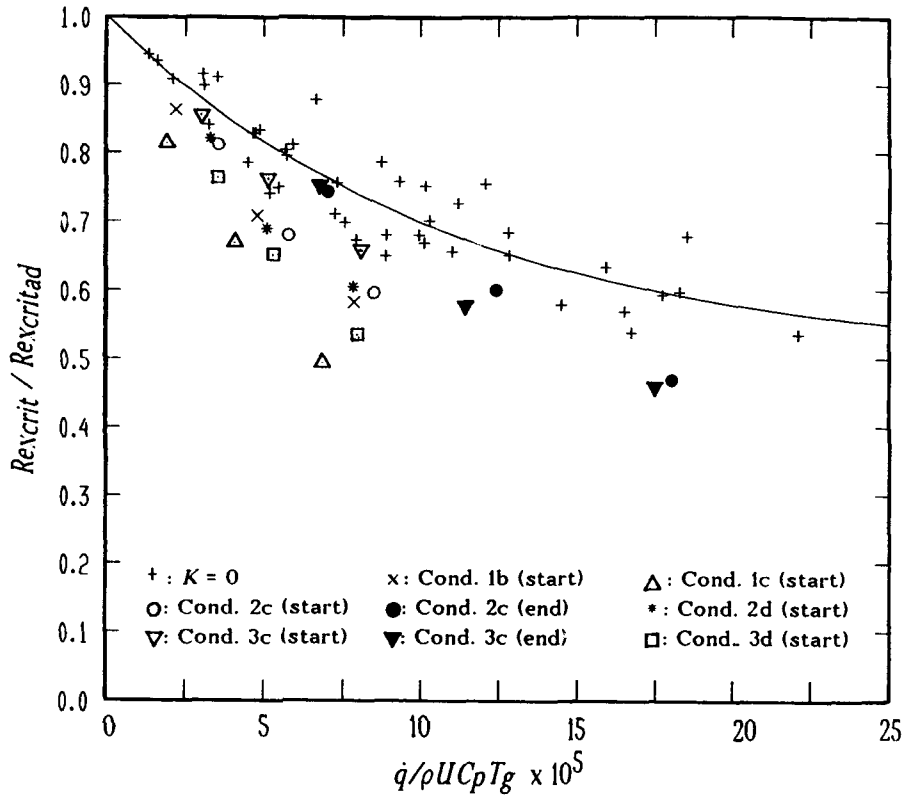

Test Conditions

Flow Condition	Oncoming Speed m/s	$K \times 10^8$	Air Temperature, T_g C
1a	22.3	0.2	17
1b	22.3	1.1	17
1c	21.9	2.6	17
2a	28.7	0.0	13
2b	28.4	0.6	13
2c	27.8	1.9	13
2d	27.3	3.5	13
3a	35.0	0.2	16
3b	35.0	0.8	16
3c	34.1	2.7	14
3d	33.3	4.1	11

Figure 3.15 Influence of heating and pressure gradient on transition location.

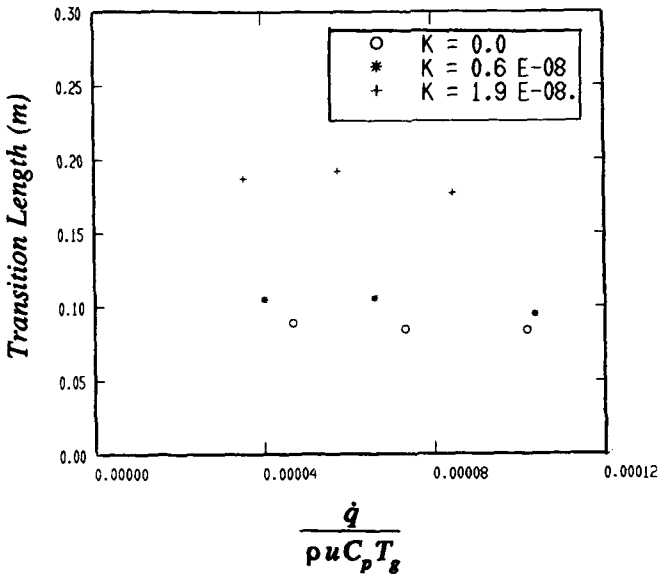

(a)

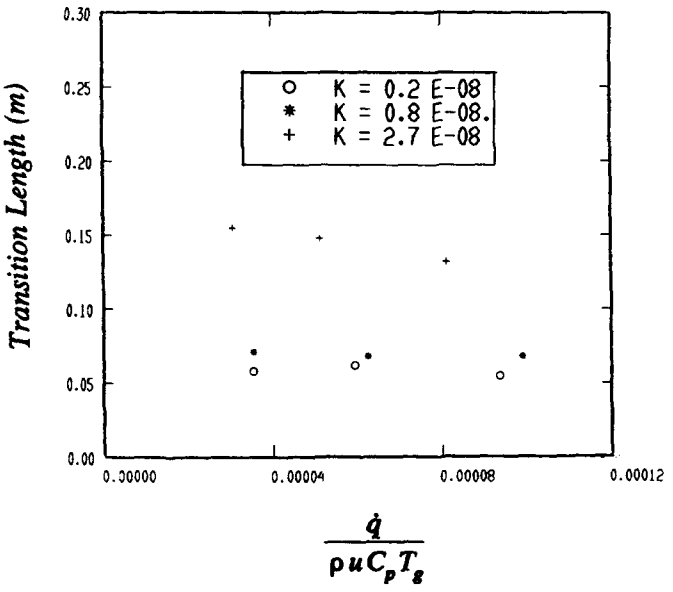

(b)

Figure 3.16 Influence of heating and pressure gradient on transition length.

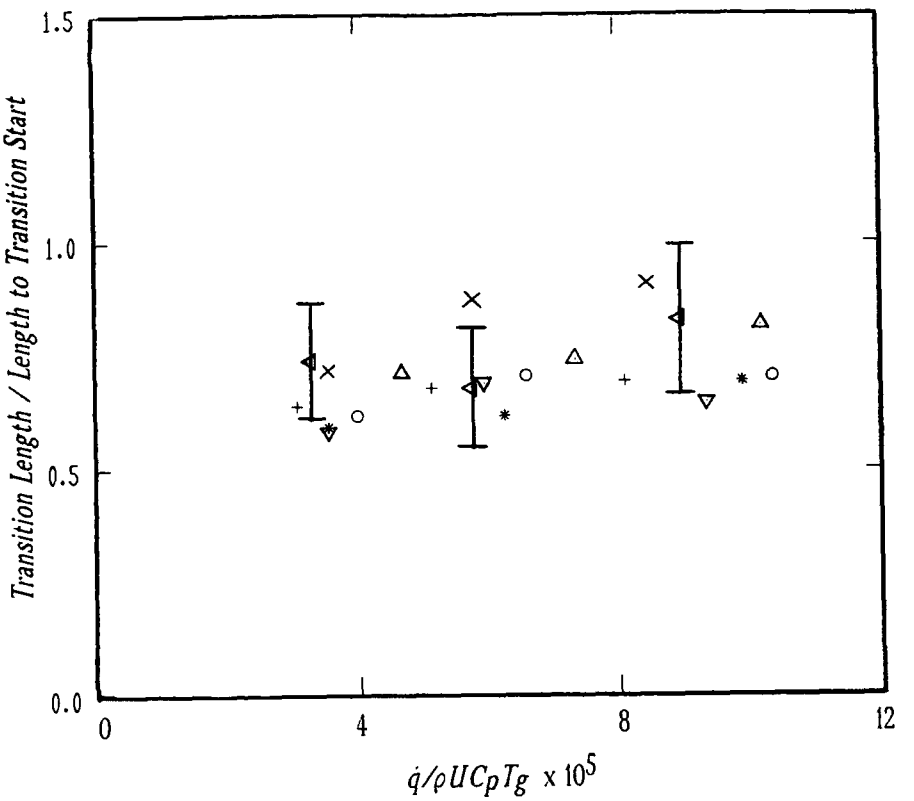

Oncoming Speed m/s	$K \times 10^8$	Air Temperature, T_g C	Figure Key
22.3	0.2	17	◁
28.7	0.0	13	△
28.4	0.6	13	○
27.8	1.9	13	×
35.0	0.2	16	▽
35.0	0.8	16	✱
34.1	2.7	14	+

Figure 3.17 Influence of heating and pressure gradient on normalised transition length.

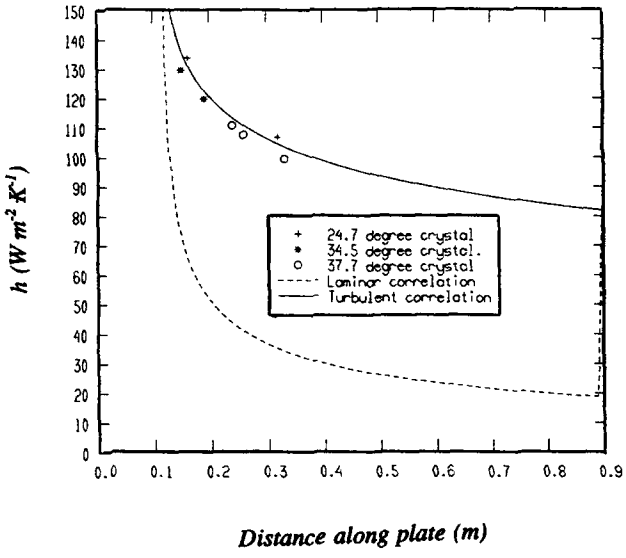

Figure 3.18 Heat transfer distribution on carbon heater. Flow speed = 34.3 m/sec.

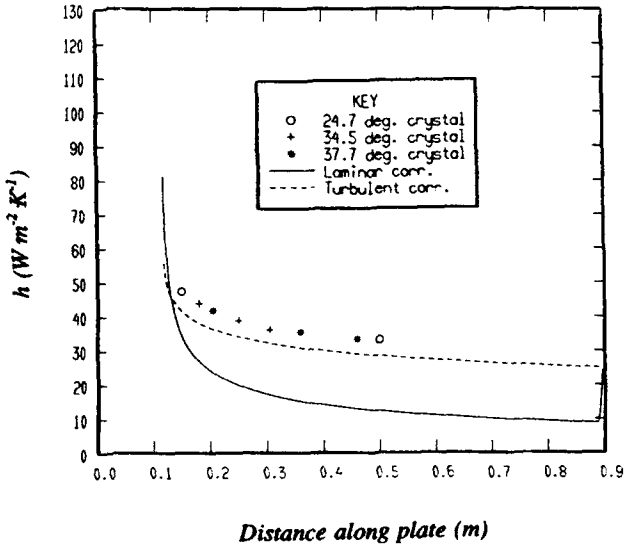

Figure 3.19 Heat transfer distribution on carbon heater. Flow speed = 34.3 m/sec.

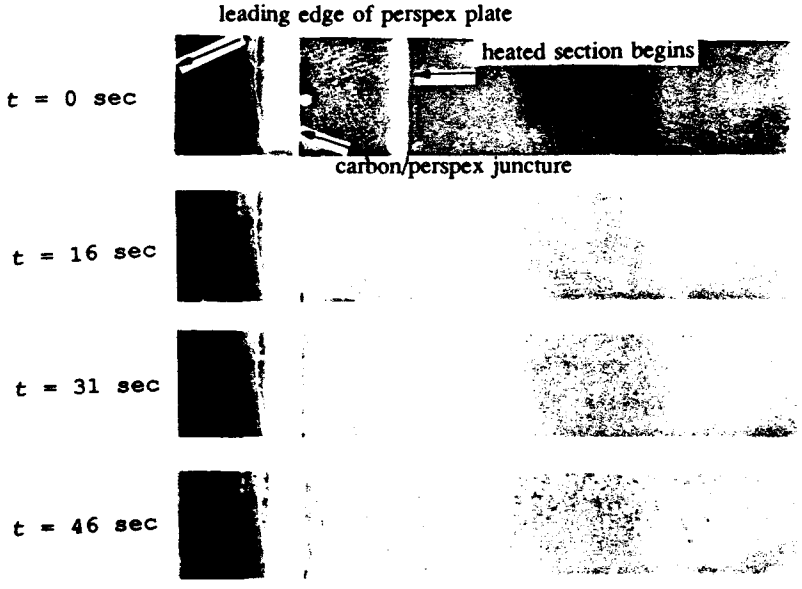

Figure 3.20 Shear sensitive liquid crystal experiment on unheated carbon plate.

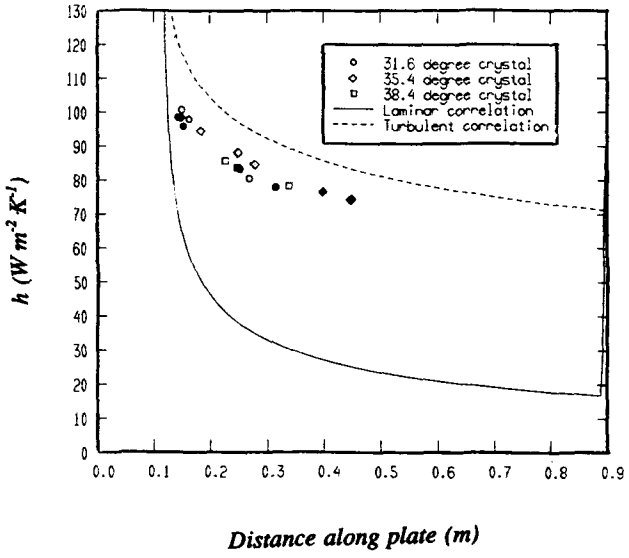

Figure 3.21 Comparison of heat transfer distributions for tripped and untripped boundary layers on carbon plate. Open symbols--untripped. Closed symbols--tripped. Flow speed = 28.9 m/sec.

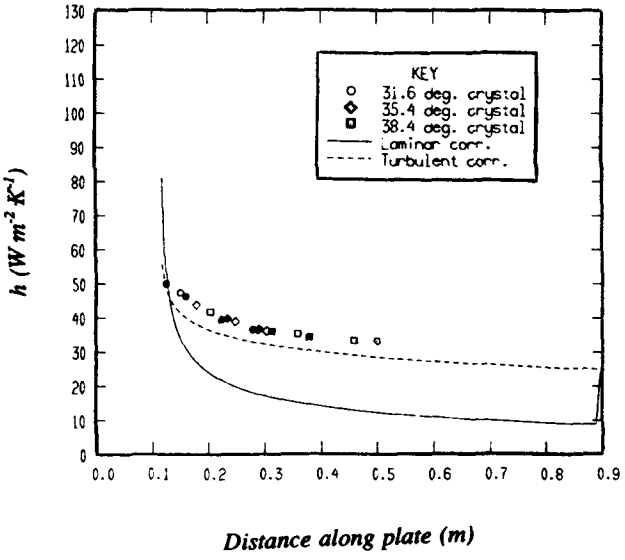

Figure 3.22 Comparison of heat transfer distributions for tripped and untripped boundary layers on carbon plate. Open symbols--untripped. Closed symbols--tripped. Flow speed = 7.9 m/sec.

Figure 3.23 Contours of constant temperature on carbon-fibre heater. Turbulent boundary layer.

Figure 3.24 Transitional boundary layer on carbon-fibre heater as indicated by temperature sensitive liquid crystals.

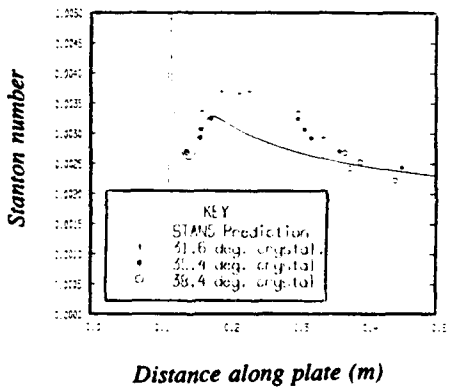

Figure 3.25 Heat transfer distribution on carbon plate. Transition boundary layer. Transition start for prediction upstream of the heated section. Flow speed = 28.9 m/s.

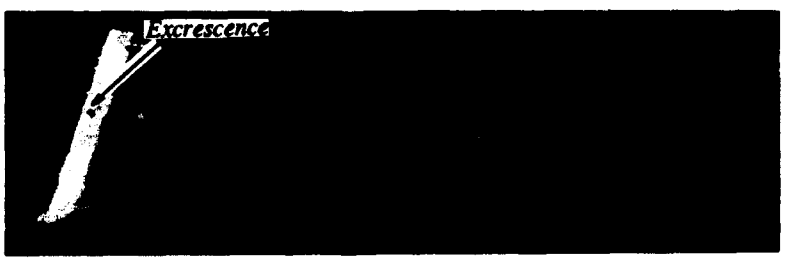

Figure 3.26 Turbulent wedge on heated carbon plate.

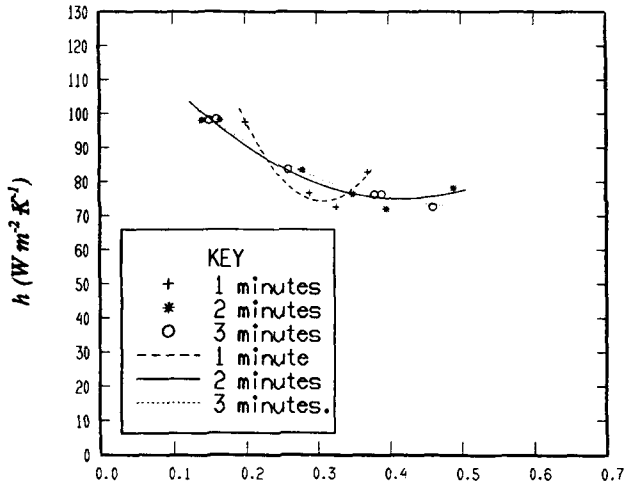

(a)

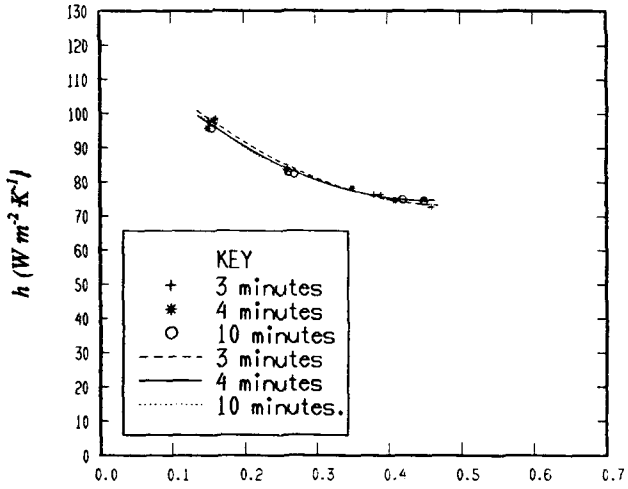

(b)

Figure 3.27 Time required for carbon plate to reach thermal stability. Flow speed = 28.9 m/sec.

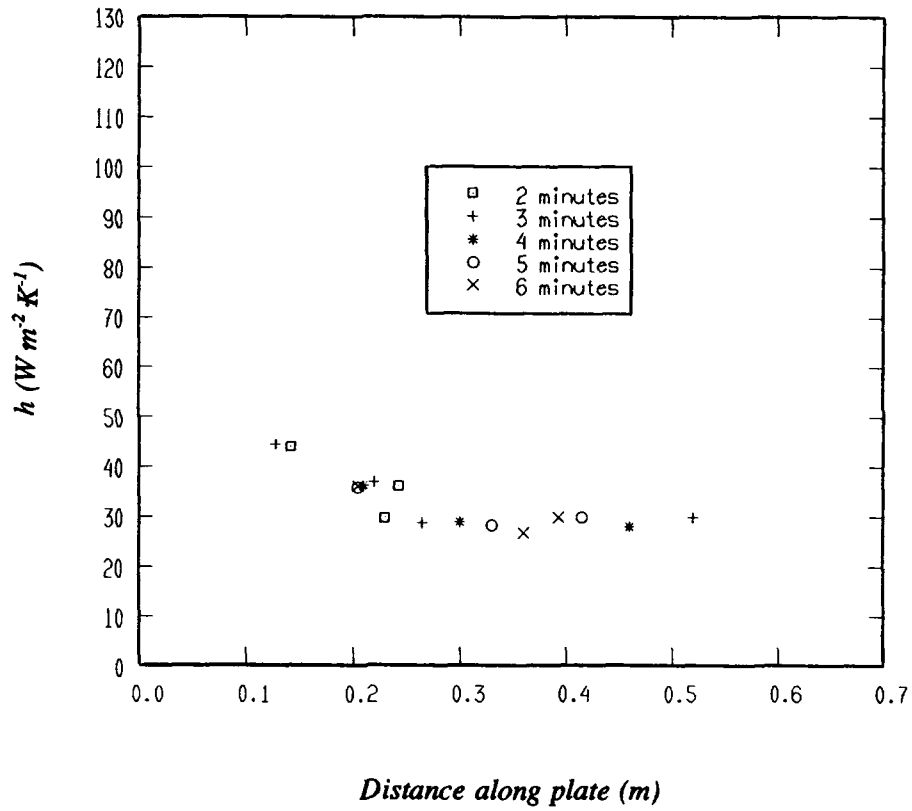

Figure 3.28 Time required for carbon plate to reach thermal stability. Flow speed = 7.9 m/sec.

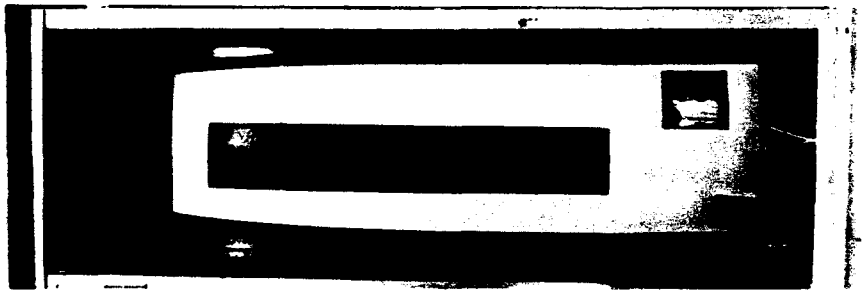

Figure 3.29 Curved carbon-fibre heater.

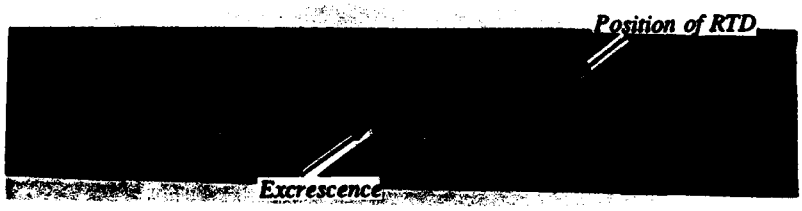

Figure 3.30 Laminar boundary layer on the curved carbon-fibre heater.

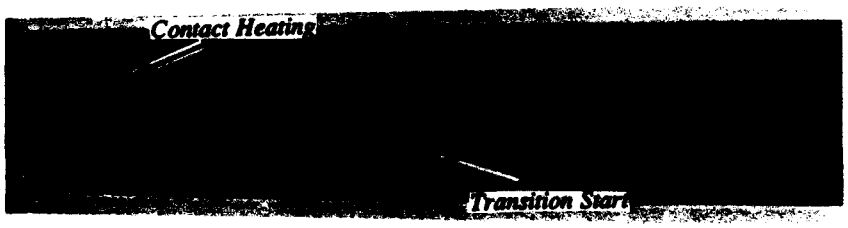

Figure 3.31 Transitional boundary layer on curved carbon-fibre heater.

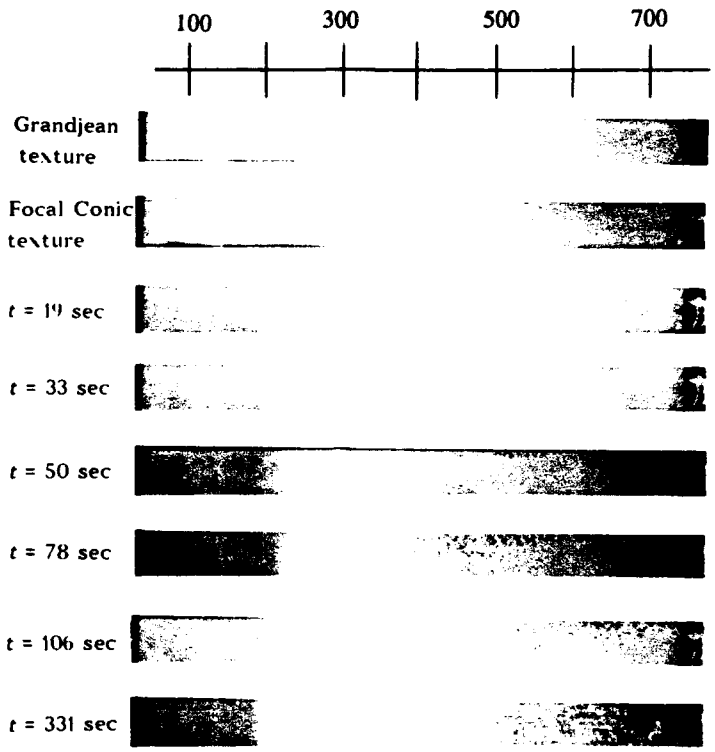

Figure 3.32 Shear sensitive liquid crystal showing transition location and used to determine absolute shear stress. Flow speed = 36.5 m/sec. (Scale in mm from leading edge of plate).

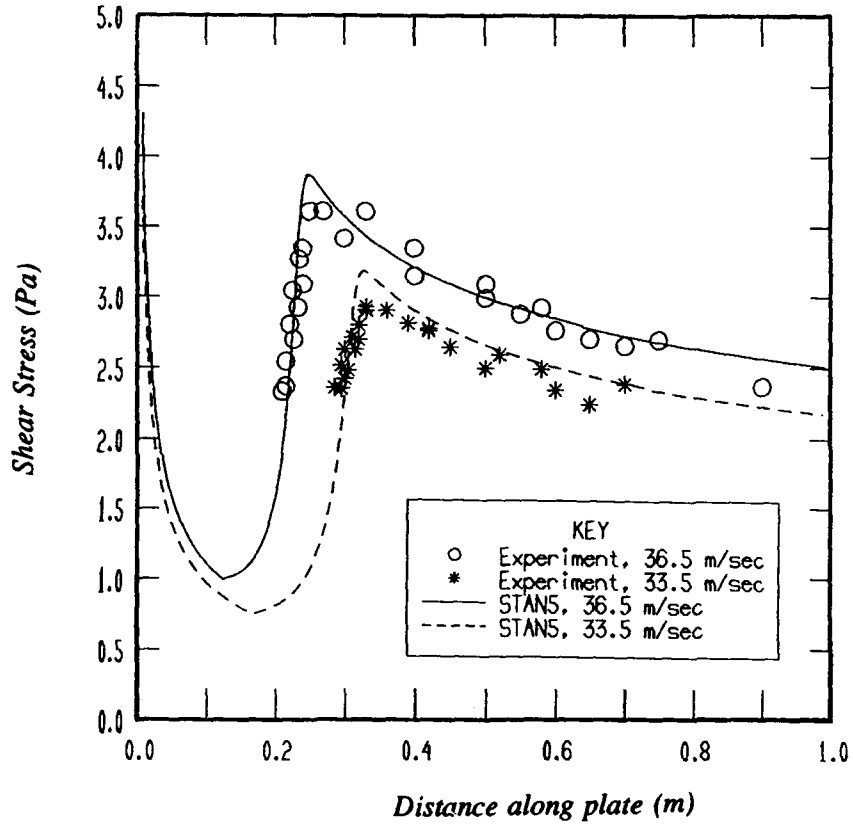

Figure 3.33 Results from two runs at 36.5 m/sec and STAN5 prediction (with specified transition location) used to calibrate the liquid crystal. This calibration is then used to determine the shear stress for two runs at 33.5 m/sec.

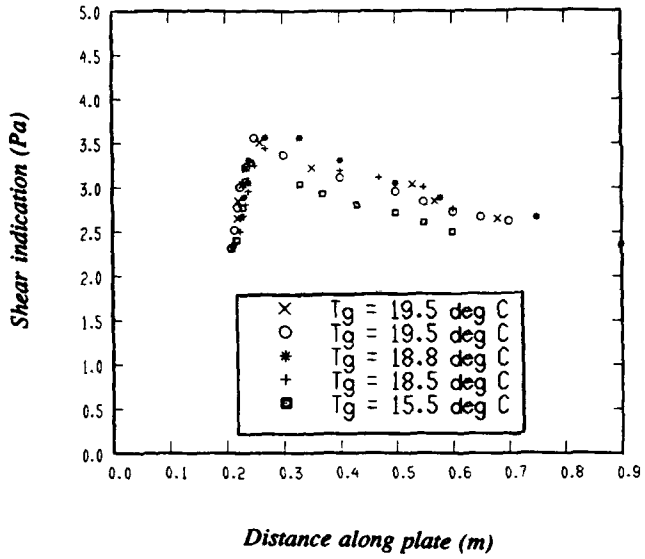

Figure 3.34 Repeatability of shear sensitive liquid crystal tests. Nominal speed = 36.5 m/sec.

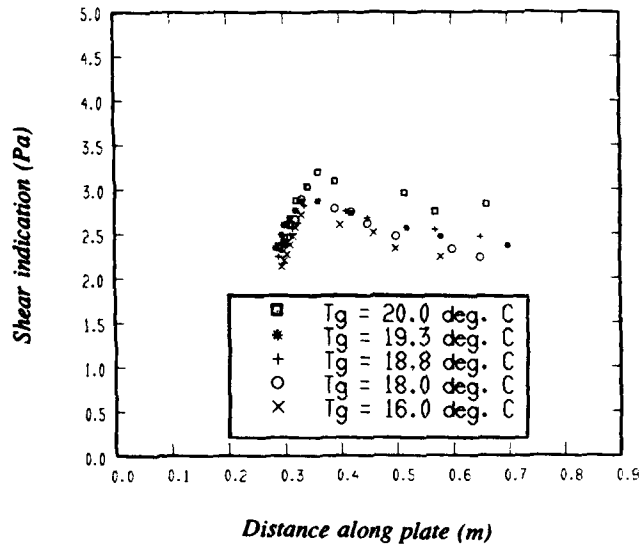

Figure 3.35 Repeatability of shear sensitive liquid crystal tests. Nominal speed = 33.6 m/sec.

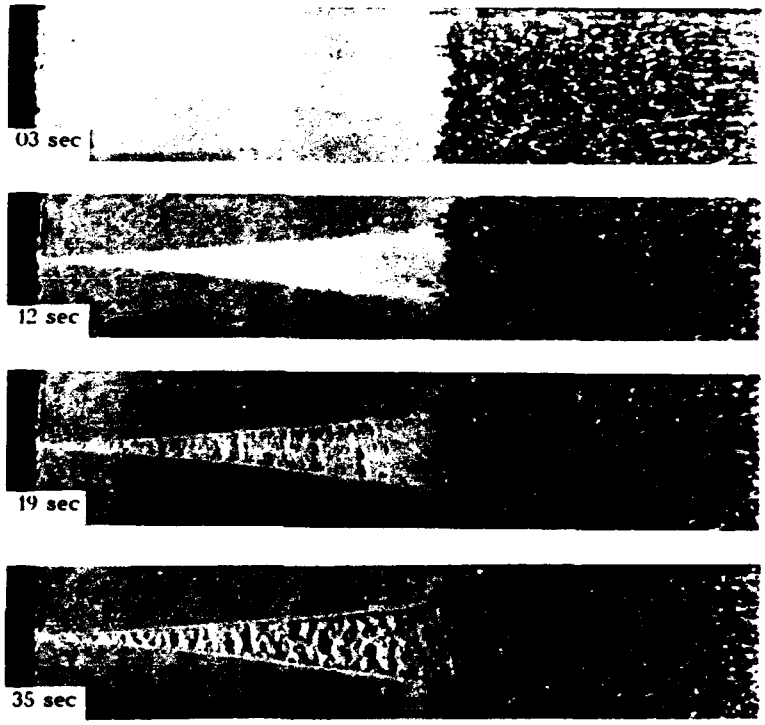

Figure 3.36 Turbulent wedge in laminar boundary layer detected with shear sensitive liquid crystal. Flow speed = 36.5 m/sec.

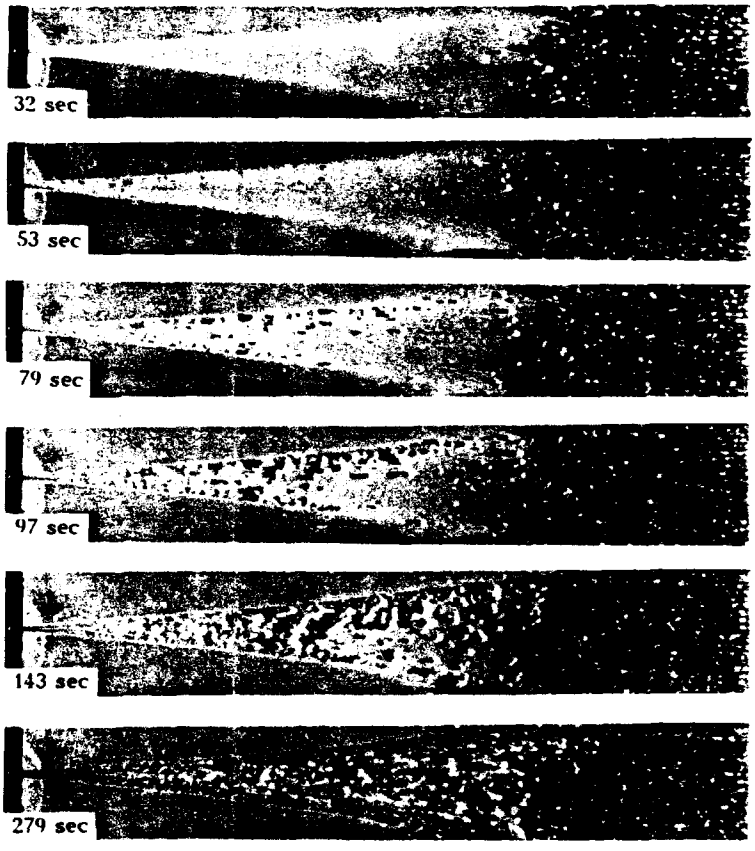

Figure 3.37 Turbulent wedge in laminar boundary layer detected with shear sensitive liquid crystal. Flow speed = 33.5 m/sec.

(a) Speed = 36.5 m/sec, 0.3 mm excrescence.

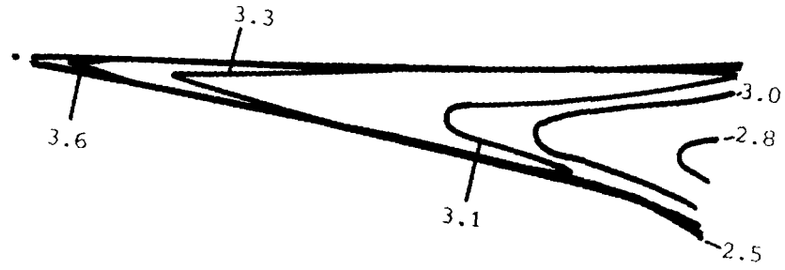

(b) Speed = 33.5 m/sec, 0.5 mm excrescence.

Figure 3.38 Contours of shear stress (Pa) in turbulent wedges.

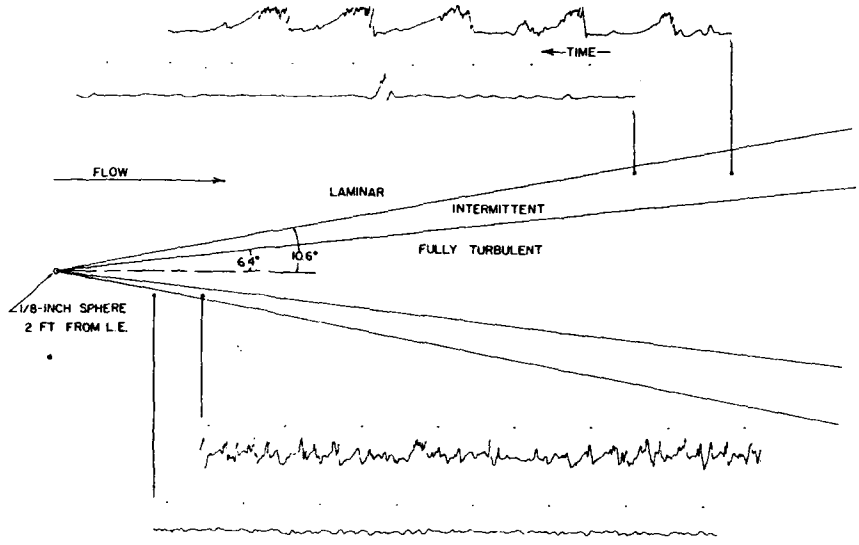

Figure 3.39 Turbulent wedge produced by three-dimensional surface excrescence, after Schubauer and Klebanoff (1955).

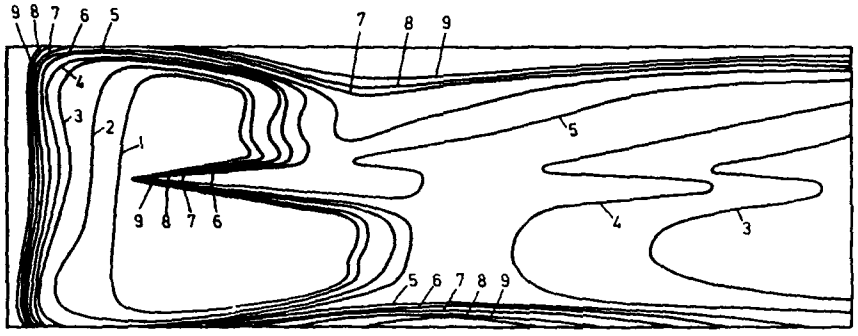

Contour	h ($W\,m^{-2}\,K^{-1}$)
1	74.4
2	92.9
3	114.3
4	125.2
5	136.9
6	150.4
7	156.8
8	161.1
9	168.6

Figure 3.40 Contours of heat transfer in a turbulent wedge, after Clark and Jones (1991).

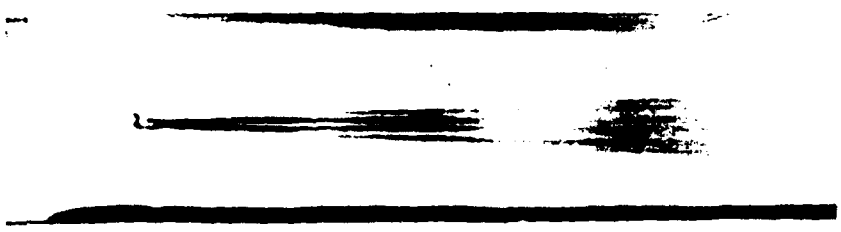

Figure 3.41 Stream-wise vortices downstream of a spherical protuberance on a flat plate, after Hama et al. (1957). Flow visualisation by sublimating acenaphthene.

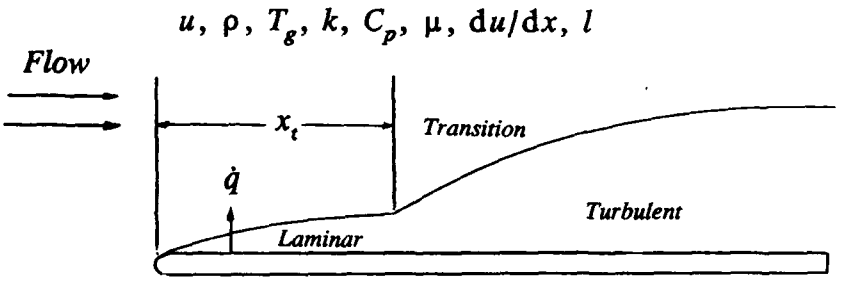

Figure A.1 Transitional boundary layer on a uniformly heated flat plate in an incompressible fluid.

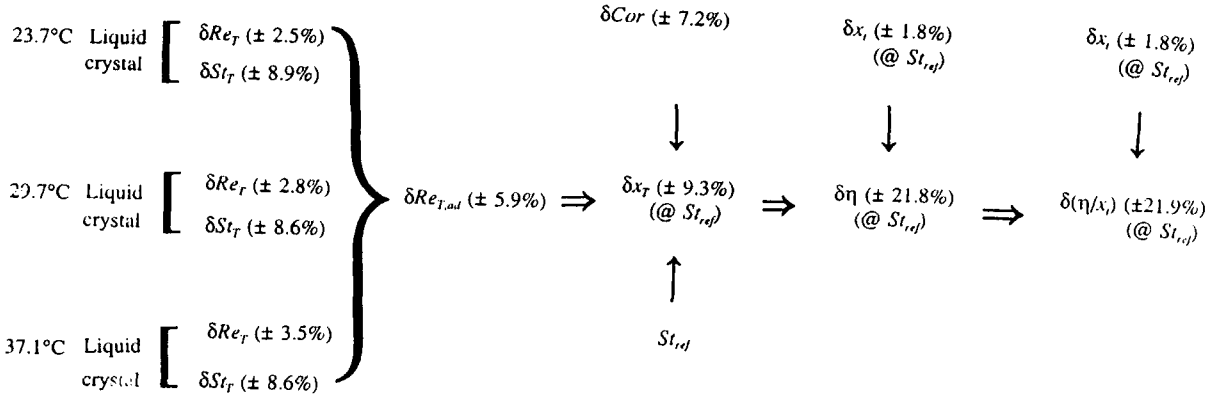

Figure B.1 Compounding of uncertainties in calculations of nondimensionalised transition length. $St_{ref} = 9.23 \times 10^{-5}$. δCor refers . Eqn. 3.10.

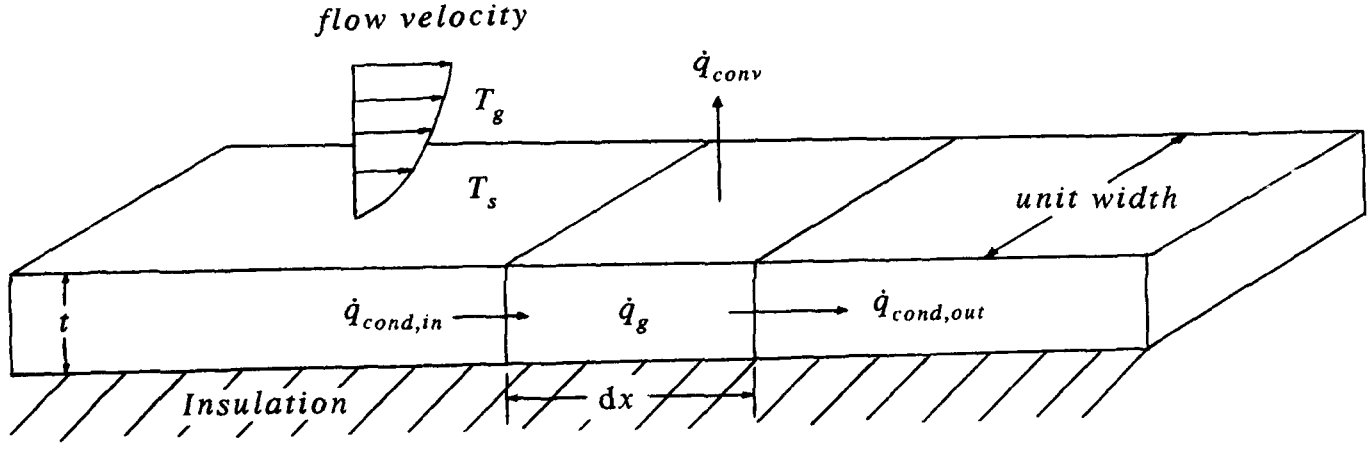

Figure C.1 Infinitesimal cross-section of heated flat plate.

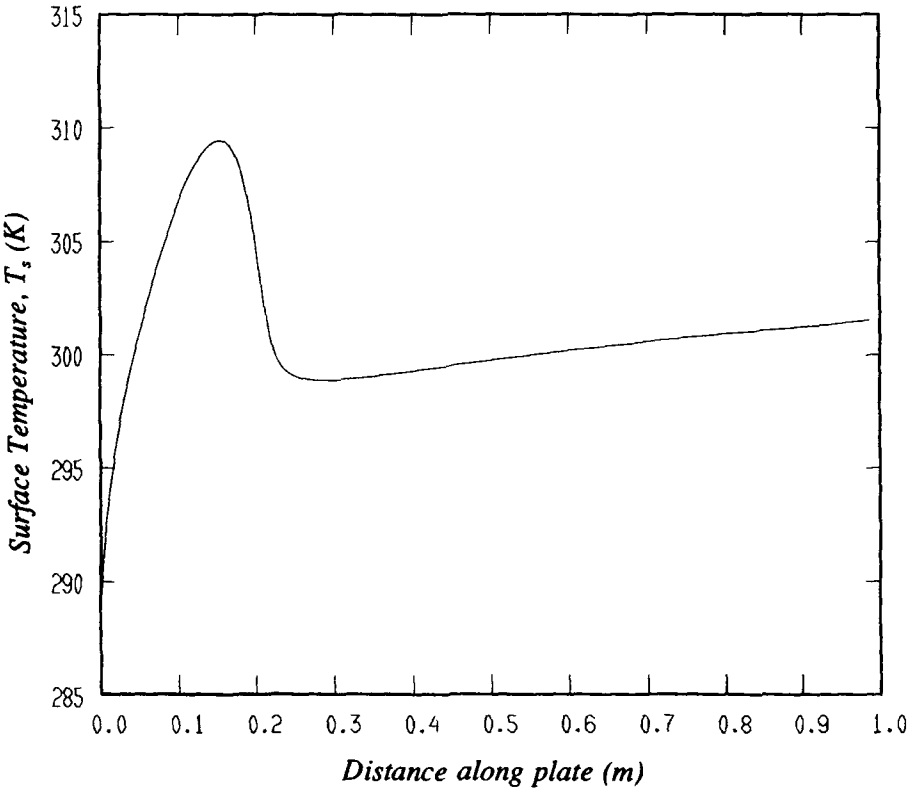

Figure C.2 Surface temperature distribution on heated flat plate as predicted by STAN5. Flow speed = 24.2 m/sec, surface heat flux = 1060 $W/m^2 \cdot K$.

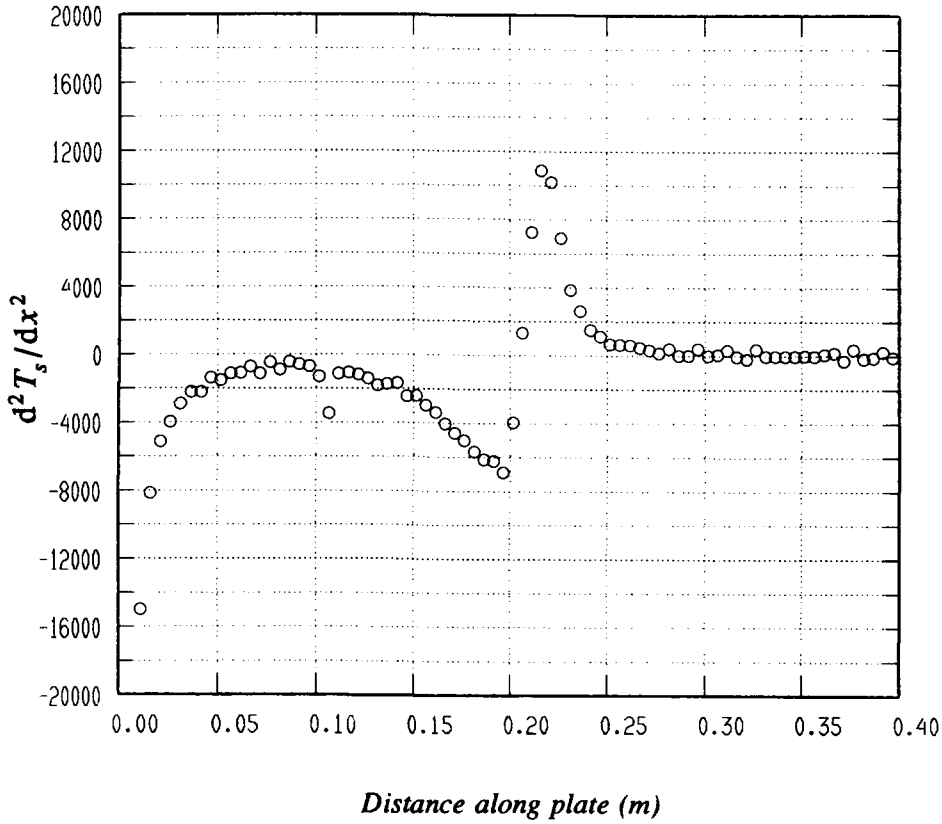

Figure C.3 Second derivative of surface temperature distribution along heated flat plate. Flow speed = 24.2 m/sec, surface heat flux = 1060 $W/m^2 \cdot K$.